
01 Jan 2023

Drainage And Sedimentary Response Of The Northern Andes And The Pebas System To Miocene Strike-slip Tectonics: A Source To Sink Study Of The Magdalena Basin

S. Zapata

L. Calderon-Diaz

C. Jaramillo

Francisca Oboh-Ikuenobe

Missouri University of Science and Technology, ikuenobe@mst.edu

et. al. For a complete list of authors, see https://scholarsmine.mst.edu/geosci_geo_peteng_facwork/2115

Follow this and additional works at: https://scholarsmine.mst.edu/geosci_geo_peteng_facwork



Part of the [Geological Engineering Commons](#), and the [Petroleum Engineering Commons](#)














Recommended Citation

S. Zapata and L. Calderon-Diaz and C. Jaramillo and F. Oboh-Ikuenobe and J. C. Piedrahita and M. Rodríguez-Cuevas and A. Cardona and E. R. Sobel and M. Parra and V. Valencia and A. Patiño and J. S. Jaramillo-Rios and M. Flores and J. Glodny, "Drainage And Sedimentary Response Of The Northern Andes And The Pebas System To Miocene Strike-slip Tectonics: A Source To Sink Study Of The Magdalena Basin," *Basin Research*, Wiley, Jan 2023.

The definitive version is available at <https://doi.org/10.1111/bre.12769>

This Article - Journal is brought to you for free and open access by Scholars' Mine. It has been accepted for inclusion in Geosciences and Geological and Petroleum Engineering Faculty Research & Creative Works by an authorized administrator of Scholars' Mine. This work is protected by U. S. Copyright Law. Unauthorized use including reproduction for redistribution requires the permission of the copyright holder. For more information, please contact scholarsmine@mst.edu.

Drainage and sedimentary response of the Northern Andes and the Pebas system to Miocene strike-slip tectonics: A source to sink study of the Magdalena Basin

S. Zapata^{1,2,3}  | L. Calderon-Diaz^{3,4}  | C. Jaramillo³  | F. Oboh-Ikuenobe²  |
 J. C. Piedrahita⁴ | M. Rodríguez-Cuevas⁴  | A. Cardona⁵  | E. R. Sobel⁶  |
 M. Parra⁷  | V. Valencia⁸  | A. Patiño⁷  | J. S. Jaramillo-Rios⁴  | M. Flores⁷  |
 J. Glodny⁹ 

¹Group of Studies in Orogenic Systems (GROSSE), Faculty of Natural Sciences, Universidad del Rosario, Bogotá, Colombia

²Department of Geosciences and Geological and Petroleum Engineering, Missouri University of Science and Technology, Rolla, Missouri, USA

³Smithsonian Tropical Research Institute, Panamá, Panama

⁴Grupo de Investigación en Geología y Geofísica (EGEO), Departamento de materiales y minerales, Facultad de Minas, Universidad Nacional de Colombia, Medellín, Colombia

⁵Grupo de Investigación en Geología y Geofísica (EGEO), Departamento de Procesos y Energía, Facultad de Minas, Universidad Nacional de Colombia, Medellín, Colombia

⁶Institute of Geosciences, University of Potsdam, Potsdam, Germany

⁷Instituto de Geociências, Universidade de São Paulo, São Paulo, Brazil

⁸School of the Environment, Washington State University, Washington, District of Columbia, USA

⁹GFZ German Research Centre for Geosciences, Potsdam, Germany

Correspondence

S. Zapata, Group of Studies in Orogenic Systems (GROSSE), Faculty of Natural Sciences, Universidad del Rosario, Bogotá, Colombia.
 Email: sebastian.zapatah@urosario.edu.co

Funding information

Bitnar fellowship; Corrigan ACGGP-ARES; HERMES 47494

Abstract

Miocene strike-slip tectonics was responsible for creating and closing short-lived (ca. 6 Ma) passages and the emergence of isolated topography in the Northern Andes. These geological events likely influenced the migration and/or isolation of biological populations. To better understand the paleogeography of the Miocene hinterland and foreland regions in the Northern Andes, we conducted a source-to-sink approach in the Magdalena Basin. This basin is located between the Central and Eastern Cordilleras of Colombia and contains an ample Miocene record, which includes Lower Miocene fine-grained strata and Middle Miocene to Pliocene coarsening-up strata. Our study presents a new data set that includes detrital U–Pb zircon ages (15 samples), sandstone petrography (45 samples) and low-temperature thermochronology from the Southern Central Cordillera (19 dates); which together with previously published data were used to construct a paleogeographical model of the Miocene hinterland and foreland regions in the Northern Andes. The evolution of the Magdalena Basin during the Miocene was characterized by playa and permanent lake systems at ca. 17.5 Ma, which may be related to a marine incursion into NW South America and western Amazonia.

The appearance of Eocene to Miocene volcanic sources in the Honda Group after ca. 16 Ma suggests the development of fluvial passages, which connected the Pacific with the western Amazonia and Caribbean regions. These passages were synchronous with a time of Miocene exhumation and topographic growth (ca. 16 to 10 Ma) in the Central Cordillera and the transition from lacustrine to fluvial deposition in the Magdalena Basin. Middle to Late Miocene strike-slip deformation promoted by oblique plate convergence and the oblique collision of the Panamá-Chocó Block likely explains the synchronous along-strike fragmentation and exhumation in the Central Cordillera.

KEYWORDS

Lake stratigraphy, low-temperature thermochronology, Northern Andes, Pebas system, sedimentary provenance, strike-slip deformation

1 | INTRODUCTION

Major tectonic events can modify relief, local climate and sedimentary routing systems (e.g., Bookhagen & Strecker, 2012; Horton, 2018a; Poulsen et al., 2010) and thus exert a first-order control on landscape and ecosystem evolution (e.g., Antonelli et al., 2018; Hoorn et al., 2018; Horton, 2018b). In particular, strike-slip tectonics can be responsible for the fragmentation and displacement of mountain belts, coeval along-strike extension and compression and major drainage rearrangements (e.g., Fossen & Tikoff, 1998; Gibson et al., 2021; Krstekanić et al., 2021; Liu et al., 2021). The Northern Andes is a cordilleran orogen that resulted from prolonged subduction, terrane accretion and oblique convergence (Cardona et al., 2020; Montes et al., 2019; Spikings et al., 2014); especially during the Miocene when oblique plate convergence and the collision of the Panamá-Chocó Block caused strike-slip deformation along the NW South America margin (Acosta et al., 2007; Escalona & Mann, 2011; Montes et al., 2019; Sanín, Mejía-Franco, et al., 2022; Siravo et al., 2021). Given that these major tectonic events in the Northern Andes were coeval with the development of the highly diverse Amazon, Caribbean and Pacific regions (e.g., Hazzi et al., 2018; Hoorn et al., 2010; Montes et al., 2019), this region is an ideal place to understand the role of major tectonic events, such as strike-slip tectonics, on landscape evolution and ultimately on diversity (e.g., Antonelli et al., 2009; Réjaud et al., 2020; Sanín, Cardona, et al., 2022).

The Pebas system was a continental-scale wetland-like ecosystem that developed during the Early Miocene in the western Amazonia and terminated due to the Middle to Late Miocene rise of the Northern and Central Andes (Costantino et al., 2021; Hoorn et al., 1995, 2010; Hoorn,

Highlights

- Drainage reorganization and mountain-belt exhumation and fragmentation due to strike slip tectonics.
- Erosion and volcanism caused the premature termination of the western border of the lacustrine Pebas system.
- Short lived connections (6 Ma) between the Northern Andes hinterland and Western Amazonia

Kukla, et al., 2021; Mora et al., 2010). Both the Andes and the Pebas systems played a role in the process of biological diversification that led to the high diversity of the Amazonia and northern South America (e.g., Antonelli et al., 2009; Hoorn et al., 2018; Hoorn, Boschman, et al., 2021; Pirie et al., 2006; Rahbek et al., 2019; Réjaud et al., 2020; Wesselingh & Salo, 2006). The question of whether land connections existed between the Pebas system and the Colombian hinterland basins, specifically the Magdalena Basin, remains a subject of research interest. This has prompted scholars to propose divergent paleogeographic models, including the hypothesis of a Miocene trans-Andean passage (Montes et al., 2021; Rodríguez-Muñoz et al., 2022) and the disconnection between the hinterland and foreland regions since the Oligocene (Anderson et al., 2016; Horton et al., 2015; Reyes-Harker et al., 2015).

The Magdalena Basin preserves an extensive Miocene record that offers an opportunity to explore possible relationships between these basins and the Pebas wetlands

and to investigate how these sedimentary systems responded to Miocene strike-slip tectonics. The refinement of the Miocene paleogeography of the Northern Andes is a key input to understanding the high diversity observed in the Amazonian, Pacific and Caribbean regions. However, despite the large amount of research dedicated to this paleogeography (Anderson et al., 2016; Costantino et al., 2021; Horton et al., 2015; Montes et al., 2021; Mora, Villagómez, et al., 2020; Parra, Mora, Sobel, et al., 2009; Restrepo-Moreno et al., 2019; Reyes-Harker et al., 2015); the lack of stratigraphic, provenance and deformation data in several segments of the Northern Andes, and the absence of regional compilations have prevented refined reconstructions of the drainage network, the sedimentary systems and the deformation patterns.

This contribution presents new stratigraphic data and multi-technique provenance data from the Miocene strata in the Magdalena Basin, and low-temperature thermochronology from the Southern Central Cordillera integrated with available provenance, thermochronological and stratigraphic data. We utilize this database to present a Miocene paleogeography of highly diverse regions, which will ultimately serve as a framework for future paleobiogeographical studies. Furthermore, our model shows how strike-slip deformation promoted surface uplift, fragmented past orographic barriers and modified the drainage network and the sedimentary systems: a tectonic scenario that controlled landscape evolution and species connectivity in NW South America.

2 | GEOLOGICAL BACKGROUND

2.1 | Tectonic evolution of the Northern Andes

The Cretaceous to Miocene tectonic evolution of the Northern Andes was characterized by oblique plate convergence which has been responsible for block displacements, the oblique collision of allochthonous terranes (Caribbean Plateau and Panamá-Chocó Block) and the formation of pull-apart basins (Jaramillo et al., 2022; Montes et al., 2010; Pindell & Erikson, 1993; Siravo et al., 2021; Spikings et al., 2014; Zapata, Cardona, et al., 2019). During the Miocene, the oblique collision of the Panamá-Chocó Block and the eastern advance of the Caribbean Plate with respect to the South American continental margin, promoted intense strike-slip deformation along the Northern Andes (Acosta et al., 2007; Amaya et al., 2017; Escalona & Mann, 2011; Galindo & Lonergan, 2020; Kennan & Pindell, 2009; Montes et al., 2012, 2019). Additionally, changes in the geometry and composition of the subducting plate and the architecture of the upper plate systems

have been responsible for the development of contrasting Cenozoic magmatic spatiotemporal patterns along the Northern Andes (Cardona et al., 2018; Jaramillo et al., 2019; Leal-Mejia, 2011; Wagner et al., 2017).

The Central, Western and Eastern Cordilleras of Colombia delimit two parallel intermountain river valleys: the Magdalena Valley in the east and the Cauca-Patia Valley in the west (Figure 1). Several NE strike-slip structures, such as the Ibagué, Chusma, and Algeciras fault systems, cut across the Central Cordillera, the Magdalena Valley and the Eastern Cordillera. The Ibagué fault separates the Antioquia Altiplano Province (AAP) from the Southern Central Cordillera, while the Algeciras and Chusma faults represent the southern limit of the Southern Central Cordillera (Figure 1).

Compressional tectonics have characterized the Northern Andes since the Cretaceous (ca. 90 Ma)—major topographic growth and foreland sedimentation started during the Late Cretaceous (ca. 72 Ma) because of the collision between the continental margin and the Caribbean Plateau (George et al., 2021; Jaramillo, Cardona, et al., 2017; Pardo-Trujillo et al., 2020; Villagómez & Spikings, 2013; Zapata et al., 2021). After this collision, arc magmatism restarted and several disconnected blocks from the northern segment of the Eastern Cordillera were uplifted (Bayona et al., 2020; Jaramillo et al., 2022). Several authors have suggested that between the Late Eocene and the Oligocene, the continental margin was characterized by the absence of major compressional events, an interpretation that is supported by low subsidence and exhumation rates in the Central and Eastern Cordilleras (Mora et al., 2010; Reyes-Harker et al., 2015; Villamizar-Escalante et al., 2021; Zapata et al., 2021).

During the Early and Middle Miocene (24–10 Ma), dynamic and flexural subsidence in Western Amazonia promoted the development of a continental-scale wetland-like system known as the Pebas system, which lacks a modern analogue (Bicudo et al., 2020; Eakin et al., 2014; Hoorn, Kukla, et al., 2021; Miller et al., 2020). By the Late Miocene (ca. 9 Ma), the Andes had major deformational and uplift events that shifted the drainage system towards the east—ending the Pebas system and starting the modern Amazonian fluvial system (Hoorn et al., 2017). Northern South America has a rich Miocene fossil record (Figure 1a) that documents diversity and the role of landscape in the paleobiogeographical evolution of this region (Carrillo et al., 2015; Montes et al., 2021; Moreno et al., 2015; Pérez-Consuegra et al., 2017). Based on fossil and phylogenetic data, several authors have proposed a lowland connection between the Northern Andes hinterland and Western Amazonia until ca. 8 Ma (Lundberg & Chernoff, 1992; Montes et al., 2021; Rodríguez-Muñoz et al., 2022). In contrast, other authors have used

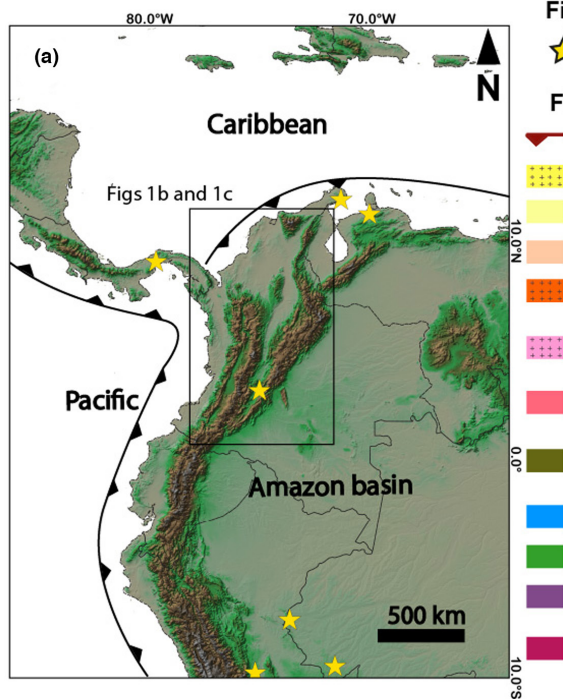


Figure 1a

★ Major Neogene neotropical fossil sites

Figure 1b

- ▬ Faults
- Neogene igneous rocks
- Neogene sedimentary rocks
- Paleocene sedimentary rocks
- Late Eocene-Oligocene igneous rocks
- Cretaceous-Early Eocene plutonic rocks
- Cretaceous metamorphic and volcanic rocks
- Cretaceous volcanic rocks with plateau affinity
- Jurassic igneous rocks
- Mesozoic sedimentary rocks
- Pre-Mesozoic Crystalline rocks
- Pre-Mesozoic sedimentary rocks

Figure 1c 1: Upper Magdalena Basin:

- 1.1: Neiva sub-Basin
- 1.2: Girardot sub-Basin
- 2: Middle Magdalena Basin
- 3: Lower Magdalena Basin
- 4: Cauca Basin
- 5: Llanos Basin
- 6: Putumayo Basin

- GF: Garrapatas Fault
- RF: Romeral Fault System
- PF: Palestina Fault
- IF: Ibague Fault
- CHF: Chusma Fault
- AF: Algeciras Fault
- GUF: Guaicaramo Fault
- CF: Conejos Fault

- SMM: Santa Marta Massif
- SL: San Lucas Range
- AAP: Antioquia Altiplano Province
- PCB: Panama-Choco Block
- WC: Western Cordillera
- EC: Eastern Cordillera
- QM: Quetame Massif
- GM: Garzon Massif
- CM: Colombian Massif
- SM: Santander Massif
- SCC: Southern Central Cordillera

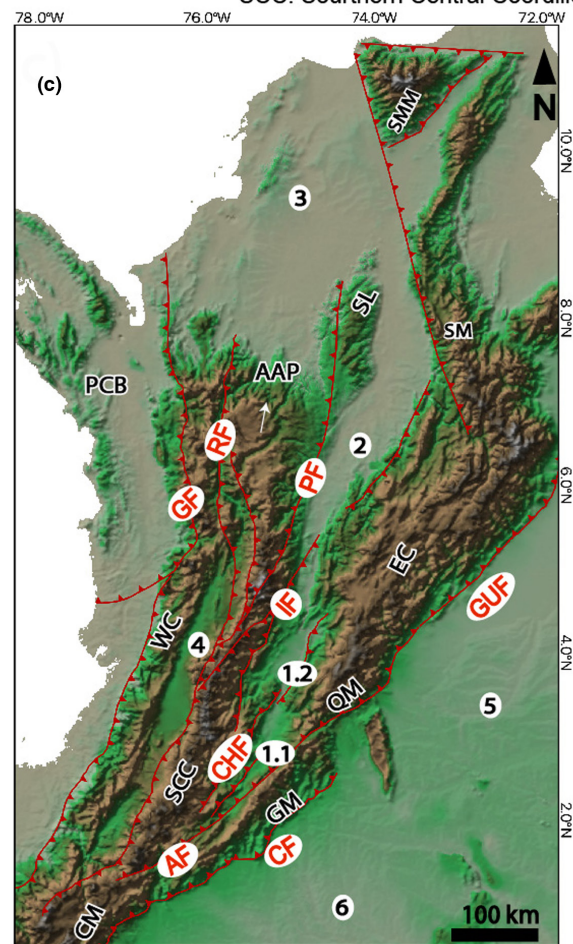
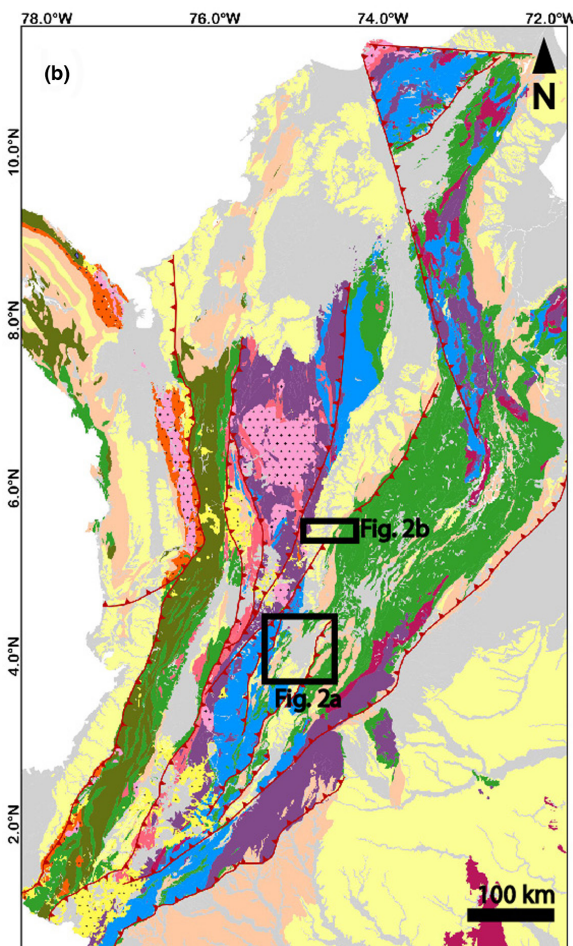


FIGURE 1 (a) Location of the study region, yellow stars indicate the most important neotropical fossil sites after Carrillo et al. (2015). (b) Geology of the Northern Andes modified from Gómez and Montes (2020). (c) Principal basins (numbers), basement-core structural blocks (black letters) and faults (red letters) from the Northern Andes; abbreviations are presented in the figure legend.

provenance and stratigraphic data to indicate a disconnection with the Pebas system before 8 Ma (Anderson et al., 2016; Horton et al., 2015; Reyes-Harker et al., 2015).

In regions such as the Western and the Southern Central Cordilleras, the deformational phases are poorly known, however, available data suggest contrasting Miocene spatiotemporal deformational patterns along the Northern Andes (Mora, Villagómez, et al., 2020; Restrepo-Moreno et al., 2019). Low-temperature thermochronology, seismic images and stratigraphy data suggest Oligocene to Pliocene deformation, exhumation and topographic growth along the northern Eastern Cordillera—deformation rates significantly increased after 13 Ma (Costantino et al., 2021; Mora et al., 2013; Mora, Tesón, et al., 2020; Reyes-Harker et al., 2015; Siravo et al., 2019). In the southern Eastern Cordillera (Colombia, Garzón and Quetame massifs), deformation and exhumation began around ca. 12 Ma, but major uplift and exhumation phases occurred between ca. 8 and 3 Ma (Anderson et al., 2016; Bayona et al., 2008; Mora et al., 2008; Pérez-Consuegra, Ott, et al., 2021; Saeid et al., 2017). Although low exhumation rates characterized the AAP during the Miocene, thermochronological and geomorphological data suggest Late Miocene to Pliocene (7–4 Ma) deformation and uplift (Pérez-Consuegra, Ott, et al., 2021; Pérez-Consuegra et al., 2022). In the Southern Central Cordillera, seismic information suggests major compressional and strike-slip deformational phases during the Miocene (Espitia et al., 2022; Jiménez et al., 2012; Ramon & Rosero, 2006); however, the lack of thermochronological data and temporal constraints in the Miocene strata have prevented a precise temporal definition of these events. Miocene deformation phases in the Northern Andes have been related to the break-up of the Farallon Plate at ca. 25 Ma, an increase in the convergence rates during the Middle Miocene, the collision of the Panamá-Chocó Block around 16 Ma and flat-slab subduction (Lara et al., 2018; Montes et al., 2015; Mora et al., 2013, 2015; Pérez-Consuegra et al., 2022; Siravo et al., 2019; Wagner et al., 2017).

2.2 | Geochronological provinces of the Northern Andes

The reconstruction of past drainage networks requires a correlation between sedimentary provenance signals and possible source areas; in this section, we describe the most important geochronological provinces in the Northern Andes. The Western, Central and Eastern Cordilleras and the intermontane Cauca and Magdalena valleys are characterized by geological units formed in contrasting tectonic settings, which have facilitated the reconstruction of past source areas in the Northern Andes (e.g., Bayona et al., 2020; Horton et al., 2015, 2020; Nie et al., 2012;

Reyes-Harker et al., 2015; Valencia-Gómez et al., 2020; Zapata, Cardona, et al., 2019).

The basement rocks of the Western Cordillera are composed of Jurassic to Lower Cretaceous (150 to 105 Ma) basaltic and sedimentary rocks that were part of the allochthons Caribbean Plateau; these rocks are intruded by Cretaceous (90 to 65 Ma) gabbros and tonalites formed in an oceanic volcanic arc (Villagómez et al., 2011; Zapata-Villada et al., 2021).

The metamorphic basement in the Central Cordillera (AAP + Southern Central Cordillera in Figure 1b,c) is mostly composed of Paleozoic to Jurassic (ca. 460 to 150 Ma) amphibolites, gneisses, granulites and low-grade schists and phyllites. These metamorphic units are characterized by major Palaeozoic (ca. 540 to 400 Ma) and Mesoproterozoic (ca. 1600 to 1000 Ma) inherited and detrital U–Pb zircon age populations (Carmona & Pimentel, 2002; Correa-Martínez et al., 2020; Martens et al., 2012; Ordóñez-Carmona et al., 2006; Restrepo et al., 2011; Villagómez et al., 2011; Vinasco et al., 2006). This Paleozoic metamorphic basement is intruded by arc-related Permian to Early Cretaceous (ca. 280 to 130 Ma) intermediate plutonic rocks formed in a continental arc (Bayona et al., 2019; Bustamante et al., 2016; Spikings & Paul, 2019).

The pre-Cretaceous crystalline basement rocks of the Central Cordillera are overlain by several volcanoclastic units deposited between 125 Ma and 80 Ma, as a result of rift and arc magmatism; these units are characterized by Cretaceous (ca. 120 to 80 Ma), Jurassic (ca. 200 to 160), Permo-Triassic (300 to 220), Paleozoic (ca. 400 to 650 Ma), Mesoproterozoic (1000 to 1600 Ma) zircon age populations (Jaramillo et al., 2014; Villagómez et al., 2011; Zapata, Cardona, et al., 2019). Finally, Late Cretaceous (ca. 100 to 70 Ma) and Paleocene to Eocene (62 to 50 Ma) granodiorites, diorites and tonalites intrude Paleozoic to Lower Cretaceous rocks from the Central Cordillera (Duque-Trujillo et al., 2019; Jaramillo et al., 2022; Leal-Mejía et al., 2019; Spikings et al., 2014).

The south-eastern segment of the Central Cordillera, the San Lucas Range and the Santander Massif are characterized by an ample record of Permian to Jurassic plutonic rocks while in the AAP the Late Cretaceous plutonic rocks and Cretaceous sedimentary strata are more abundant (Figure 1b,c). In summary, the Central Cordillera is mostly composed of Pre-Cretaceous metamorphic rocks overlain by Cretaceous volcanoclastic strata and intruded by abundant Mesozoic and Paleogene plutonic rocks; these units represent source areas with distinctive Mesoproterozoic (1000 to 1600 Ma), Paleozoic to Triassic (650 to 400 Ma and 300 to 220 Ma), Jurassic (ca. 200 to 160), Cretaceous (ca. 120 to 70 Ma) and Paleogene (62 to 50 Ma) U–Pb zircon age populations.

The Eastern Cordillera is characterized by a Paleozoic sedimentary basement covered by rift-related Cretaceous

strata, which have detrital zircon ages from the eastern cratons—older than 900 Ma—and minor syn-depositional ages (Bayona et al., 2020; Horton et al., 2010, 2020). Paleogene to Miocene foreland sedimentary units preserved in the Eastern Cordillera are characterized by the appearance of Permian to Eocene zircons derived from the Central Cordillera (Horton et al., 2020 and references therein). North of the Eastern Cordillera, the Santander Massif is characterized by Paleozoic plutonic and metasedimentary rocks intruded by Jurassic plutons (Bayona et al., 2019; van der Lelij et al., 2016). The Garzón and Quetame massifs are composed of Proterozoic (1500–900 Ma) metamorphic rocks intruded by Ordovician plutons (ca. 450 Ma) (Horton et al., 2010; Ibanez-Mejia et al., 2015) (Figure 1b,c).

The spatiotemporal distribution of Cenozoic arc volcanism in the Northern Andes provides an additional provenance constraint (Figure 1). The plutonic record of the post-collisional Paleocene to Early Eocene volcanic arc (66 to 50 Ma) is restricted to minor intrusive rocks distributed along the Central Cordillera, several Caribbean crustal blocks and the Panamá-Chocó Block (Bayona et al., 2012; Bustamante et al., 2017; Duque-Trujillo et al., 2019). Additionally, Paleocene-Eocene volcanic zircon grains and reworked volcanoclastic rocks were preserved in the Eocene units in the Magdalena Basin and the Eastern Cordillera (Bayona et al., 2012; Bustamante et al., 2017; Cardona et al., 2018; Jaramillo et al., 2022). After a magmatic gap of ca. 7 Ma, Late Eocene to Oligocene (40 to 30 Ma) igneous rocks restricted to the allochthonous Panamá-Chocó Block and the southern segment of the Western Cordillera (Barbosa-Espitia et al., 2019; Cardona et al., 2018). Between 20 and 8 Ma, the volcanic arc migrated from the Western Cordillera to the Cauca Basin and the western flank of the Central Cordillera (Wagner et al., 2017). The migration towards the eastern flank of the Southern Central Cordillera occurred after ca. 8 Ma, resulting in the deposition of volcanoclastic rocks in the Magdalena Basin (Anderson et al., 2016).

2.3 | Stratigraphy of the Upper and Middle Magdalena Basins

The Magdalena Basin has been divided into the Upper, Middle and Lower Magdalena basins, these definitions refer to their relative topographic positions along the Magdalena Valley. The limit between the Upper and Lower Magdalena basins is the Guataqui High (Figures 1c and 2). The Upper Magdalena Basin is divided into the Girardot and Neiva sub-basins, which are separated by the Pata and Natagaima highs (Figures 1c and 2). The basements of these basins comprise Jurassic volcanoclastic

and plutonic rocks in the Upper Magdalena Basin and pre-Mesozoic metamorphic rocks and Jurassic plutons in the Middle Magdalena Basin; in both basins, basement rocks are unconformably overlain by rift-related Cretaceous strata (Gómez et al., 2003; Sarmiento & Rangel, 2004; Sarmiento-Rojas et al., 2006). A pronounced angular unconformity separates deformed Cretaceous and Lower Paleocene units from the Middle Eocene to Oligocene Gualanday Group in the Upper Magdalena Basin and from the San Juan de Rio Seco Formation in the Middle Magdalena Basin (Gómez et al., 2005; Ramon & Rosero, 2006; Sarmiento & Rangel, 2004). The Gualanday Group is characterized by pebble-to-boulder conglomerates interpreted as alluvial fans sourced from the Southern Central Cordillera, while the San Juan the Rio Seco Formation is composed of sandstones and mudstones deposited in a fluvial system (Gómez et al., 2003, 2005; Ramon & Rosero, 2006).

During the Lower Miocene, fine-grained lacustrine strata were deposited on top of the Cretaceous, Eocene and Oligocene rocks in the Middle (Santa Teresa and La Cira formations) and the Upper (Barzalosa Formation) Magdalena basins. Several authors have used palynological biostratigraphy to constraint the depositional age of these sedimentary units, a technique commonly used in many tropical American sedimentary basins (Carvalho et al., 2021; Jaramillo, Ochoa, et al., 2010; Jaramillo, Romero, et al., 2017; Parra, Mora, Jaramillo, et al., 2009). The most up-to-date biostratigraphic zonation for these basins (Jaramillo et al., 2011) is based on the information from 70 sections and 6707 samples covering the entire Cenozoic. This zonation was calibrated with published data, including magnetostratigraphy (Herrera, 2008), carbon isotopes (Carvalho et al., 2021; Jaramillo et al., 2006), zircon U–Pb geochronology (Carvalho et al., 2021; Jaramillo, Torres, et al., 2010) and foraminifera data (Linares, 2004; Wozniak & Wozniak, 1987). Therefore, this method provides a reliable tool to precisely constrain Cenozoic depositional ages in the Northern Andes. Fossil palynological data suggest an Early Miocene ca. 17.7 Ma to 16.1 Ma (palynological zone T13 of Jaramillo et al., 2011) depositional age for the La Cira, Santa Teresa and Barzalosa formations (de La Parra et al., 2019; Gómez et al., 2003; Guzmán-Speziale et al., 2005; Jaramillo, Romero, et al., 2017; Nuttall, 1990).

The Barzalosa Formation has been divided into three members, which include a lower member dominated by siltstones and conglomerates, a middle member composed of monotonous claystones and siltstones that exhibit distinctive gypsum veins, and an upper member dominated by conglomerates and siltstones (de La Parra et al., 2019). The Santa Teresa, La Cira and Barzalosa formations were deposited in lacustrine sedimentary systems, similar to the Lower and Middle Miocene strata

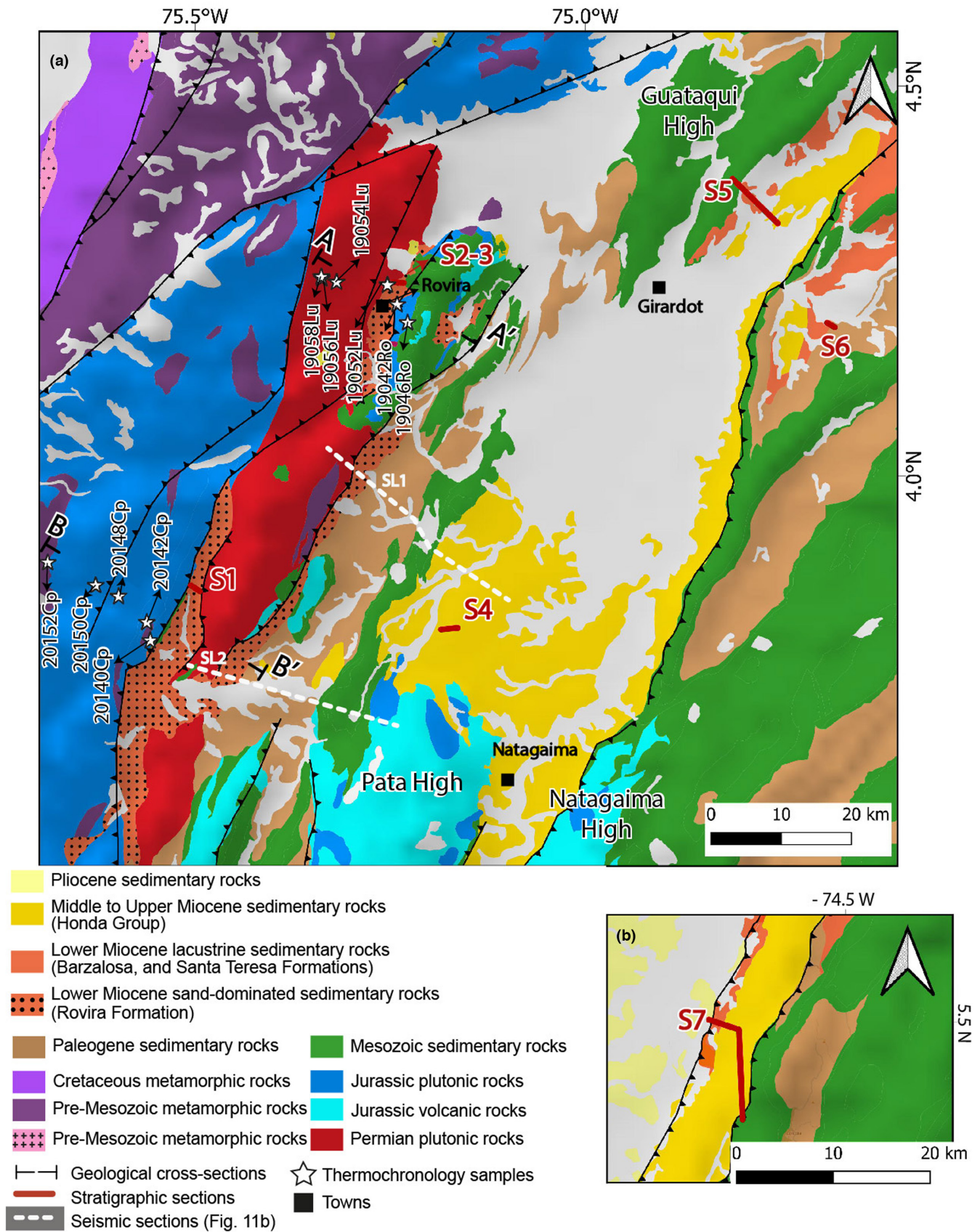


FIGURE 2 Geology of the Upper and Middle Magdalena Basin (a) Girardot sub-basin in the Upper Magdalena Basin and the (b) Middle Magdalena Basin. Map locations are presented in Figure 1b and available seismic lines are presented in Figure 11b.

deposited in the Llanos and Putumayo basins during the development of the Pebas system in Western Amazonia (de La Parra et al., 2019). However, the lacustrine strata in the Upper and Middle Magdalena basins were deposited in a freshwater system, while the Pebas system included two major marine Caribbean incursions during the Lower Miocene (ca. 18.1 to ca. 17.2 Ma) and the Middle Miocene (ca. 16.1 to ca. 12.4 Ma) (Jaramillo, Romero, et al., 2017).

Middle to Upper Miocene sand-dominated clastic strata deposited in braided to meandering depositional systems have been described as the Honda Group. Our results suggest that clastic strata in the western segment of the Girardot sub-basin are not correlatable with the Honda Group, and thus a new unit (Rovira Formation) is presented in this contribution. In the Neiva sub-basin, the Honda Group is divided into the Victoria and Villavieja formations. At the top of the Honda Group, an erosional contact separates the Villavieja Formation from the Gigante Formation, which is composed of boulder conglomerates and abundant volcanoclastic strata deposited between 10 Ma and 6 Ma (Anderson et al., 2016; Montes et al., 2021; van der Wiel et al., 1992). In the Middle Magdalena Basin, the Pliocene volcanoclastic strata of the Mesa Formation are unconformably deposited on top of the Honda Group (de Porta, 1966).

3 | METHODS

We used a source-to-sink approach in the Upper and Middle Magdalena basins and combine it with data from previous studies; this dataset is used to reconstruct the Miocene paleogeography of the Northern Andes hinterland region and the western border of the Pebas system and to understand their response to tectonic events, such as terrane accretion and oblique convergence. We obtained 19 new thermochronological ages from two transects in the Southern Central Cordillera (Figure 2). Additionally, we described seven stratigraphic sections accompanied by provenance data that include 15 samples with U–Pb detrital zircon ages, 45 petrography samples and 8 clast counts. Sample locations are presented in Table 1. Thermochronological and zircon U–Pb data are fully available in the Geochron database (https://www.geochron.org/dataset/html/geochron_dataset_2023_03_11_pOaYX).

3.1 | Stratigraphy and provenance methods

The stratigraphic sections were measured using Jacob's staff and facies identification and description were

carried out following Miall's method (Miall, 1977, 1985). The stratigraphic columns were plotted using the package of R: Stratigraphic Data Analysis (SDAR) (Ortiz & Jaramillo, 2018). The petrographic compositional analyses were carried out following the Gazzi-Dickinson method (Dickinson, 1985); we counted at least 300 points in each sample, including framework, matrix and cement. For the metamorphic lithics, a textural classification was made according to Garzanti and Vezzoli (2003) and the categories proposed therein, detailed data are presented in Table S1. Eight conglomerate counts were performed, following the ribbon counting method (Howard, 1993).

3.2 | U–Pb zircon geochronology

Fifteen detrital zircon U–Pb geochronological analyses were performed. Zircon grains were separated from sandstones using standard techniques. A random selection of zircons from each sample was analyzed using laser ablation inductively coupled plasma mass spectrometry (LA-ICP-MS) at Washington State University and following the standard procedures presented in Chang et al. (2006). The $^{206}\text{Pb}/^{207}\text{Pb}$ zircon age is reported for all grains older than 1500 Ma, while for younger grains, the $^{206}\text{Pb}/^{238}\text{U}$ age is reported (Spencer et al., 2016). Kernel Density Estimation (KDE) was obtained using the software DensityPlotter (Vermeesch, 2012). Two different maximum depositional ages (MDA) were calculated for each sample using the youngest single grain (YSG) and the weighted average age from two or three youngest zircons that overlap at 2 sigmas (Y2Z and Y3Z) (Coutts et al., 2019; Gehrels, 2012). Zircon ages older than 250 Ma and with discordance >30% were not considered. Complete single-grain zircon data are fully available in the Geochron database and Table S2.

To compare and visualize the similarities between the zircon age distributions from the Miocene strata and several basements of the Northern Andes, we used the software Isoplot R (Vermeesch, 2018a) to implement a multi-dimensional scaling (MDS) method, which uses the Kolmogorov–Smirnov (KS) statistics. The MDS method creates a map where the Euclidian distances between the samples are proportional to their disparities (Vermeesch, 2013, 2018b).

3.3 | Low-temperature thermochronological methods

The apatite fission-track (AFT) method is based on the quantification of damage (tracks) caused by the spontaneous fission of ^{238}U to the apatite crystal lattice. Between ca. 60 and 120°C, these tracks are partially annealed:

TABLE 1 Samples localization.

Sample ID	Longitude (°)	Latitude (°)	Elevation (m.a.s.l.)	Petrography	Zircon U-Pb	AHe	AFT	Unit
21158Bz	-74.7523	4.3236	305		x			Honda Group
21159Bz	-74.7523	4.3236	305	x				Honda Group
34001Cy	-75.1622	3.8090	409	x				Honda Group
34002Cy	-75.1752	3.8012	416	x				Honda Group
21144To	-74.6484	4.4231	364	x				Honda Group
JC-T001	-74.6024	5.4888	270	x				Honda Group
JC-T004	-74.5981	5.4295	465	x				Honda Group
JCM-T007	-74.6034	5.4799	336	x				Honda Group
JC-T007	-74.6052	5.4943	228	x				Honda Group
JC-T008	-74.5992	5.4479	508	x				Honda Group
JC-M009	-74.6024	5.4888	270		x			Honda Group
JC-M012	-74.6011	5.4654	438	x				Honda Group
JC-M015	-74.5978	5.4441	498	x				Honda Group
JC-M017	-74.6961	5.1943	279	x				Honda Group
JC-M018	-74.7002	5.1902	274	x				Honda Group
JC-M019	-74.7084	5.1894	309	x	x			Honda Group
JC-M020	-74.7127	5.1889	265	x				Honda Group
JC-M022	-74.7166	5.1926	227	x				Honda Group
JC-M023	-74.7186	5.1984	234	x				Honda Group
JC-M024	-74.7239	5.2023	234	x				Honda Group
JC-M025	-74.7263	5.2028	256	x				Honda Group
19033Ro	-75.1479	4.1230	554		x			Rovira Formation
19043Ro	-75.2410	4.2197	854	x				Rovira Formation
19048Ro	-75.2532	4.2244	909		x			Rovira Formation
20112Ro	-75.2411	4.2483	890	x				Rovira Formation
20113Ro	-75.2411	4.2483	890	x				Rovira Formation
20114Ro	-75.2404	4.2484	897	x				Rovira Formation
20116Ro	-75.2401	4.2485	910	x				Rovira Formation
20118Ro	-75.2401	4.2486	912	x				Rovira Formation
20120Ro	-75.2366	4.2493	889	x				Rovira Formation
20121Ro	-75.2350	4.2486	912	x				Rovira Formation
20125Ro	-75.2426	4.2488	897	x				Rovira Formation
20122Ro	-75.2364	4.2503	902		x			Rovira Formation
21162Cp	-75.5064	3.8599	1057	x				Rovira Formation
21166Cp	-75.5055	3.8557	1011		x			Rovira Formation
21167Cp	-75.5055	3.8557	1011	x				Rovira Formation
21169Cp	-75.5035	3.8535	1002	x				Rovira Formation
21170Cp	-75.5035	3.8535	1002		x			Rovira Formation
19036Bz	-74.7947	4.3605	330		x			Barzalosa Formation
19037Bz	-74.7947	4.3605	330	x				Barzalosa Formation
19038Bz	-74.7967	4.3526	329	x				Barzalosa Formation
20133Bz	-74.7978	4.3649	354	x				Barzalosa Formation
20134Bz	-74.7960	4.3627	345	x				Barzalosa Formation

(Continues)

TABLE 1 (Continued)

Sample ID	Longitude (°)	Latitude (°)	Elevation (m.a.s.l.)	Petrography	Zircon			Unit
					U-Pb	AHe	AFT	
20135Bz	-74.7953	4.3609	345	x				Barzalosa Formation
20137Bz	-74.7969	4.3557	342	x				Barzalosa Formation
20138Bz	-74.7931	4.3554	325	x				Barzalosa Formation
21141Bz	-74.7953	4.3575	331	x				Barzalosa Formation
21143Bz	-74.7949	4.3561	330		x			Barzalosa Formation
21148Me	-74.6744	4.1938	323		x			Barzalosa Formation
21149Me	-74.6744	4.1938	323	x				Barzalosa Formation
21151Me	-74.6744	4.1938	323	x				Barzalosa Formation
21154Me	-74.6840	4.1957	358	x				Barzalosa Formation
20155Bz	-74.7801	4.3479	315	x				Barzalosa Formation
21156Me	-74.6840	4.1957	358		x			Barzalosa Formation
JC-M002	-74.6228	5.4989	227	x				Santa Teresa Formation
JC-M003	-74.6194	5.4989	219		x			Santa Teresa Formation
JC-M007	-74.6100	5.4983	218	x				Santa Teresa Formation
21147Me	-74.6744	4.1938	323		x			Eocene strata
20130Bz	-74.8042	4.3683	468		x			Cretaceous strata
19042Ro	-75.2410	4.2197	854			x		Jurassic plutonic rocks
19046Ro	-75.2277	4.1965	1424			x		Permian plutonic rocks
19052Lu	-75.2535	4.2449	999			x	x	Permian plutonic rocks
19054Lu	-75.3187	4.2486	1399			x	x	Permian plutonic rocks
19056Lu	-75.3375	4.2531	1740			x	x	Permian plutonic rocks
19058Lu	-75.3383	4.2552	1799			x		Permian plutonic rocks
20140Cp	-75.5575	3.7887	1299			x	x	Jurassic plutonic rocks
20142Cp	-75.5619	3.8123	1665			x	x	Jurassic plutonic rocks
20148Cp	-75.5979	3.8454	1982			x	x	Jurassic plutonic rocks
20150Cp	-75.6276	3.8596	1754			x	x	Jurassic plutonic rocks
20152Cp	-75.6889	3.8889	1865			x	x	Jurassic plutonic rocks

a temperature interval defined as the apatite partial annealing zone (APAZ) (Wagner et al., 1989). The detailed procedures for etching, Dpar measurements and sample preparation are presented in Text S1 (Dunkl, 2002; Galbraith & Laslett, 1993; Green, 1981). Analyses were carried out using the External Detector Method in the thermochronology laboratory and research centre (CPGeo_LTC) at the University of Sao Paulo, Brazil (USP). Complete single-grain data is presented in the Geochron database and Table S3.

Apatite U-Th-Sm/He thermochronology is based on the production and accumulation of helium that forms from the alpha decay of uranium (U), thorium (Th) and samarium (Sm). In apatites, this method provides information on the thermal history between 40 and 90°C, and this temperature interval is known as the apatite partial retention zone (APRZ) (Farley, 2002). The helium retentivity of the crystal can be affected by the effective

uranium content ($eU = U + 0.235 * Th$), size, geometry and cooling rate (Brown et al., 2013; Flowers, 2009; Guenther et al., 2013; Shuster et al., 2006). The analyses were carried out at the Potsdam University Alphachron laboratory. Detailed procedures are presented by Zhou et al. (2017).

3.4 | Thermal modelling approach and parameters

We performed inverse modelling with the QTQt software (v.5.7.0), which uses a Bayesian transdimensional statistical approach to extract the most probable thermal history from a given dataset (Gallagher, 2012; Gallagher et al., 2009). QTQt finds thermal histories by considering multiple thermochronometers, the natural dispersion of data and the kinetic models of each thermochronometer. We used the radiation damage models from Flowers

et al. (2009) for AHe data and the annealing model of Ketcham et al. (2007) for AFT data. Only U-Th/He single-grain aliquots with reproducible ages or dispersed ages with possible size or eU age controls were included in the models. We consider ages to be reproducible when the 1σ SD is <25% of the mean age (e.g., Flowers et al., 2009; Flowers & Kelley, 2011).

Major basement structures and positive elevation versus age relationship were used to identify blocks with presumably similar thermal histories. Geological constraints and modelling time intervals were fixed according to rock crystallization and thermochronological ages. In all the models, the initial iterations were discarded (burn-in) and the subsequent iterations were used for the inference of the thermal history (Gallagher, 2012). During inverse modelling in QTQt, the coldest and hottest samples represent the rocks assumed to have relatively colder and hotter thermal histories within a rock body. After identifying a coherent basement block, the elevation was used as a proxy for paleodepth, and consequently a proxy for relative past temperatures. Model constraints and parameters are presented in Table S4 and likelihood chains are presented in Figure S1.

4 | RESULTS

4.1 | Stratigraphy of the Miocene units in the Girardot sub-basin in the Upper and Middle Magdalena Basins

4.1.1 | Rovira formation

We described this unit for the first time near the Rovira town, in the Girardot sub-basin (Figure 2a). The Rovira Formation has been previously mapped as part of the Honda Group, but differences in the observed facies were enough to describe this unit separately. The Rovira Formation was described in sections 1–3. This unit constitutes a clastic wedge parallel to the eastern flank of the Southern Central Cordillera. In sections 1 and 2, this unit was observed overlying the Permo-Triassic igneous basement of the Southern Central Cordillera (Figure 2a).

The Rovira Formation is characterized by facies association I (Tables 2 and 3), which is mostly composed of thick beds (1 to 4 m) of massive, parallel laminated and graded sandstones and conglomerates (Sm, Gp and Gm) interbedded with red and grey mudstones and paleosols (Fmr, Fmg and P in Figures 3a–c, and 4a,b). Paleosols are composed of grey and red mudstones (argisols and oxisols) characterized by the absence of sedimentary textures; occasionally, paleosols also exhibit gypsum and carbonate veins

and nodules (Tables 2 and 3). This facies association is characterized by beds that are 1 m to 5 m thick, and some laterally continuous beds (up ca. 50 m) with tabular geometries; occasionally coarse-grained facies are presented in discontinuous beds (channels and splay deposits) that lateral transition to fine-grained facies (Figure 3a). Lateral facies variation is evident in sections 2 and 3: in the west, section 2 is characterized by the prevalence of coarse-grained clastic strata, while in the east (section 3) fine-grained strata are more abundant (Figure 4a). The absence of tractive structures and the presence of massive sandstones and gravels (Gm and Sm) with channel and sheet bed geometries suggest that this unit was deposited by successive confined and unconfined high-density and more diluted flows (Miall, 2014; Zavala et al., 2011) accumulated in a well-developed flood plain characterized by periods of sub-areal exposition.

4.1.2 | Barzalosa and Santa Teresa formations

The Barzalosa Formation was described in sections 5 and 6 in the NE segment of the Girardot sub-basin while the Santa Teresa Formation was described in the lower segment of section 7 (Figures 2a,b, 5, and 6). The Barzalosa Formation unconformably overlies the Cretaceous (section 5) and Eocene (section 6) strata while the lower contact of the Santa Teresa Formation was not observed (Figure 5). In the Barzalosa Formation, three different facies associations were identified (II, III, IV); facies assemblages II and V were described in the Santa Teresa Formation (Tables 2 and 3; Figures 5 and 6). Facies association II is composed of conglomerates and sandstones with trough or cross-stratification and imbrication (Figures 3d, 5, and 6)(Gt, St, Sc and Gi) interbedded with fine-grained red and grey mudstones and paleosols (Fmr, Fmg and P). Coarse-grained rocks are presented in very thick (1 to 2 m) beds with channel geometries while fine-grained facies are in very thick and laterally continuous tabular beds. Facies assemblage III is dominated by red-mottled paleosols (oxisols) and massive sandstones presented in relatively thin (<1 m) beds with channelized geometries (Figures 3e, and 5a,b). Facies association IV is characterized by planar laminated mudstones and sandstones (Sp and Fp) organized in tabular beds that are between 1 cm and 10 cm thick (Figures 3f and 5b). Facies association V contains organic-rich laminated mudstones and siltstones interbedded with massive sandstones and coal beds (Figure 6).

Facies assemblages II, III and IV described above are interpreted as part of the marginal facies of a playa lake or ephemeral lacustrine system (Briere, 2000; Nichols, 2009), where facies assemblage II corresponds to marginal

lacustrine facies characterized by the presence of bedforms deposited by unidirectional currents (Gt, St and Sc); facies assemblages III and IV correspond to inner lake deposits. The fine-grained facies in assemblage III are interpreted as fallout lake deposition and Sm facies are interpreted as lake underflows (Carroll & Bohacs, 1999). The development of paleosols suggests that lake deposits experienced periods of subaerial exposition characteristic of an intermittent water body, which is indicative of a playa lake depositional system (Briere, 2000). The preservation of the lamination and the absence of paleosols in facies assemblage IV suggest times when the water body was more permanent. Paleosol facies interbedded with stagnant water conditions suggest constant submergence and emergence of the lake bottom (Hatano & Yoshida, 2017; Nichols, 2009). In contrast, continuous mud-rich sedimentation and the preservation of organic matter in facies association V are indicative of sediments deposited in an anoxic lake bottom under a permanent water body (Renaut et al., 2010).

4.1.3 | Honda Group

The Honda Group was described in the central and eastern segments of the Girardot sub-basin in the Upper Magdalena Basin (sections 4 and 5, Figure 2a) and the northern Middle Magdalena Basin (section 7, Figure 2b). We observed the Honda Group conformably overlying the Barzalosa and Santa Teresa formations in sections 5 and 7 (Figures 5b and 6). This unit is composed of facies association VI and VII (Tables 2 and 3). Facies association VI is characterized by laterally discontinuous and very thick (1 to 2 m) beds of conglomerates and sandstones with trough stratification (Gt and St) and sandstones with cross lamination (Sc) interbedded with massive sandstones (Sm) presented in thick and very thick (0.5 to 2 m) tabular and laterally continuous beds (Figure 3g,h). These lithofacies are interbedded with tabular beds of red and green mudstones (Fmr and Fmg).

Facies association VII is characterized by a succession of laterally continuous thick beds with fallout ashes (As), tuffaceous sandstones and conglomerates with pumice fragments (Stf) interbedded with massive sandstones and conglomerates (Gm and Sm) (Figure 3i). The two facies assemblages described in the Honda Group are interpreted as part of a fluvial system characterized by abundant tractive bedforms (Gt, Sc, St), overbank deposits (Sm) and a well-developed flood plain (Fmr and Fmg) (Miall, 2014). Facies association VII represents segments of the fluvial systems that were close or proximal to volcanic sources. Similar fluvial depositional environments have been described in the Victoria and Villavieja formations (Honda Group)

in the Upper Magdalena Basin (Anderson et al., 2016; Guerrero, 1993; van der Wiel et al., 1992; Wellman, 1970).

4.2 | Sandstone petrography and conglomerate clast counting

The Rovira Formation comprises sandstones mostly composed of quartz, feldspars and metamorphic lithics while conglomerates are composed of chert, quartz and distinctive plutonic and metamorphic clasts (Figure 7a–c). Sandstones exhibit medium to coarse, rounded and subrounded grains embedded in a mud-rich matrix. Sandstone composition is characterized by 45% to 83% of quartz, followed by 8% to 35% of feldspar (Figure 7b and Table 4). The lithic fraction varies between 7% and 27% and is composed of metamorphic and plutonic lithics (Figure 7c,d). One conglomerate clast count in this unit presents 48% of milky coloured quartz, 22% of chert and 11% of lidites and mudstones, 9% of gneisses, 7% of plutonic rocks and 2% of volcanic fragments (Figure 7a and Table 5).

The Barzalosa and the Santa Teresa formations are characterized by quartz-rich sandstones and conglomerates with abundant sedimentary lithics and clasts (Figure 7a–c). The sandstones are characterized by sub-rounded to rounded grains embedded in a mud-rich matrix with siliceous and ferruginous cement. Compositionally, these sandstones have quartz content varying between 55% and 90%, feldspar content between 1% and 11% and lithics between 3% and 40%, with abundant sedimentary lithics (>50% of the lithic fraction; Figure 7c,e). Two conglomerate clast counts were carried out in the Barzalosa Formation, with both showing a predominance of sedimentary clasts, including chert and lidites (55% and 76%), sandstones (16% and 22%) and 27% of mudstones in one of the counts (Figure 7a). One conglomerate clast count from the Santa Teresa Formation presents 80% of milky coloured quartz, 10% of metamorphic lithic fragments, 9% of chert and lidites and 2% of mudstones (Figure 7a and Table 5).

The Honda Group marks the appearance of a massive volcanic component in the Upper and Middle Magdalena basins, evidenced in volcanic lithics and clasts (Figure 7a–c). Samples correspond to medium to very coarse-grained sandstones characterized by sub-rounded to angular grains and a mud-rich matrix with siliceous cement. These sandstones are characterized by a high content of lithics (16% to 55%) with a predominance of sedimentary and volcanic lithics (Figure 7c,f) and variable amounts of metamorphic fragments (10% to 40%). The quartz content varies between 15% to 50% and feldspar content is between 3% and 21%. One conglomerate clast count was carried out in the Honda Group in the Upper Magdalena Basin, and the results show milky-coloured quartz (48%), volcanic

TABLE 2 Facies description; codes were modified from Miall (1985b).

Code	Description	Interpretation
Gp	Pebble and granule matrix-supported conglomerates with a planar lamination defined by normally graded centimetric sets	Fast deposition of high-density flows
Gi	Pebble and granule class-supported and imbricated conglomerates	Channel fills formed by bedload migration
Gm	Structureless pebble and granule matrix-supported conglomerates	Fast deposition of high-density flows
Gt	Pebble matrix-supported conglomerates with trough stratification	Channel fill formed by 3D bedform migration
Sm	Fine- to coarse-grained structureless sandstones with floating clasts and scour bases	Rapid deposition and aggradation of suspended load during the waning of high-density flows
Sp	Fine- to coarse-grained sandstones with planar bedding with internal normal grading	Rapid deposition of diluted high-energy flows
Sc	Medium- to coarse-grained grey sandstones with well-defined and incipient stratification	Channel fill formed by 2D bedform migration
St	Medium- to coarse-grained sandstones with trough stratification	Development of 3D dunes under unidirectional flows
Stf	Tuffaceous medium- to coarse-grained sandstones	Reworked pyroclastic materials
Fmr	Red mudstones with horizontal lamination organized in tabular beds	Deposition of fine-grained suspended load in oxidant conditions.
Fmg	Dark grey to green mudstones with horizontal lamination organized in tabular beds	Deposition of fine suspended load in reductive conditions.
P	Iron-rich layers of mottled massive red to brownish mudstones (oxisols) and grey massive mudstones (argillisols) with carbonate noodles and occasional gypsum veins	Fine-grained strata exposed to subaerial conditions
C	Metric coal beds characterized by sharp tops and	Flood plains with abundant organic material
As	Fallout ashes	Fallout ashes

lithics (33%), chert and lidites (11%) and sandstones (7%). Three conglomerate clast counts were made in the Middle Magdalena Basin, and they show a predominance of calcareous sedimentary clasts ca. 40%, followed by volcanic (20%), chert (14%), milky-coloured quartz (10%) and metamorphic clasts (8%) (Figure 7a and Table 5).

4.3 | Detrital zircon U–Pb geochronology

We obtained single-grain zircon U–Pb data from fifteen samples from Miocene Rovira, Barzalosa and Honda sedimentary units and the underlying Cretaceous and Eocene

strata. In the Rovira Formation, between 45% and 80% of the zircon grains have Jurassic to Early Cretaceous ages (200 to 120 Ma), with age peaks between ca. 160 and ca. 152 Ma. Four of the samples (19048Ro, 20122Ro, 21166Cp, 21177Cp) have Permo-Triassic zircon populations with age peaks between ca. 269 and ca. 275 Ma (Figure 4); samples from section 1 exhibit Eocene zircon age populations with age peaks around 50 Ma. The maximum depositional ages in this unit are between ca. 150 and ca. 48 Ma (Y3Z) (Table 6).

Single-grain U–Pb zircon ages from the Barzalosa Formation in the Upper Magdalena Basin include data from four samples in sections 5 and 6 and one

TABLE 3 Facies associations.

Facies association	Constituent facies	Description	Interpretation
Facies association I	Gm, Gp, Sm, Sp, Sc, Fmr, Fmg, P	Amalgamated confined and unconfined high-density flows, characterized by lateral facies transition to floodplain deposits with the development of paleosols	Alluvial deposits formed by high energy flows, with minor fluvial reworking deposited adjacent to a well-developed floodplain
Facies association II	Gm, Gt, Gi, St, Sc, Fmg, Fmr, P	Fine-grained sedimentation with the development of paleosols and bedforms deposited by unidirectional currents	Marginal lake conditions characterized by floodplain deposition and unidirectional flows
Facies association III	Sm, P	Fine-grained strata with the development of paleosols and minor confined high-density flows	Profundal fluctuating lake deposits characterized by massive underflows, fall-out deposition and periods of subaerial exposition
Facies association IV	Sp, Fp	Tabular thin laminae of horizontally laminated mudstones and massive fine-grained sandstones and siltstones	Lake sedimentation characterized by suspension deposition
Facies association V	Sp, Fp, C	Tabular thin laminae of horizontally laminated black mudstones, rich in organic matter and interbedded with coal beds	Lake sedimentation in anoxic conditions and high-density underflows
Facies association VI	Gt, Sm, Sc, St, Fmg, Fmr, C	Amalgamated 2D and 3D bedforms organized in channelized beds that laterally transition to fine-grained flood plains—large tabular sheet floods	Well-developed fluvial system
Facies association VII	Stf, As, Gm and Sm	Fall-out ash deposition and reworked pyroclastic materials	Volcanic activity coeval with sedimentation

sample from the equivalent Santa Teresa Formation in the Middle Magdalena Basin (section 7, Figures 5 and 6). Sample 19036Bz from section 5 exhibits a single age peak of 80 Ma, which corresponds to ca. 80% of the ages while sample 21143Bz also from section 5 exhibits major age peaks at 1540, 278, 176, 144 and 85 Ma. The Cretaceous strata underlying the Barzalosa Formation in section 5 exhibit ca. 65% of grains older than 400 Ma and younger age peaks at ca. 266, ca. 150 and ca. 72 Ma (Figure 5b and Table 6).

The samples collected in section 6—in the eastern segment of the basin—are characterized by more than 75% of zircon ages older than 900 Ma and minor (<20%) Permo-Triassic and Cretaceous peaks (Figure 5a and Table 6). A sample from the underlying Eocene strata (21147Me) also exhibits more than ca. 75% of zircon grains older than 900 Ma, with minor younger peaks at 158 Ma and 80 Ma (Figure 5a and Table 6). Maximum depositional ages (Y2Z and YSG) from the Barzalosa Formation are between 140 Ma and 57 Ma. Sample JC-M003 from the Santa Teresa Formation (section 7) exhibits major age peaks at 1490, 155, 83 and 58 Ma (Figure 6 and Table 6).

Three samples from the Honda Group in the Upper and Middle Magdalena basins were analyzed (21158Bz, JC-M019; JC-M009), these exhibit a high percentage (>34%) of zircons with ages between ca. 5 and 40 Ma; the minor age populations have peaks around 75, 150, 235 and 560 Ma. This unit exhibits maximum depositional ages between ca. 15 and 9 Ma (Y3Z). A positive correlation between the stratigraphic position and the MDA values was observed in section 7 (Figure 6 and Table 6).

4.4 | Low-temperature thermochronology analytical and modelling

We obtained AFT and AHe data from eleven samples collected at elevations between 1 and 2 km a.s.l. along two NW–SE transects in the eastern flank of the Southern Central Cordillera (Figure 2a). Given that sample locations are separated by several faults and exhibit contrasting thermochronological age patterns, the transects were divided into several coherent structural blocks (A1, A2, B1, B2 and B3 in Figure 8a).

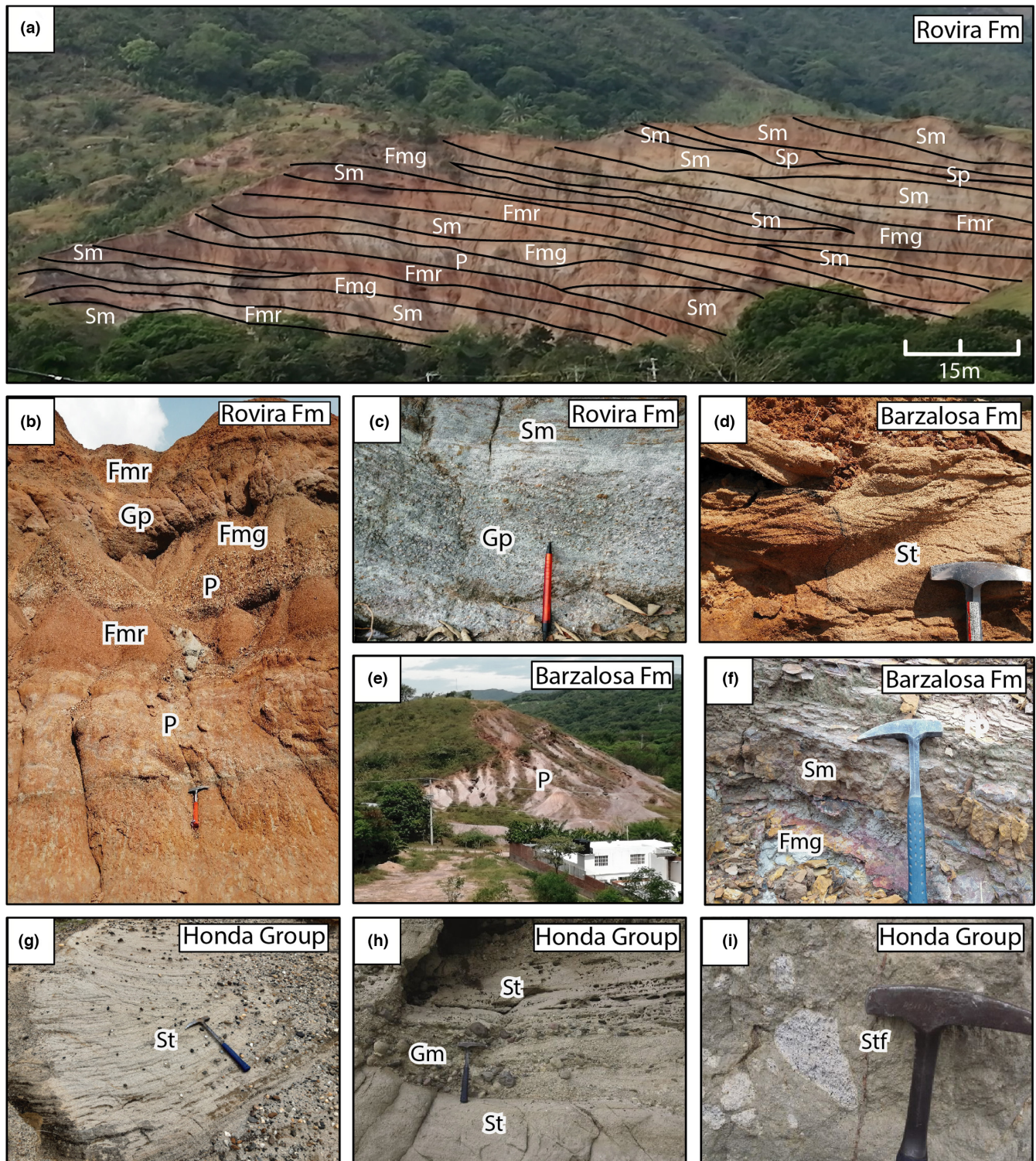


FIGURE 3 (a) Panoramic view of section 2 (Rovira Formation) white letters denote the sedimentary facies described in Table 2. (b) Interbedded pebbly conglomerates (Gp), red mudstones (Fmr) and Paleosols (P). (c) Massive sandstones (Sm) and pebbly conglomerates with planar stratification (Gp). (d) Medium-grained sandstones with trough stratification. (e) Thick paleosol from the Barzalosa Formation. (f) Black mudstones with parallel lamination (Fp), interbedded with massive sandstones (Sm) and massive grey mudstones (Fmg). (g) Sandstones with trough stratification (St). (h) Interbedded cobble conglomerates (Gm) and sandstones with trough stratification (St) in the Honda Group. (i) Tuffaceous sandstones with pyroclastic fragments (Stf).

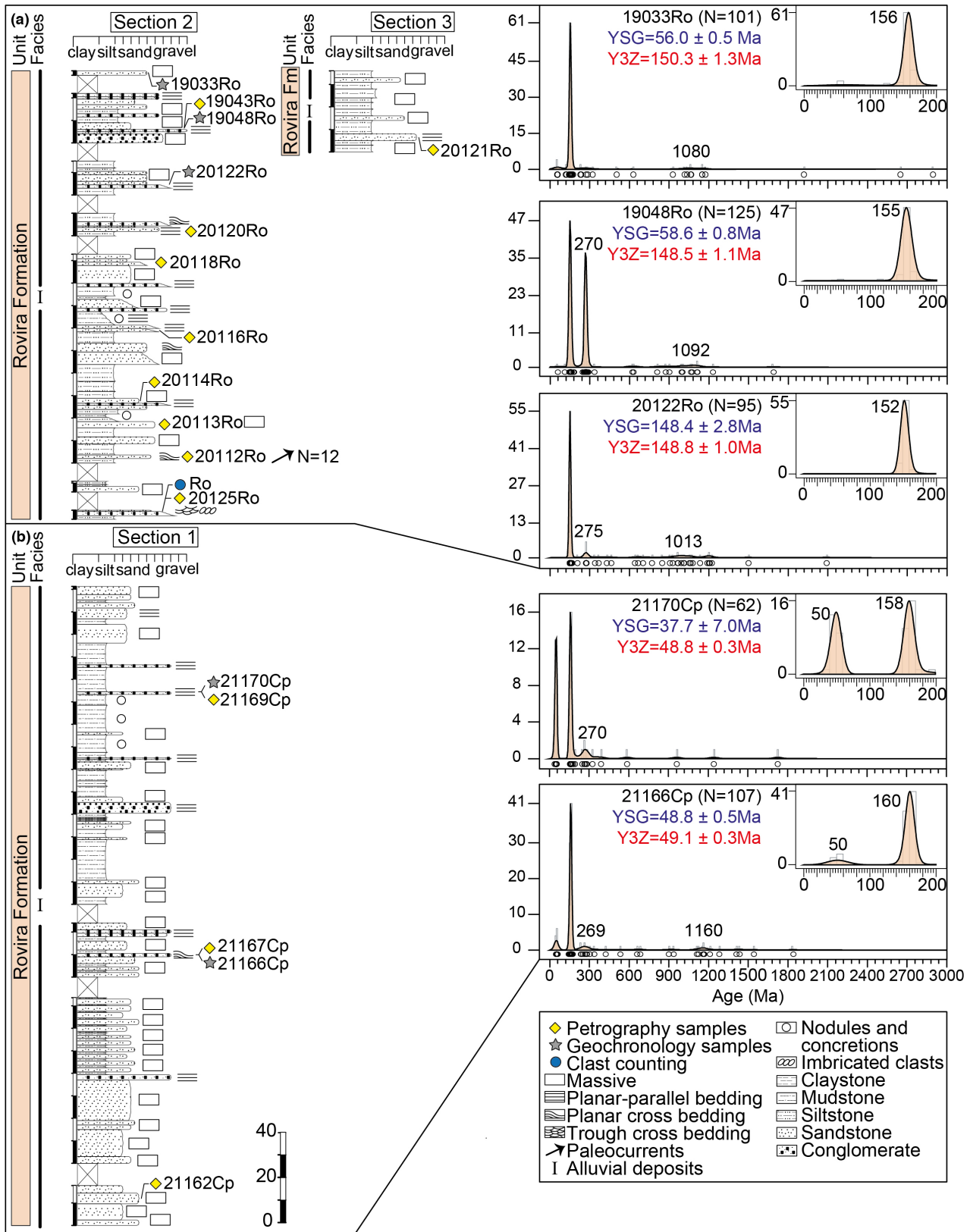


FIGURE 4 Stratigraphic sections from the Rovira Formation with the stratigraphic position of the petrography samples (yellow rhombus), geochronology (grey stars) and clast counting (blue dots) data. Zircon U-Pb data is presented in the right panel. YSG: youngest zircon grain, Y2Z: weighted average of the youngest two grains and Y3Z: weighted average of the youngest three grains. The locations of the stratigraphic sections are presented in Figure 2.

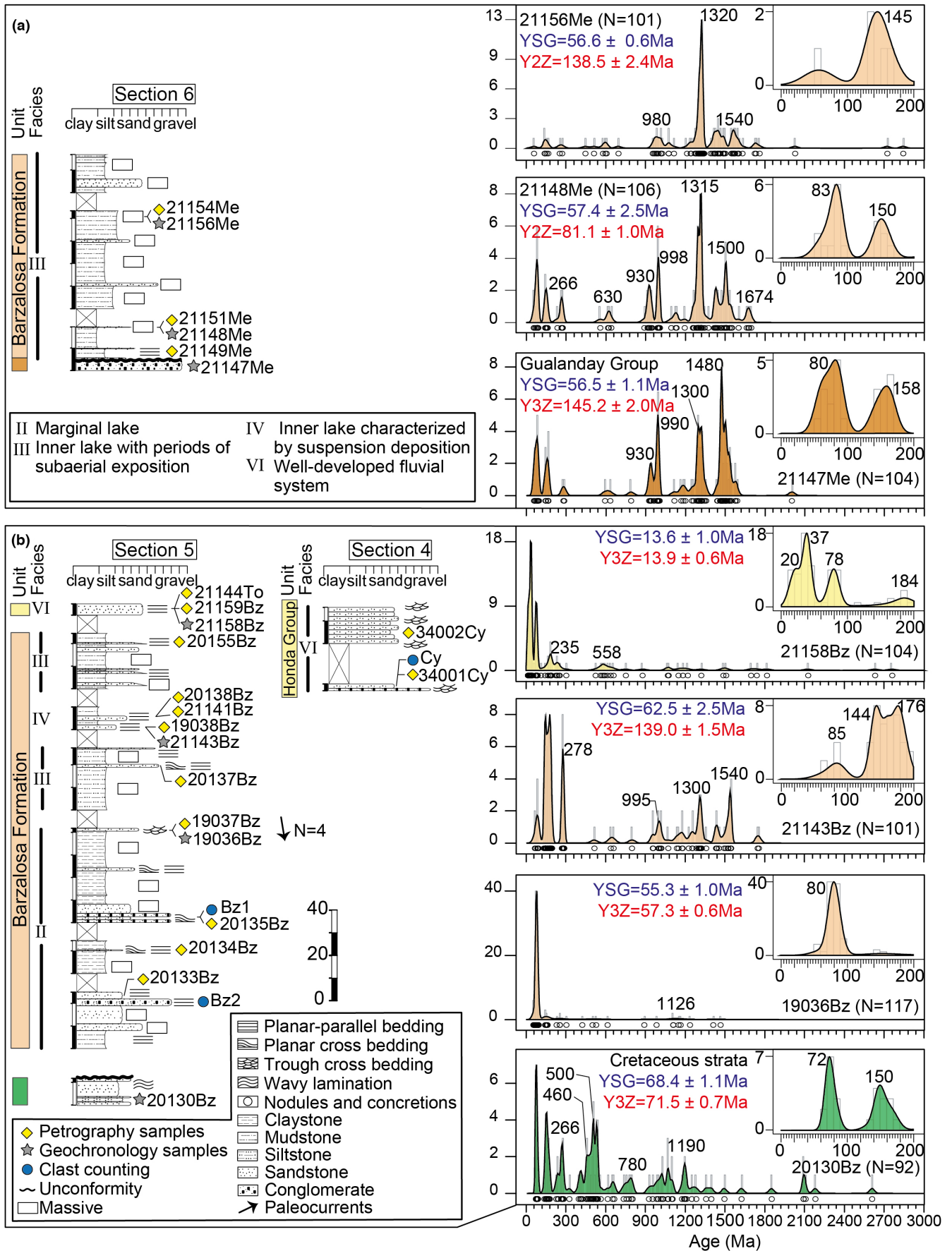


FIGURE 5 Stratigraphic sections from the Barzalosa Formation and the Honda Group; for a detailed caption, see Figure 4.

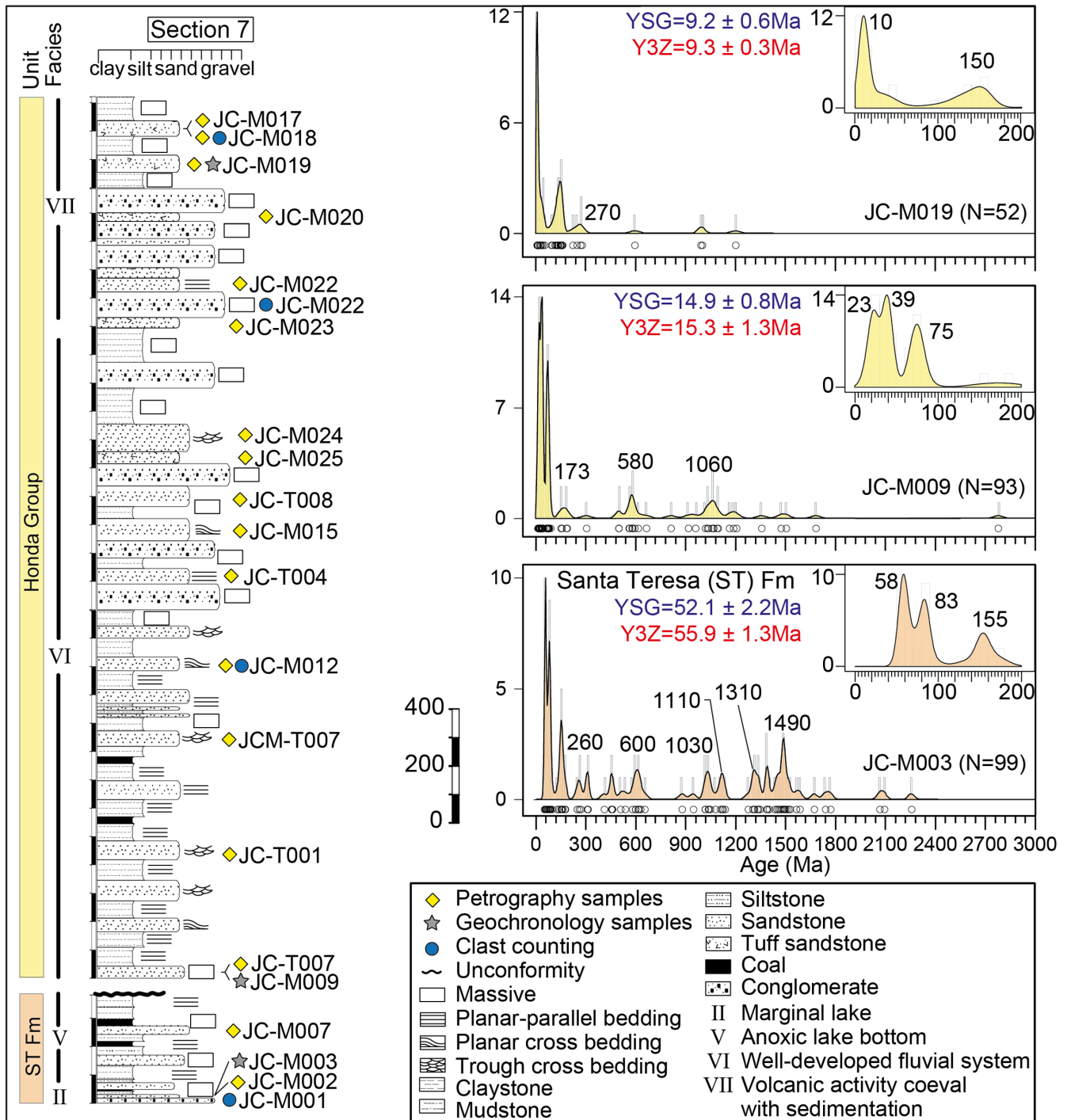


FIGURE 6 Stratigraphic sections from the Honda Group in Middle Magdalena Basin; for a detailed caption, see Figure 4. ST, Santa Teresa Formation.

The northern transect (A-A') includes data from the Permo-Triassic igneous basement of the Central Cordillera (A1) and Jurassic plutonic rocks from an intra-basin high (A2) (Figure 8a). Four samples were collected within block A1. The three lower samples have AFT ages between ca. 19 and ca. 59 Ma, which exhibit a weak positive correlation between age and elevation (Figure 8a). Transect A1 includes eighteen aliquots from four samples that exhibit

AHe ages between ca. 4.1 and 31.8 Ma. Thirteen aliquots with intra-sample reproducibility and ages between 4 and 7 Ma were included in the model; two aliquots with older ages (ca. 11 and 16 Ma) and relatively high eU and/or grain size values were also included (Table 7; Figure 8b). The multi-sample thermal history model from block A1 exhibits slow cooling after 15 Ma (hot sample); followed by accelerated cooling starting at 6 Ma. This model reproduces

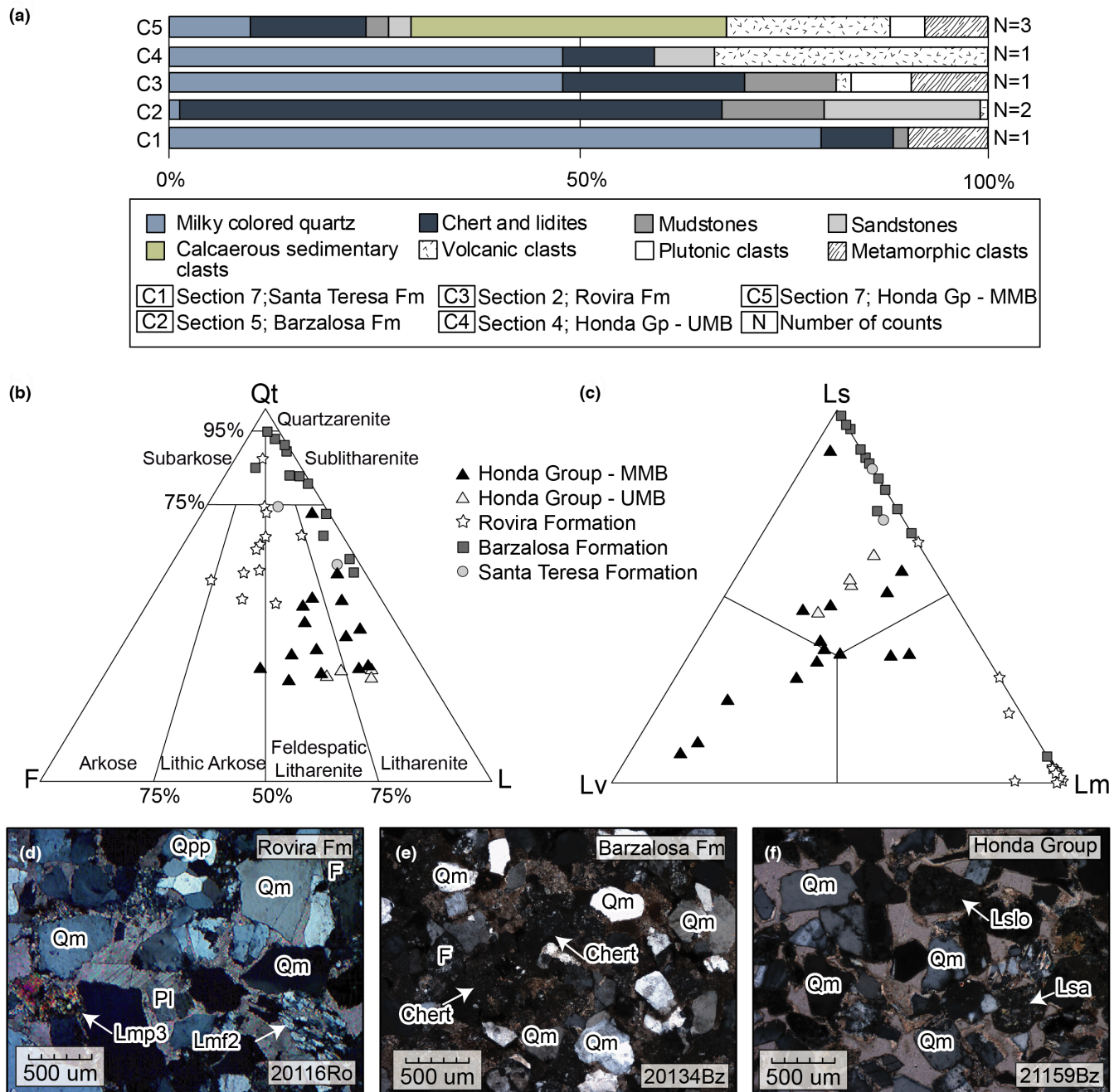


FIGURE 7 (a) Combined clast counting results, N# indicates the number of counting stations. (b) Sandstone classification diagram from Folk (1980) Qt: total quartz, F: total feldspar, L: total lithics. (c) Lithics abundance diagram; Lv: volcanic lithics, Ls: sedimentary lithics and Lm: metamorphic lithics. (d–f) Thin section photographs with cross Nichols; Qm: monocrystalline quartz, Pl: plagioclase, F: feldspar, Lsa: sandstone lithic fragment, Lslo: mudstone lithic fragment, Lmp3: Micaceous schist lithic fragment; Lmf2: Quartz-sericite lithic fragment with strong cleavage. MMB, middle Magdalena Basin; UMB, upper Magdalena Basin.

most of the observed AHe ages and predicts AFT ages that exhibit discrepancies up to 10 Ma with respect to the observed data (Figure 9).

Block A2 contains samples 19042Ro and 19046Ro, which have AHe single grain ages between ca. 2.9 and ca. 8.0 Ma and are characterized by a slightly positive intra-sample correlation between age and eU (Figure 8b and Table 7), all aliquots were included in the model. The

thermal history model from segment A2 suggests a cooling event of at least 50°C after 16 Ma. The model reproduced all the observed AHe ages and the positive relationship between age and eU (Figure 9).

Transect B-B' was divided into three different structural blocks. Block B1 includes the samples 20152Cp and 20150Cp, which have AFT ages of 23.8 ± 6.0 and 15.9 ± 1.7 Ma, respectively (Table 8). These AFT ages

TABLE 4 Summary of the petrographic analyses. Detailed data is presented in Table S1.

Unit	Sample	Quartz (%)				Feldspar (%)				Metamorphic lithics (%)	Volcanic lithics (%)	Sedimentary lithics (%)	Accessory minerals (%)
		Qm	Qpf	Qpp	Qpd	Pl	Fk	F	F				
Honda Group	21159Bz	22.1	0.3	0.7	5.7	10.4	0.0	7.7	13.4	6.0	30.2	3.4	
	34001Cy	21.1	1.0	1.7	3.0	16.2	0.0	4.6	9.2	16.2	21.5	5.6	
	34002Cy	21.0	0.0	1.0	4.9	8.1	0.0	3.6	14.6	11.3	29.1	6.5	
	21144To	21.1	0.3	0.6	4.9	7.1	0.0	4.5	14.0	11.4	27.3	8.8	
	JC-M007	45.2	5.7	0.0	0.0	4.2	0.3	0.0	7.8	2.4	22.3	12.0	
	JC-T001	22.8	1.3	0.0	0.0	5.8	0.0	3.7	9.9	19.4	13.9	23.3	
	JC-T007	34.2	2.7	0.0	0.0	3.0	0.0	0.0	8.5	3.8	12.0	35.8	
	JC-M012	22.0	3.4	0.0	0.0	8.6	1.7	0.0	10.5	5.4	16.1	32.3	
	JC-T004	22.0	0.0	0.0	0.0	4.1	0.0	0.0	10.4	17.9	13.2	32.4	
	JC-M015	23.0	1.6	0.6	0.0	5.7	2.2	0.0	8.2	14.2	9.1	35.5	
	JC-T008	25.6	2.6	0.0	0.0	7.7	1.4	0.0	14.5	10.5	10.8	27.0	
	JC-M025	30.9	3.4	0.0	0.0	11.6	3.4	0.0	9.7	8.4	6.9	25.6	
	JC-M024	33.3	3.2	0.0	0.0	7.2	2.9	0.0	6.6	13.2	12.6	21.0	
	JC-M023	21.2	0.0	0.0	0.0	6.4	3.8	0.0	7.8	11.9	15.7	33.1	
	JC-M022	34.2	1.6	0.0	0.0	5.8	1.9	0.0	9.6	11.2	10.2	25.6	
	JC-M020	28.3	1.8	0.0	0.0	12.8	2.8	0.0	5.4	11.2	5.6	32.1	
	JC-M019	21.0	2.0	0.0	0.0	7.5	7.8	0.0	2.9	21.6	2.0	35.3	
JC-M018	16.4	1.5	0.0	0.0	11.4	2.6	0.0	3.5	21.6	2.9	40.1		
JC-M017	15.0	0.0	0.0	0.0	16.6	0.8	0.0	2.4	10.5	3.5	51.2		
Rovira Formation	19043Ro	44.2	0.7	9.9	18.2	5.3	1.0	6.3	11.9	1.3	0.0	1.3	
	20125Ro	30.7	2.1	10.3	15.5	21.3	0.6	0.0	15.5	0.0	0.0	4.0	
	20112Ro	36.3	1.2	8.4	10.2	19.9	0.9	0.0	14.9	0.0	0.6	7.5	
	20113Ro	16.6	3.0	5.0	28.5	23.5	4.6	6.6	10.9	0.0	0.0	1.3	
	20114Ro	30.6	3.7	6.2	21.6	11.4	4.0	4.6	15.7	0.9	0.0	1.2	
	20116Ro	29.6	1.6	3.6	19.7	14.1	3.6	3.9	19.7	0.3	0.0	3.6	
	20118Ro	30.9	0.0	3.0	11.5	12.5	3.9	11.8	18.8	0.0	0.7	6.9	
	20120Ro	21.2	1.0	6.8	16.7	8.0	5.1	9.6	26.7	0.0	0.3	4.5	
	20121Ro	30.0	1.3	5.9	17.8	4.6	2.3	19.5	17.2	0.0	0.0	1.3	
	21162Cp	71.5	0.3	0.3	11.3	0.0	0.0	7.9	2.3	0.0	4.3	2.0	
	21167Cp	32.7	1.0	0.7	28.7	6.3	0.0	3.3	18.0	0.0	7.3	2.0	
	21169Cp	42.2	0.7	2.3	25.1	5.0	0.0	7.9	10.9	0.3	2.6	3.0	

TABLE 4 (Continued)

Unit	Sample	Quartz (%)				Feldspar (%)			Metamorphic lithics (%)	Volcanic lithics (%)	Sedimentary lithics (%)	Accessory minerals (%)
		Qm	Qpf	Qpp	Qpd	Pl	Fk	F				
Barzalosa Formation	20133Bz	85.4	0.0	2.7	2.7	0.7	1.7	0.0	1.3	0.0	5.0	0.7
	20134Bz	52.1	1.9	7.0	11.8	0.0	1.9	0.3	3.2	0.6	10.9	10.2
	20135Bz	76.3	0.0	1.5	1.5	0.0	1.2	0.0	5.1	0.0	14.4	0.0
	19037Bz	70.2	0.0	1.6	7.9	3.2	0.3	6.7	1.0	0.0	4.4	4.8
	20137Bz	76.3	0.0	5.0	7.7	0.0	0.0	1.0	1.3	0.0	8.7	0.0
	20138Bz	80.0	0.0	1.7	2.7	0.0	2.3	0.0	0.3	0.0	3.0	10.0
	19038Bz	55.5	0.0	5.7	13.0	0.0	0.0	0.8	7.4	0.0	0.6	17.0
	20155Bz	62.0	0.0	6.3	6.0	0.0	3.7	0.0	4.3	0.0	9.0	8.7
	21141Bz	50.2	0.3	0.3	4.3	0.0	0.0	2.3	1.7	0.0	39.9	1.0
	21149Me	50.2	0.3	0.3	6.6	0.7	0.0	1.0	2.0	0.0	36.1	3.0
21151Me	60.8	1.0	0.3	6.4	0.3	0.0	1.3	0.6	0.0	26.4	2.9	
21154Me	59.2	0.3	0.0	3.3	0.3	0.0	3.9	4.3	0.0	25.0	3.6	
Santa Teresa Formation	JC-M002	58.1	3.2	0.0	0.0	6.5	1.8	0.0	2.1	0.0	10.9	17.4
	JC-T007	52.3	2.6	1.5	0.0	7.3	0.0	3.2	0.9	1.5	16.7	14.0

Note: Qm: monocrystalline quartz; Qpf: foliated polycrystalline quartz; Qpp: Polygonal polycrystalline quartz; Qpd: diffuse polycrystalline quartz; Pl: plagioclase; Fk: potassium feldspar; F: undifferentiated feldspar.

TABLE 5 Clast counting results.

Station code	Section 2	Section 5		Section 4	Section 7			
	Ro	Bz1	Bz2	Cy	JC-M001	JC-M012	JC-M022	JC-M018
Milky colored quartz	52	1	2	52	90	10	33	27
Chert and lidites	24	88	55	12	10		42	24
Mudstones	12	0	27	0	2	1	11	7
Sandstones	0	25	16	8			3	10
Calcareous sedimentary						90		
Volcanic	2	2	0	36			15	79
Plutonic	8						9	10
Metamorphic	10				11		28	8
Total	108	116	100	108	113	101	141	165

exhibit a positive correlation with elevation. AHe data from block B1 include single grain ages between ca. 1.5 and ca. 10.3 Ma that exhibit a negative correlation between age and elevation (Figure 8a). The thermal history model from this block suggests slow cooling between ca. 21 and 12 Ma, followed by a final phase of rapid cooling around 3 Ma (Figure 9). The model predicts most of the observed AHe and AFT data, including the negative correlation between AHe ages and elevation and the positive correlation between AFT ages and elevation. This negative correlation is explained by the relatively low eU values of the grains from the upper sample (Figure 8b), which facilitated full resetting during reheating (Flowers, 2009; Flowers et al., 2009).

Sample 20148Cp was collected in the structural block B2, it has an AFT age of 42.3 ± 6.7 Ma and three single grain AHe ages between ca. 5.3 and ca. 9.9 Ma — the two older and reproducible aliquots were included in the model. The thermal history model exhibits continuous cooling after ca. 15 Ma. Two samples from the structural block B3 exhibit overlapping ca. 70 Ma AFT ages (Table 8) and eight AHe single grain ages between ca. 12 and ca. 45 Ma. Data from four aliquots with reproducible ages between ca. 11 and ca. 16 Ma and one aliquot with a relatively older age and a high ESR value were included in the model (Figure 8b). The inverse thermal history model suggests continuous cooling after ca. 16 Ma, this model reproduces most of the observed data, including the positive relationship between age and grain size (Figure 9).

5 | DISCUSSION

We present a source-to-sink analysis of the Girardot sub-basin in the Upper Magdalena Basin and one section from the Middle Magdalena Basin integrated with published data to present a paleogeographic model of the Miocene

hinterland and foreland regions in the Northern Andes. Our results present a case study of how the strike slip-tectonics was responsible for active deformation in the hinterland region and a dynamic drainage network in the Northern Andes, a tectonic scenario that promoted the development of permeable and discontinuous orographic barriers, and modified the northwestern border of the Pebas system.

5.1 | Facies distribution, provenance and age of the Miocene units in the Girardot sub-basin

We identified three Miocene sedimentary successions in the Upper Magdalena Basin Girardot sub-basin and two in the southern Middle Magdalena Basin. Our results add a new stratigraphic unit—the Rovira Formation—to the Miocene stratigraphic record of the Girardot sub-basin that previously only included the Barzalosa Formation and Honda Group. The Rovira Formation was mapped as part of the Middle to Upper Miocene Honda Group, but, as we show in this section provenance and stratigraphic data suggest that this unit is older than the Honda Group and was likely deposited during the Early Miocene.

The present study integrates petrographic and zircon geochronological data from the Upper and Middle Magdalena basins—2022 zircon grains and 65 petrography samples in total (Figures 10) (Anderson et al., 2016; Echeverri et al., 2015; Lara et al., 2018; Montes et al., 2021). The compilation shows that Middle to Upper Miocene sedimentary rocks from the Honda Group exhibit a significant volcanic provenance component, as evidenced by the presence of lithic fragments (>25%) that include abundant volcanic lithics (>10%) (Figure 10a), volcanic clasts (ca. 10% to ca. 30%) and zircons younger than 40 Ma (>30%) (Figures 7 and 10b). These observations are consistent

TABLE 6 Summary of the geochronology results; single grain U–Pb ages are presented in Table S2.

Unit	Sample ID	n	YSG			Y3Z/Y2Z			Ages (%)				
			Age (Ma)	2 σ Abs error (Ma)	Age (Ma)	2 σ Abs error (Ma)	Age (Ma)	2 σ Abs error (Ma)	0–40 Ma (%)	40–120 Ma (%)	120–200 Ma (%)	200–400 Ma (%)	400–900 Ma (%)
Honda Group	JC-M019	52	9.2	0.6	9.3	0.3	46.2	13.5	25.0	7.7	1.9	5.8	
	JC-M009	93	14.9	0.8	15.3	1.3	33.3	30.1	4.3	1.1	11.8	19.4	
	21158Bz	104	13.6	1.0	13.9	0.6	33.7	29.8	8.7	5.8	9.6	12.5	
Rovira Fm.	19033Ro	101	56.0	0.5	150.3	1.3	0.0	4.0	80.2	3.0	2.0	10.9	
	19048Ro	125	58.6	0.8	148.5	1.1	0.0	1.6	47.2	40.8	3.2	7.2	
	20122Ro	95	148.4	2.8	148.8	1.0	0.0	0.0	69.5	7.4	5.3	17.9	
	21170Cp	62	37.7	7.0	48.8	0.3	1.6	35.5	45.2	11.3	1.6	4.8	
	21166Cp	107	48.8	0.5	49.1	0.3	0.0	9.3	69.2	7.5	1.9	12.1	
Barzalosa Fm.	21143Bz	101	62.5	2.5	139.0	1.5	0.0	5.9	38.6	9.9	4.0	41.6	
	19036Bz	117	55.3	1.0	57.3	0.6	0.0	82.1	5.1	1.7	4.3	6.8	
	21156Me	101	56.6	0.6	138.5	2.4	0.0	1.0	4.0	1.0	3.0	91.1	
	21148Me	106	57.4	2.5	81.1	1.0	0.0	10.4	5.7	3.8	4.7	75.5	
	JC-M003	99	52.1	2.2	55.9	1.3	0.0	26.3	10.1	6.1	14.1	43.4	
Eocene	21147Me	104	56.5	1.1	145.2	2.0	0.0	11.5	6.7	1.9	2.9	76.9	
Cretaceous	20130Bz	92	68.4	1.1	71.5	0.7	0.0	13.0	13.0	8.7	33.7	31.5	

Abbreviations: Y2Z/Y3Z, youngest two/three zircons; YSG, youngest single grain.

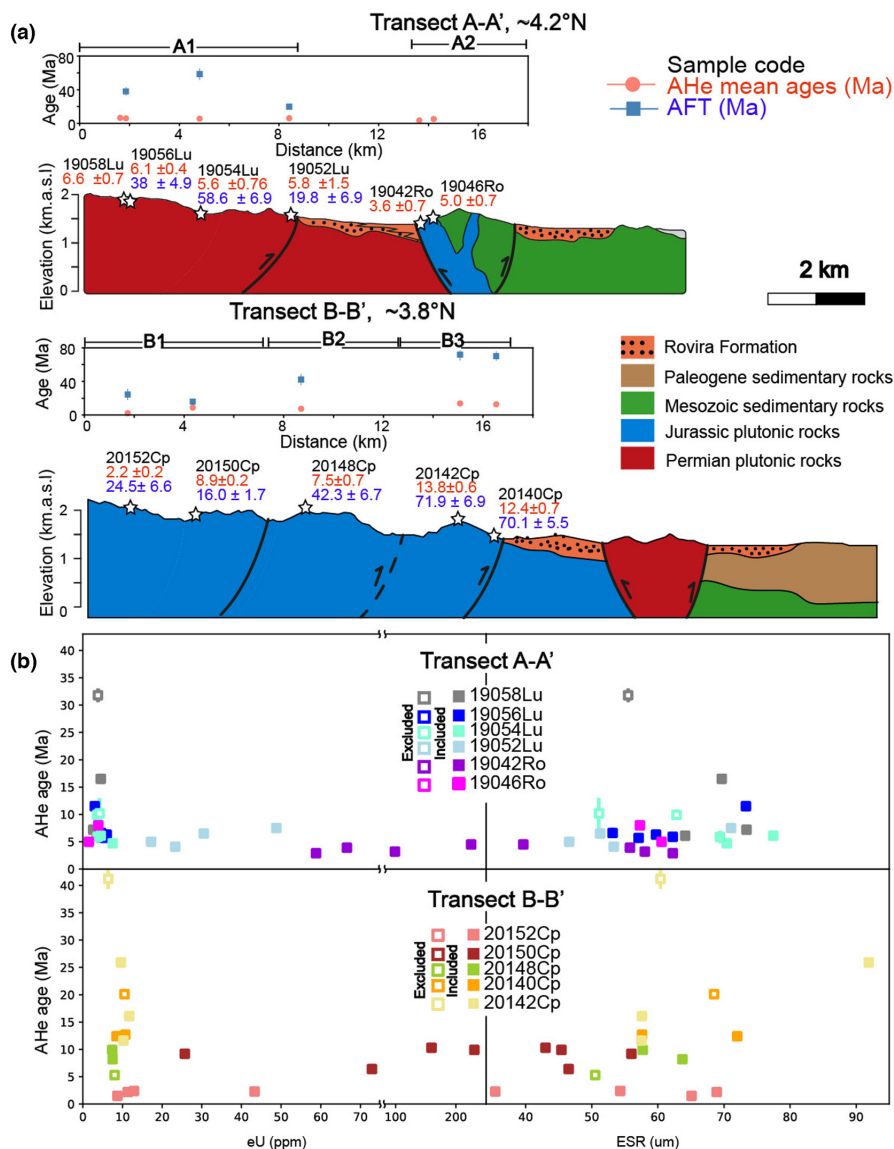


FIGURE 8 (a) Cross-sections and thermochronological data from the Southern Central Cordillera; white stars indicate the sample location. Sample codes and thermochronological ages are presented for each sample. The locations of the geological transects are presented in Figure 2a, cross-sections are separated from each other by ca. 60 km. Older aliquots with higher eU and ERS values were not considered to calculate AHe mean ages (Table 6). (b) Effective uranium (eU) versus age and grain size (equivalent spherical radius: ESR) versus age plots for the two geological transects. Colour code denotes the sample and hollow markers indicate the apatite aliquots excluded from the inverse thermal history models.

with several studies indicating that Upper Eocene to Middle Miocene volcanic sources characterized Middle Miocene to Pliocene strata in the Cauca and Magdalena basins (Anderson et al., 2016; Echeverri et al., 2015; Lara et al., 2018; Montes et al., 2021).

In contrast, despite analyzing over ca. 500 zircon grains from the Rovira Formation, zircon ages younger than 40 Ma were not obtained, similar to the results obtained in the Santa Teresa and the Barzalosa formations (Figures 5, 6, and 10b). The absence of young volcanic zircons explains the results of the multidimensional scaling (MDS) test, where samples from the Rovira Formation plot distant from the Middle Miocene zircon data from the Magdalena and Cauca basins (Figure 10c).

The very low abundance of Eocene to Miocene volcanic sources in zircon age populations in the Rovira Formation is consistent with sandstone petrography and conglomerate clast composition, which are characterized by low percentages of volcanic lithics (<1%) and volcanic

clasts (<10%) (Figures 7a,c, and 10). Furthermore, differences in the sedimentary facies were also observed, as the rocks from the Rovira Formation were deposited in an alluvial system dominated by high-density confined and unconfined flows, while abundant tractive structures in the Honda Group were interpreted as evidence of a well-developed fluvial system that flowed to the east (Anderson et al., 2016; van der Wiel et al., 1992). Provenance and stratigraphic data suggest that the Rovira Formation was deposited prior to the availability of volcanic sources in the Magdalena Basin.

The depositional age of the Rovira Formation remains uncertain, but based on several lines of evidence, we hypothesize that this unit was accumulated at some point between 20 Ma and 16 Ma and is likely a lateral facies variation of the Barzalosa Formation (Figures 11a and 12). The evidence supporting this includes: (1) maximum depositional ages suggest deposition after 50 Ma (Figure 11a); (2) both the Rovira and Barzalosa formations lack a volcanic

TABLE 7 Single-grain Apatite He/(U-Th-Sm) data.

Block	Sample ID-aliquot ^a	Corr. age (Ma) ^b	±2σ (Ma)	U (ppm)	Th (ppm)	Sm (ppm)	eU (ppm)	He (nmol/g)	Mass (ug)	Ft	ESR (μm)	Terminations
A1	19058Lu-1	31.8	1.2	1.8	8.4	15	3.8	0.48	3.3	0.7	52.9	2
	19058Lu-2	6.1	0.7	1.8	7.5	21.4	3.5	0.09	4.5	0.8	61.1	2
	19058Lu-3	7.2	0.6	1.2	5.7	20.2	2.6	0.08	8.2	0.8	72.0	2
	19058Lu-4	16.5	0.8	2.9	6.9	17.6	4.5	0.32	6.4	0.8	68.0	2
	19056Lu-1	6.3	0.6	3.5	10.8	33.7	6	0.2	4.14	0.7	57.4	1
	19056Lu-2	5.9	0.8	2.5	8.5	17.5	4.5	0.1	4.67	0.8	60.1	2
	19056Lu-3	5.7	0.8	3.3	9.3	15	5.5	0.1	3.52	0.7	54.6	2
	19056Lu-4	11.5	0.9	1.7	5.8	30.8	3	0.2	7.86	0.8	71.9	2
	19056Lu-5	6.6	0.9	2.7	7.8	25.7	4.6	0.1	2.81	0.7	50.4	2
	19054Lu-1	9.9	1	2	6.8	24.1	3.6	0.2	4.88	0.8	60.7	1
	19054Lu-2	6.1	0.4	2.6	7.8	27.5	4.5	0.1	11.56	0.8	76.3	2
	19054Lu-3	4.7	0.3	5.1	10	13.6	7.5	0.2	7.3	0.8	68.8	2
	19054Lu-4	10.2	2.7	2.2	8.2	33.8	4.2	0.2	3.07	0.7	48.2	2
	19054Lu-5	5.9	1.1	2	7.3	26.2	3.7	0.1	7.19	0.8	67.7	2
	19052Lu-1	5	0.5	11.2	25.4	14.2	17.2	0.3	1.7	0.7	43.4	2
19052Lu-2	4.1	0.3	17.8	23.3	15.1	23.3	0.4	2.83	0.7	50.6	2	
19052Lu-3	6.5	0.5	22.7	32.9	14.9	30.5	0.7	2.57	0.7	48.4	2	
19052Lu-4	7.5	0.3	31.4	74	29.2	48.8	1.6	6.89	0.8	69.5	1	
A2	19042Ro-a1	2.9	0.1	7.7	217.7	72.1	58.8	0.8	4.62	0.85	60.1	1
	19042Ro-a2	3.9	0.1	14.4	222.3	83.5	66.6	1.1	3.35	0.76	53.2	2
	19042Ro-a3	3.2	0.1	6.7	392.7	43.6	99.0	1.3	3.4	0.7	55.6	2
	19042Ro-a4	4.5	0.2	62.5	692.7	179.2	225.3	3.8	1.2	0.7	36.0	1
	19046Ro-a1	8.0	0.6	2.3	6.9	26.6	6.3	0.1	4.2	0.7	84.5	2
	19046Ro-a4	5.0	0.7	1.0	1.9	5.1	1.5	0.0	14.1	0.7	58.3	2

(Continues)

TABLE 7 (Continued)

Block	Sample ID-aliquot ^a	Corr. age (Ma) ^b	$\pm 2\sigma$ (Ma)	U (ppm)	Th (ppm)	Sm (ppm)	eU (ppm)	He (nmol/g)	Mass (ug)	Ft	ESR (μm)	Terminations	
B1	20152Cp-1	2.2	0.1	7.2	17.4	10.6	11.3	0.1	6.7	0.8	68.9	1	
	20152Cp-2	1.5	0.2	4.9	16.1	12.3	8.7	0.1	5.9	0.8	65.1	0	
	20152Cp-3	2.3	0.2	24.7	79.2	34.8	43.3	0.4	1.18	0.7	35.4	2	
	20152Cp-4	2.4	0.3	7.1	24.5	11	12.9	0.1	3.27	0.8	54.3	1	
	20150Cp-1	9.9	0.1	156.6	314.5	34.2	231	9.4	2.61	0.8	45.4	1	
	20150Cp-2	9.2	0.2	12.9	54.3	23.5	25.7	1	3.82	0.8	56.0	2	
	20150Cp-3	6.4	0.2	46	114.3	10.7	72.9	1.8	2.41	0.7	46.5	2	
	20150Cp-4	10.3	0.2	103.3	239.5	25.8	160	6.6	1.89	0.7	43.0	1	
	B2	20148Cp-1	5.3	0.4	4.2	16.1	27.4	8	0.2	2.8	0.8	50.5	2
		20148Cp-3	9.9	0.7	3.9	14.7	27.4	7.4	0.3	4	0.7	57.7	1
20148Cp-4		8.2	0.5	4.4	13.1	21.9	7.5	0.2	5.6	0.7	63.7	2	
20140Cp-1		12.4	0.3	7.8	2.8	12.4	8.5	0.5	8.2	0.8	72.0	2	
B3	20140Cp-2	20.1	0.4	10.2	1.3	12.4	10.5	0.9	6.8	0.8	68.5	2	
	20140Cp-3	12.7	0.5	9.2	6.2	11.5	10.7	0.6	4.1	0.8	57.6	2	
	20142Cp-1	11.6	0.4	4.9	22.2	26.2	10.2	0.5	4.7	0.8	57.5	2	
	20142Cp-2	16.1	0.6	6.1	23.7	24.3	11.7	0.8	4.5	0.8	57.6	2	
	20142Cp-3	25.9	0.8	5.2	18.7	23.6	9.6	1	17.2	0.8	91.9	2	
	20142Cp-4	41.2	1.8	3.4	13	20.6	6.4	1.3	5.1	0.9	60.4	2	

Abbreviation: ERS, equivalent spherical radius.

^aBold letters denote the aliquots excluded from the inverse thermal models, see Figure 8b.^bCorrected AHe age.

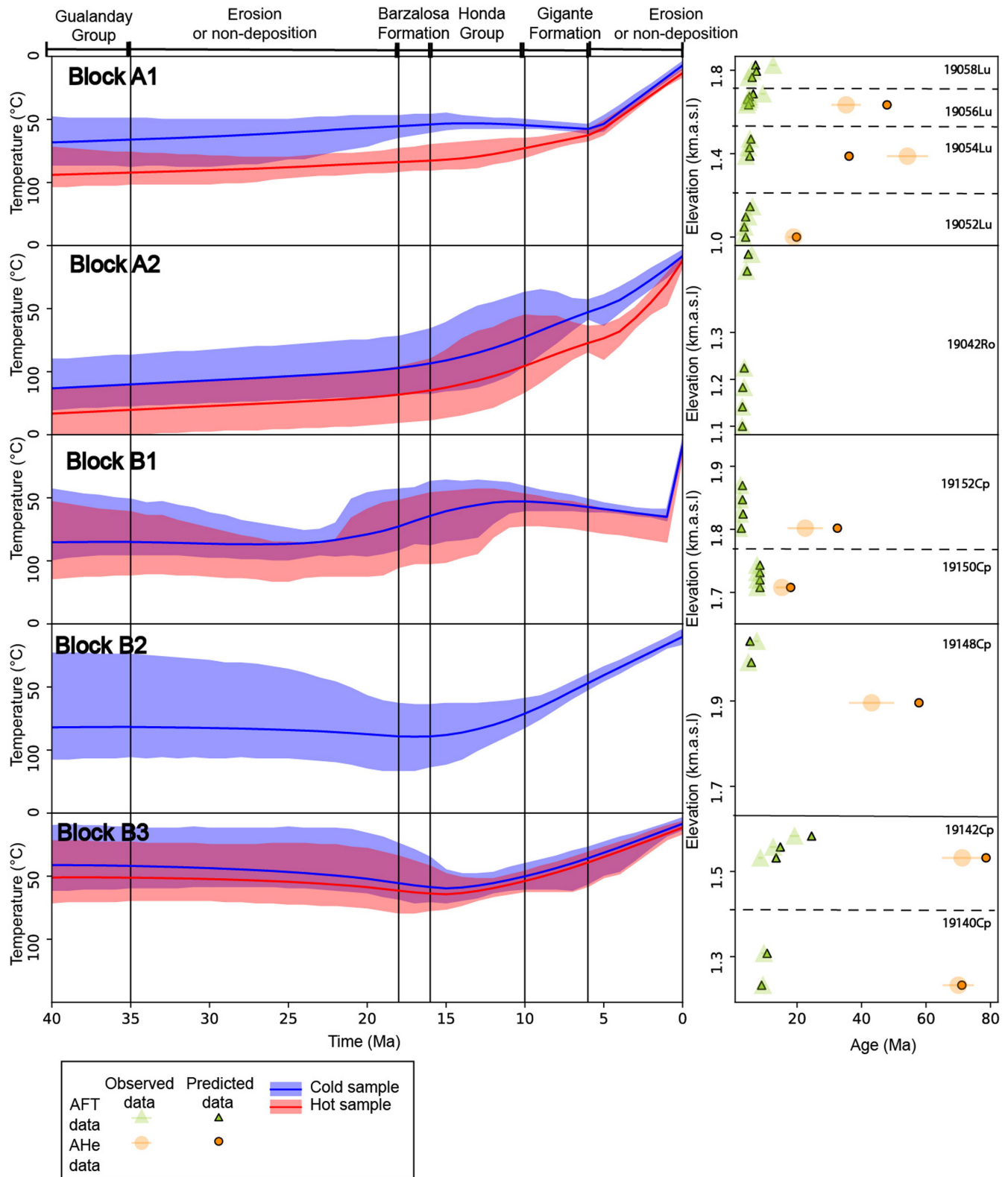


FIGURE 9 Thermal history inverse models from the bedrock data collected in the western segment of the Girardot sub-basin. Thermal histories and 2-sigma confidence intervals cold-sample (blue) and hot-sample (red) from each structural block are presented in the left panel; observed and predicted data are shown in the right panel. Marker colour and shape indicate the thermochronological system while light colours denote the observed data. Vertical black lines represent the depositional ages of the sedimentary units in the Girardot sub-basin. Note that the older portions of the models are not shown, complete models are presented in [Figure S2](#).

TABLE 8 Apatite fission-track data (AFT). No track lengths were measured for any sample. Complete single-grain data are presented in Table S3.

Sample code	N ^a	Ns	Ni	Nd	RhoD (x105) ^b	Age (Ma) ^c	± 2σ (Ma)	P(χ) (%)	Dpar (μm)	± 2σ (μm)	ζ (zeta)	± 2σ
19052Lu	30	135	1005	10,176	21.81230	19.8	2.0	42	1.9	0.37	135.4	5.2
19054Lu	30	113	287	10,176	22.06710	58.6	6.9	83	1.2	0.3	135.4	5.2
19056Lu	30	82	326	10,176	22.35350	38	4.9	70	1.41	0.23	135.4	5.2
20140Cp	30	331	674	9944	21.18100	70.1	5.5	67	1.8	0.4	135.4	5.2
20142Cp	30	195	397	9944	15.51250	71.9	6.9	58	2.2	0.41	135.4	5.2
20148Cp	12	55	157	1610	6.87842	42.3	6.7	98	2.1	0.52	100.1	1.9
20150Cp	13	110	851	1610	49.19075	15.91	1.6	20	2.3	0.56	100.1	1.9
20152Cp	6	19	100	1610	10.17812	23.79	6.0	100	1.2	0.23	100.1	1.9

^aNumber of counted grains.

^bDosimeter track density.

^cPooled age.

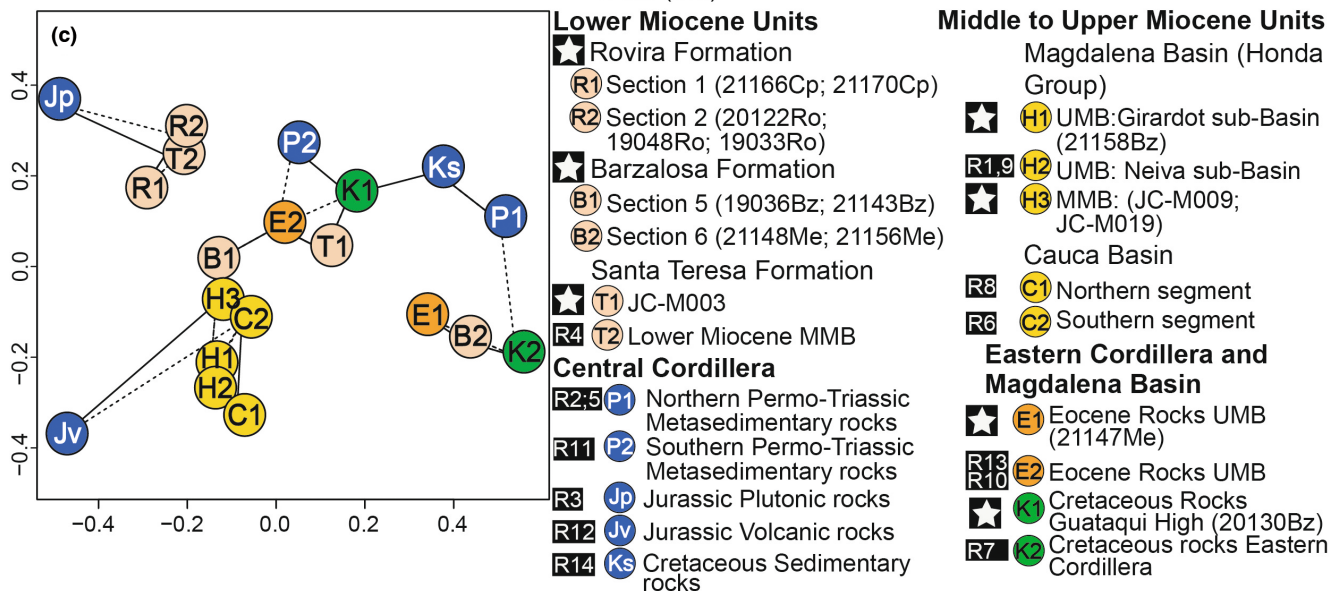
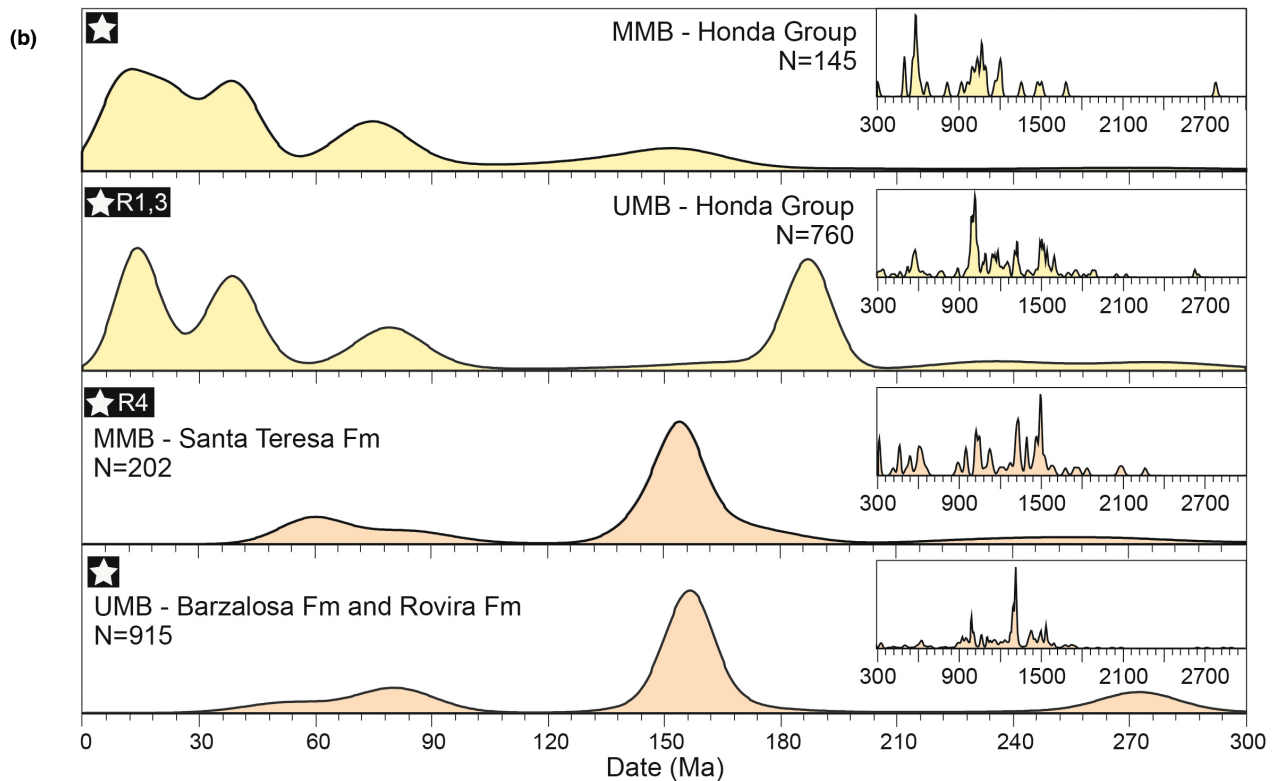
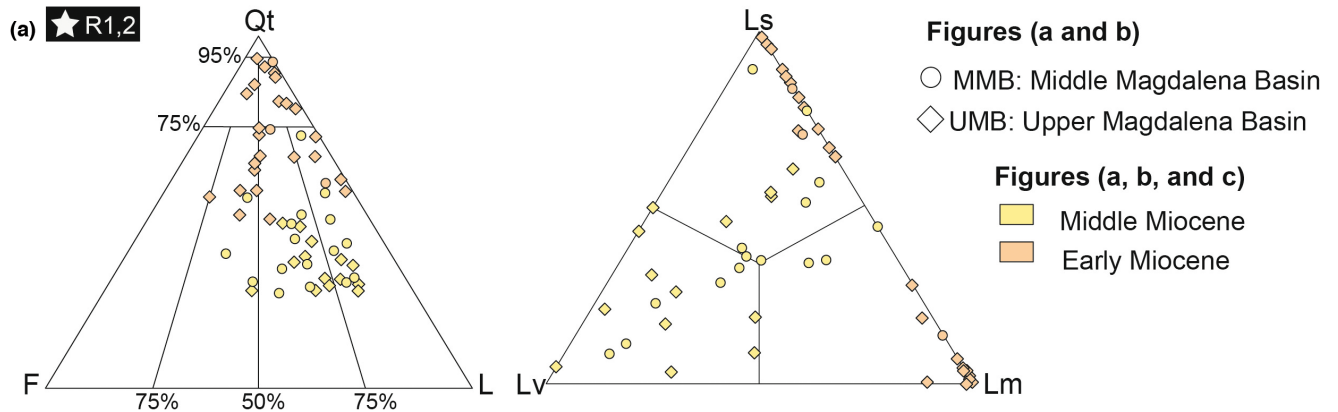
provenance signature—zircon grains younger than 40 Ma and volcanic clasts and lithics (Figure 10). Given that sedimentary rocks from the Honda Group have a significant presence of volcanic sources; the Rovira Formation should be older than 16 Ma; (3) seismic data suggest that both the Rovira and Barzalosa formations overlie the Oligocene strata of the Gualanday Group (Ramon & Rosero, 2006) (Figure 11b); (4) the Rovira Formation is restricted to a clastic wedge in the west of the basin that disappears towards the east, where the Honda Group directly overlies the Barzalosa Formation (Figures 5 and 11a); and (5) the Rovira Formation contains distinctive beds of mudstones with gypsum veins that have been described in the Barzalosa Formation (de La Parra et al., 2019). Lateral facies over relatively short distances (<50 km) is a distinctive characteristic of alluvial fan depositional systems; which accumulate in close proximity to topography (0.5 to 10 km) (Abdul Aziz et al., 2003; Blair, 2003). This may be the case of the Rovira Formation, which was deposited in the vicinity of the Central Cordillera positive relief (Figures 11a and 12).

The Rovira, Santa Teresa and Barzalosa formations were deposited during the Early Miocene in basins characterized by a non-volcanic sediment supply. However, several variations in the provenance signals were observed between these units. The Rovira Formation is characterized

by dominant Cretaceous, Jurassic and Permo-Triassic zircon age populations (Figure 4), which are characteristic of the plutonic and metamorphic basements of the Central Cordillera. Additionally, the MDS shows similarities between the samples from the Rovira Formation and plutonic basements and metamorphic basements of the Southern Central Cordillera (Figure 10c). The presence of feldspars, metamorphic lithics and granitic and metamorphic clasts confirm that the adjacent Southern Central Cordillera was the main source area of this unit. In contrast, the Barzalosa and Santa Teresa formations are characterized by sedimentary sources evidenced in more diverse zircons signatures, dominant sedimentary lithics (>60%) and sedimentary clasts (Figures 7 and 10).

Zircon data suggest contrasting sedimentary sources for the Santa Teresa and Barzalosa formations; as explained in chapter 2.2 two distinctive zircon signatures can be identified in the Cretaceous sedimentary rocks from the Central and Eastern Cordilleras, and the Magdalena Basin: strata from the Central Cordillera and the Magdalena Basin are characterized by the presence of diagnostic Permian to Cretaceous zircon populations while rocks from the Eastern Cordillera are characterized by the prevalence of older cratonic zircon ages (>900 Ma) (Bayona et al., 2020; Horton et al., 2020). The samples from section 5 and one from the Santa Teresa Formation indicate source areas

FIGURE 10 Compiled petrography and zircon data from the Northern Andes Miocene strata and the basements of the Central and Eastern Cordilleras, black squares contain the references of the compiled data while white stars denoting the data presented in this contribution (R1: Anderson et al., 2016; R2: Blanco-Quintero et al., 2014; R3: Bustamante et al., 2016, Bustamante et al., 2010; R4: Caballero et al., 2013; R5: Cochrane et al., 2014; R6: Echeverri et al., 2015; R7: Horton et al., 2010; R8: Lara et al., 2018; R9: Montes et al., 2021; R10: Muñoz Granados, 2019; R11: Naranjo et al., 2018; R12: Rodríguez et al., 2016; R13: Villamizar-Escalante et al., 2021; R14: Zapata, Cardona, et al., 2019). (a) sandstone classification diagram after Folk (1980) Qt: total quartz, F: total feldspar, L: total lithics, Lv: volcanic lithics, Ls: sedimentary lithics and Lm: metamorphic lithics. (b), Kernel Density Estimates of zircon U–Pb ages data from the Upper (UMB) and Middle Magdalena (MMB) basins. (c) Multi-dimensional scaling (MDS) using the Kolmogorov–Smirnov statistic (KS) (Vermeesch, 2013).



from the Cretaceous strata in Magdalena Basin (K2 in Figure 10c) and the Central Cordillera (Ks in Figure 10c), which are characterized by the presence of Jurassic and Cretaceous age populations (>23%). Similar Permian to Cretaceous zircon ages were also observed in the results from sample 20130Bz collected from the Cretaceous strata in the Guataqui High, north of section 5 (Figure 2a). In contrast, the samples from section 6—closer to the Eastern Cordillera—exhibit a higher percentage of zircons older than 900 Ma (>75%). One sample from the underlying Eocene strata in this section exhibits similar percentages of zircon grains older than 900 Ma (Figure 5a).

The MDS plot confirms that the zircon age populations from sections 5 to 7 (Barzalosa and Santa Teresa formations) have more affinity with the basements and the sedimentary cover from the Central Cordillera and the Magdalena Basin while samples from the eastern segment of the Girardot sub-basin (section 6) are related to the strata from the Eastern Cordillera (Figure 10c). These provenance patterns suggest that during the Early Miocene, the igneous basements from the Central Cordillera, the Cretaceous rocks from the Guataqui High and the Cretaceous and Eocene strata from the Eastern Cordillera were exposed and locally sourced the Rovira, Santa Teresa and Barzalosa formations (Figures 12).

Around 16 Ma, the appearance of syn-sedimentary and reworked (Upper Eocene and Oligocene) volcanic sources in the Magdalena Basin (Figure 10b) imply a major regional change in the source areas of the Upper and Middle Magdalena basins. Volcanic sources are evidenced in a regional increase in the lithic fraction (>40%), the appearance of volcanic lithics and an increase (>33%) in zircon ages younger than 40 Ma (Figure 10).

5.2 | Miocene paleogeography of the Colombian hinterland and foreland regions

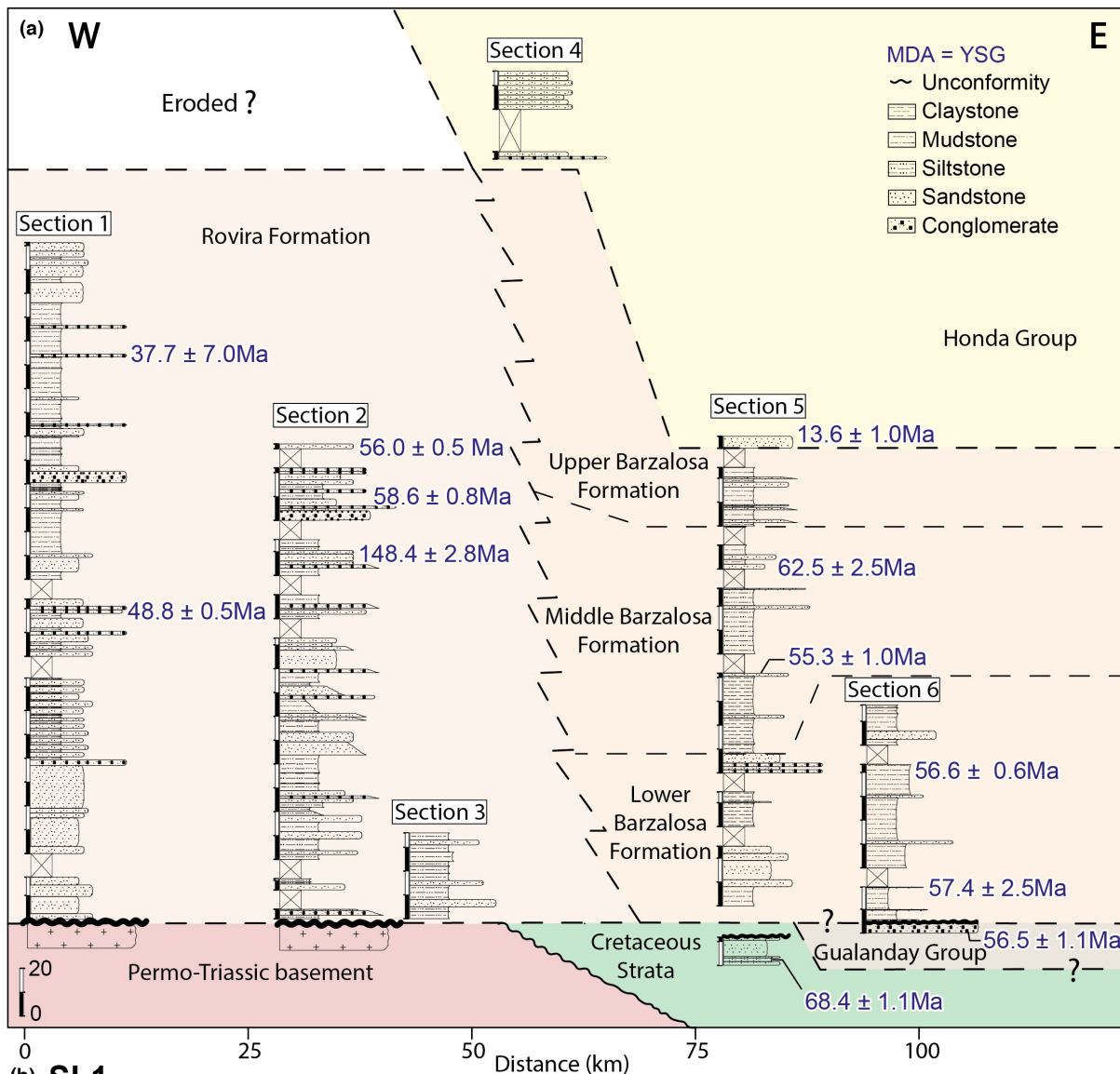
Miocene sedimentation in the Upper and Middle Magdalena basins commenced with the deposition of the Barzalosa and Santa Teresa formations at ca. 17.5 Ma. The Barzalosa Formation was deposited in an elongated freshwater playa lake system. The deepest facies of this lacustrine system within the Upper Magdalena Basin are found in the Neiva sub-basin (de La Parra et al., 2019), about 120 km south of sections 5 and 6 (Figure 12). The playa lake system described in the Girardot sub-basin was

characterized by an intermittent water body that facilitated the development of paleosols and fluvial currents on the lake pan. These shallow facies could correspond to the northern boundary of the lacustrine system that ended in the Guataqui High (Figure 12). In contrast, continuous fine-grained sedimentation and the preservation of coal beds and organic matter in the Middle Magdalena Basin suggest deposition under a permanent water body, which differs from the ephemeral system described in the Upper Magdalena Basin (Gómez et al., 2003, 2005). These distinct lake depositional systems in the Upper and Middle Magdalena basins may have been related to differences in the hydrological balance of each basin, suggesting that these lake systems were disconnected from each other.

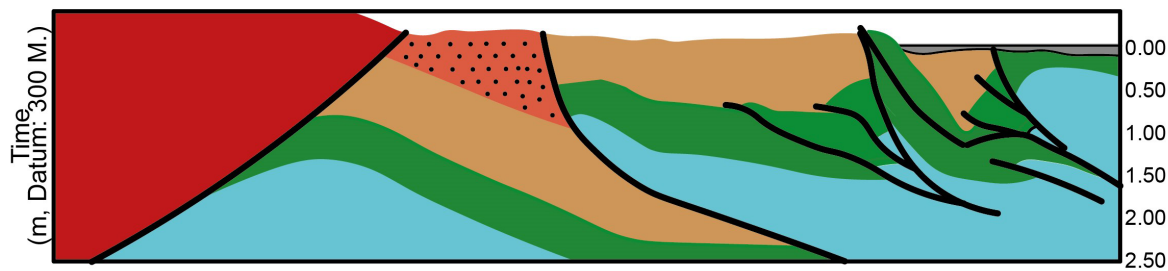
Paleontological and phylogenetic data suggest that the Upper Magdalena Basin was connected to the western Amazonia between 16 Ma and 10 Ma, supporting the existence of a trans-Andean passage (Montes et al., 2021; Rodríguez-Muñoz et al., 2022). Available thermochronological, provenance and structural data suggest that the Middle Magdalena Basin and the Llanos Basin were separated since the Paleocene due to the uplift of the Northern Eastern Cordillera (Bayona et al., 2020; Gómez et al., 2005; Horton et al., 2015; Parra, Mora, Sobel, et al., 2009; Reyes-Harker et al., 2015). However, these uplift patterns cannot be extrapolated to the Colombian, Garzón and Quetame massifs, which have been interpreted to have undergone an episodic Late Oligocene to Pliocene uplift history (Costantino et al., 2021; Pérez-Consuegra, Hoke, et al., 2021; Saeid et al., 2017), opening the possibility of a lowland connection between the Upper Magdalena Basin and the Pebas system before the uplift of the southern segment of the Eastern Cordillera.

In order to investigate the potential connection between the Upper Magdalena Basin and western Amazonia, Figure 13 presents a compilation of available thermochronological data from the basement blocks of the Southern Eastern Cordillera (CM, GM and QM in Figure 1c) (Anderson et al., 2016; Costantino et al., 2021; Parra, Mora, Sobel, et al., 2009; Pérez-Consuegra, Hoke, et al., 2021; Villagómez & Spikings, 2013). The results suggest that both the Barzalosa and Honda sedimentary units were deposited prior to the main phases of exhumation (<10 Ma) of these blocks. Specifically, the thermochronological data indicates minor or no exhumation before or during the deposition of the Barzalosa Formation and the Pebas System, which suggests that the Upper Magdalena

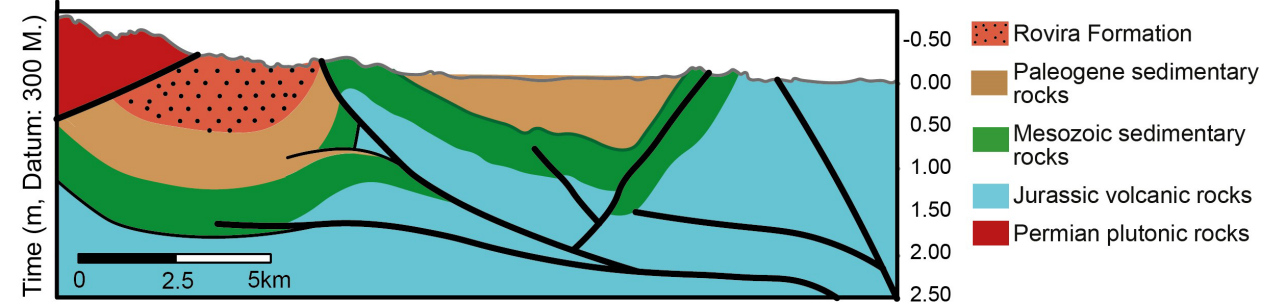
FIGURE 11 (a) West to east distribution of the described stratigraphic sections, facies association and the MDAs in the Girardot sub-basin, single stratigraphic sections are presented in Figures 4–6. (b) Interpreted seismic lines close to sections SL1–SL3, showing the subsurface disposition of the Rovira Formation. Seismic profiles were modified from Ramon and Rosero (2006). The location of these profiles is presented in Figure 2.



(b) SL1



SL2



Basin was connected to the Pebas System between ca. 19 and 13 Ma (Figure 13a,b), as also suggested by the SE deepening of the lacustrine facies (Figure 14). The transition from freshwater to marine conditions can be explained by the presence of continental rivers and meteoric waters toward the west.

Furthermore, the upper segment of the Honda Group (13–10 Ma) was deposited during the onset of exhumation in some segments of the Colombian, Quetame and Garzón massifs. It is, therefore, possible that during these initial phases, the formation of low and discontinuous topography allowed for narrow fluvial connections between the Upper Magdalena Basin and the Pebas System, as suggested by fossil and phylogenetic data. The complete disconnection between the Upper Magdalena Basins and the western Amazonia occurred between 9 Ma and 3 Ma, during the major exhumation phases of these blocks (Costantino et al., 2021; Pérez-Consuegra, Hoke, et al., 2021; Saeid et al., 2017) (Figures 13 and 14).

Coeval with the deposition of the Barzalosa Formation, a marine incursion flooded the Pebas system in the Llanos and Putumayo basins, resulting in the deposition of a thick succession of claystones with organic matter and marine palynomorphs (Jaramillo et al., 2017). As already discussed, the Upper Magdalena Basin and the Pebas System may have been connected, leading to the interpretation that the formation of the freshwater lacustrine system of the Barzalosa was a direct consequence of the rise in the fluvial base-line level driven by marine flooding, as it is often the case when playa-lake deposits accumulate along elongated and narrow basins (Figure 11) (e.g., Dumont, 1993; Gaupp et al., 2000).

In the Middle Magdalena Basin, the Santa Teresa and La Cira formations were disconnected from the Upper Magdalena Basin and Western Amazonia but connected to the Caribbean region (Gómez et al., 2003, 2005). Despite being deposited farther from the coastline in the north, the Early Miocene marine incursion from the Caribbean could have also facilitated the development of these lake systems (de La Parra et al., 2019). The slow cooling trends observed in the Southern Central cordillera and the AAP (Zapata et al., 2021) between the Oligocene and the Lower Miocene (Figure 9), may have facilitated the development of the lacustrine systems in the Upper and Middle Magdalena basins.

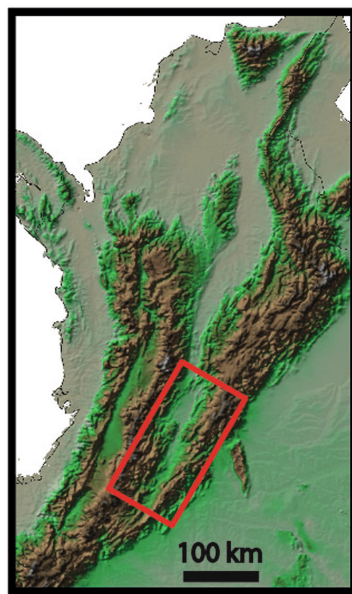
Active arc volcanism characterized the Cauca Basin to the west of the Central Cordillera between 40 Ma and 12 Ma (Cardona et al., 2018; Echeverri et al., 2015). Montes et al. (2021) proposed a trans-Andean passage between the Pacific and the Amazon around 13 Ma, this interpretation was based on the presence of Late Eocene to Miocene zircons—interpreted to be sourced from the Cauca Basin—in Middle Miocene rocks from the Upper

Magdalena Basin. Our data from the Upper and Middle Magdalena basins support and reinforce the existence of this passage. However, Lower Miocene strata from both basins lack Eocene to Miocene volcanic sources (50–18 Ma) (Figure 10), suggesting that the Central Cordillera acted as a continuous barrier between the Late Eocene and the Lower Miocene, preventing sub-aerial and drainage connections between the Cauca and the Magdalena basins. The hydrological connections between the Cauca and the Upper and Middle Magdalena basins probably started around 16 Ma (Figure 14).

During the Middle Miocene (ca. 16 to 12.4 Ma), similar to the Early Miocene, the Pebas system dominated most of the Putumayo and Llanos basins landscape, when a second marine incursion occurred into western Amazonia (Jaramillo, Romero, et al., 2017). Despite the Upper Magdalena Basin being connected to the Pebas System, a lacustrine system did not form, and instead, the well-developed fluvial system of the Honda Group (ca. 16–10 Ma) accumulated. This shift in the depositional systems coincides with thermochronological data and thermal history models from sections A-A' and B-B', which suggest that between ca. 16 and 8 Ma, the Southern Central Cordillera experienced a phase rock uplift and exhumation (Figure 9). Consequently, we interpret that during this time, a rapid increase in sediment influx associated with orogenic erosion and the arrival of volcanoclastic sediments from the Cauca Basin prevented the establishment of lacustrine systems in the Upper Magdalena Basin. Similar responses of lacustrine systems to major shifts in sediment supply and relief have been widely documented in the geological record (García-Castellanos, 2006; Pietras et al., 2003; Zapata, Sobel, et al., 2019).

In the Middle Magdalena Basin, the Middle Miocene deposition of the Honda Group coincides with the exhumation and uplift of the Eastern Cordillera and a period of low exhumation in the AAP (Costantino et al., 2021; Mora et al., 2013; Zapata et al., 2021). Analogously to the processes described in the Upper Magdalena Basin, the topographic growth of the Eastern Cordillera may have raised the base level of the Middle Magdalena Basin and increased the sediment influx, leading to the lacustrine system's termination. Additionally, the Middle Magdalena Basin is characterized by the presence of primary and proximal volcanic facies; which may have favoured the termination of the lacustrine system by the construction of volcanic edifices and the production of volcanic materials (Figure 14).

Strike-slip fault deformation can cause sudden modifications in drainage networks and source areas, leading to significant changes in the provenance signals that are recorded in neighbouring basins (e.g., Gibson et al., 2021;



- Drainages
- Positive topography
- Low elevation sediment transfer zones

Pebas system

- Fluvial Facies
- Wetland and ephemeral fluvial
- Marine incursion

Barzalosa Formation

- Marginal playa lake system
- Fresh water deep lacustrine facies

Rovira Fomation

- Alluvial facies
- Active faults
- - - Inactive faults
- Towns
- ☆ Wells from De la Parra et al. (2019)
- ★ Surface stratigraphic sections of the Barzalosa and Rovira Formations

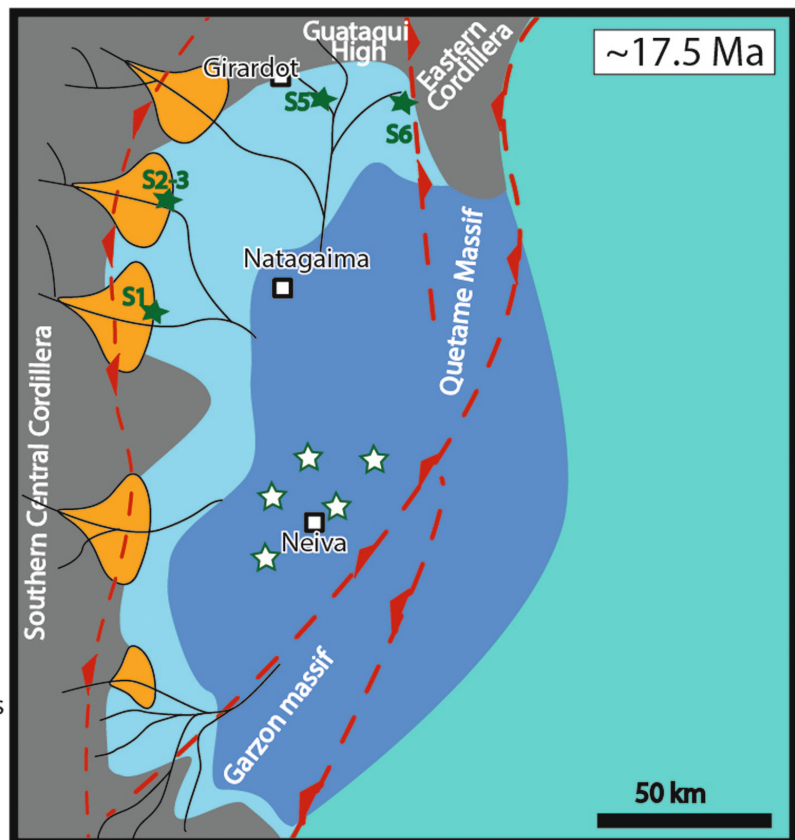
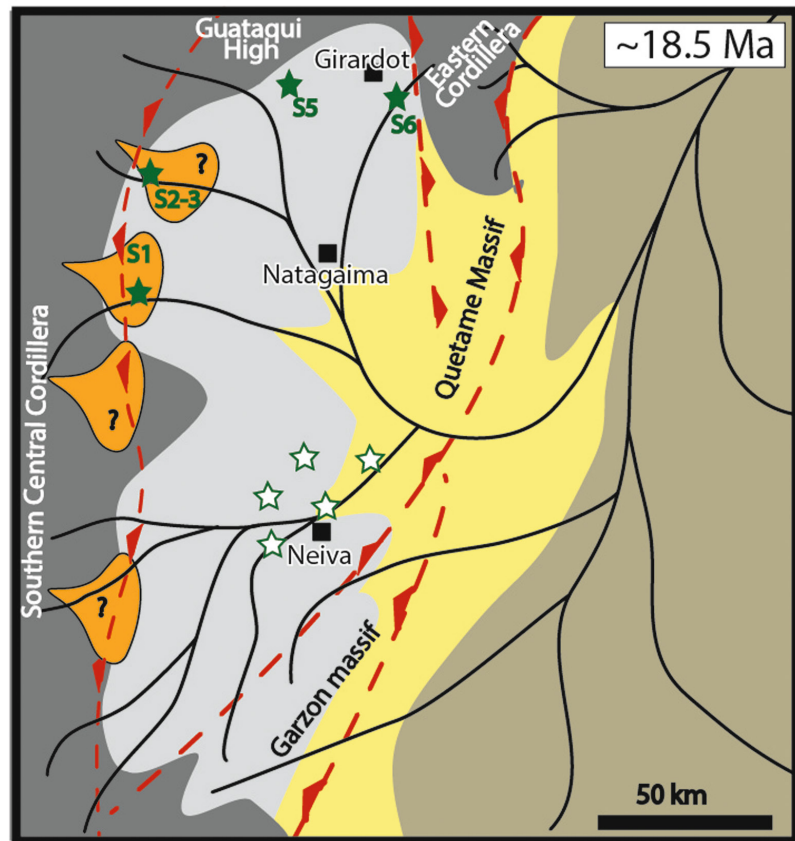


FIGURE 12 Schematic palaeogeography and facies distribution of the Upper Magdalena Basin. Towns are presented as geographic references. Stars denote the surface stratigraphic sections and the well data of the Barzalosa and Rovira formations.

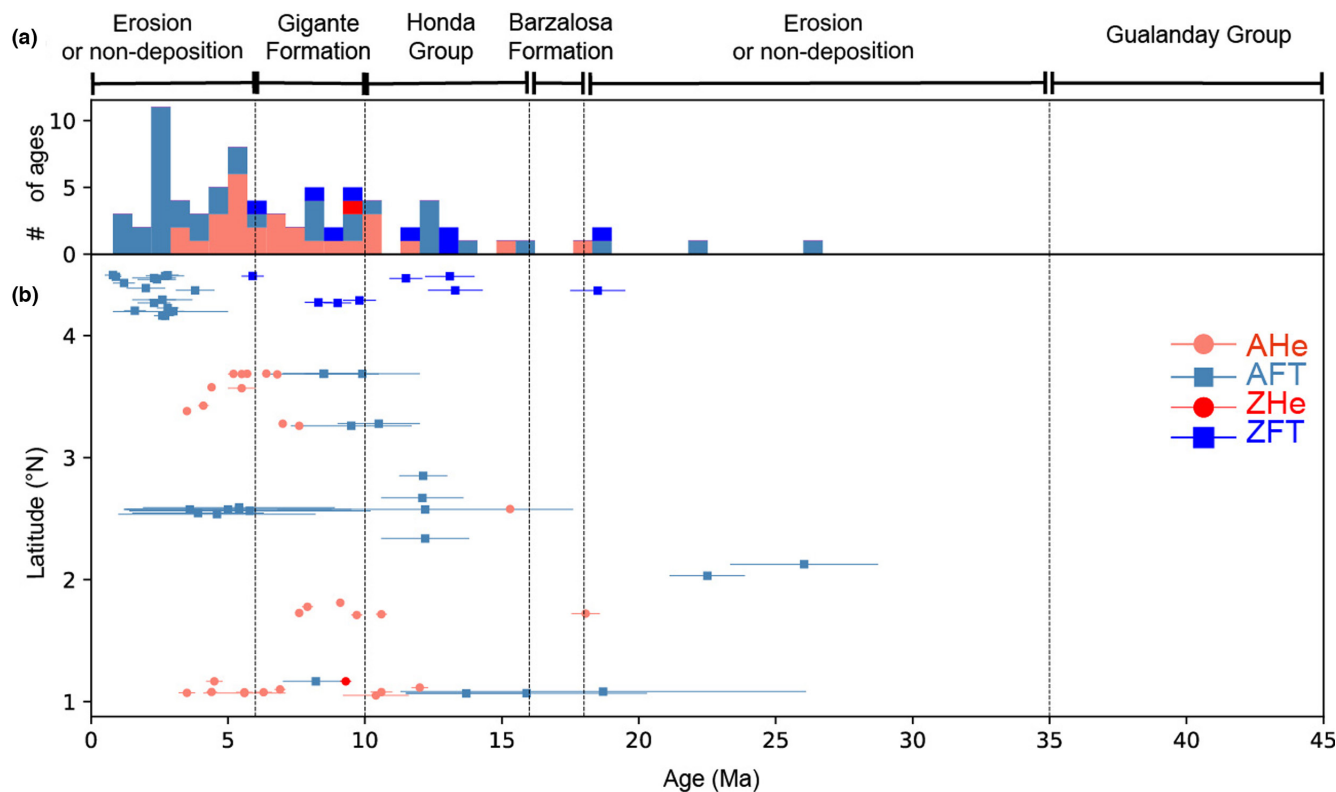


FIGURE 13 Available thermochronological data from the Colombian, Garzón and Quetame massifs (Anderson et al., 2016; Costantino et al., 2021; Parra, Mora, Sobel, et al., 2009b; Pérez-Consuegra, Hoke, et al., 2021; Villagómez & Spikings, 2013), including fission tracks and U-Th/He ages in apatite and zircon. (a) stacked histogram with the thermochronological data. (b) Age versus latitude diagram.

Liu et al., 2021; Zhou et al., 2022). Moreover, orogens controlled by strike-slip tectonics are characterized by along-strike variations in deformational styles, resulting in the coexistence of rock subsidence, displacement and uplift (e.g., Cunningham & Mann, 2007; Forero-Ortega et al., 2020; Lin & Yamashita, 2013). Based on our provenance and thermochronological data, we suggest that the Southern Central Cordillera experienced exhumation and uplift coeval with the development of fluvial connections that required the fragmentation of this mountain belt between ca. 16 and ca. 10 Ma. A sedimentation and deformation pattern that could be explained by active Miocene strike-slip tectonics (Figure 14). Given that strike-slip tectonics characterized the Cenozoic evolution of the North-Andean continental margin (Montes et al., 2019; Spikings et al., 2014); this is the most plausible tectonic mechanism to explain the along-strike fragmentation and exhumation of the Central Cordillera.

The Upper and Middle Magdalena basins exhibit similar provenance signals, however, given that these basins were disconnected since the Early Miocene, a single drainage connection through the south can not explain the input of volcanic materials from the west in both basins, thus, a direct connection between the Cauca and the Middle Magdalena Basin is also required (Figure 14).

Several structural studies conducted in the Magdalena Basin and the bounding Cordilleras have suggested the occurrence of strike-slip deformation during the Oligocene to Miocene, which was associated with multiple NE faults that traverse the Central Cordillera (Acosta et al., 2007). To the north of the Guataqui High, several NE faults, including the Ibagué fault, cross the Central Cordillera, the Middle Magdalena Basin and the western flank of the Eastern Cordillera. In this region, structural studies have documented several phases of dextral transpression that began in the Late Cretaceous and included a Miocene deformation phase (Acosta et al., 2004; Acosta et al., 2007; Montes et al., 2005). These faults may have played a role in the connection between the Amagá and the Middle Magdalena Basin (Figure 14). Other authors have also proposed similar connections based on geomorphological and thermochronological data (Pérez-Consuegra et al., 2022).

Both the Chusma and the Algeciras fault systems cross the Central Cordillera and Upper Magdalena Basin (Figure 1). Structural and paleomagnetic data suggest that there was Miocene rotation and right-lateral deformation along the Chusma Fault System (Jiménez et al., 2012). Although the Algeciras Fault System has been described as an active dextral NE strike-slip fault, the pre-Pliocene

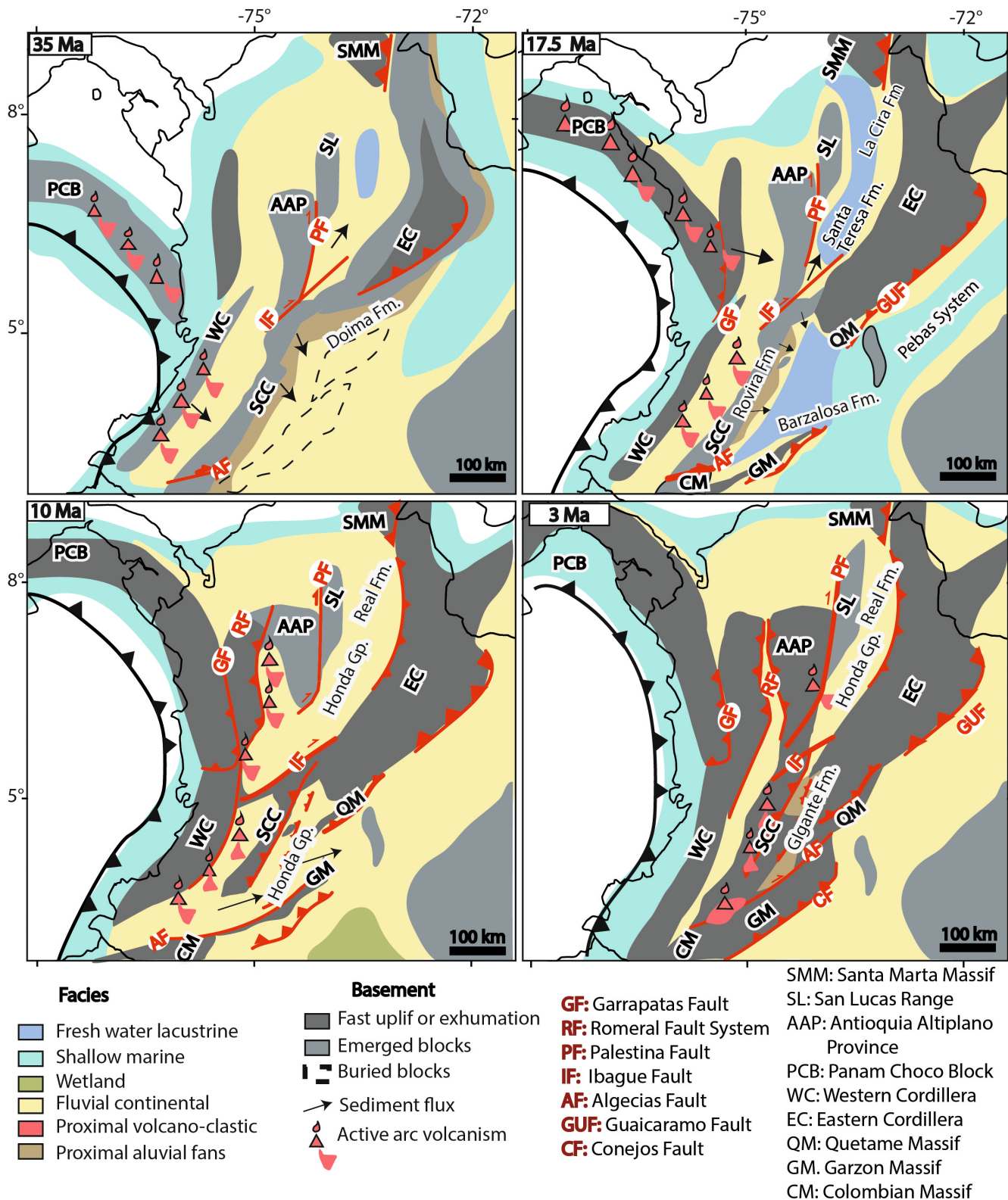


FIGURE 14 Schematic Late Eocene to Pliocene paleogeography of the Northern Andes. Red letters denote the fault names while black letters indicate sedimentary units and structural blocks, abbreviations are presented in the figure legend. Grey colours represent exposures of basement blocks and coloured polygons the sedimentary facies. Outside of the study area, previous publications were used to reconstruct the paleogeography, sedimentary facies, volcanism and deformational events (Caballero et al., 2013; Echeverri et al., 2015; Horton et al., 2020; Jaramillo, Romero, et al., 2017; Lara et al., 2018; Montes et al., 2019; Pérez-Consuegra, Ott, et al., 2021; Pérez-Consuegra et al., 2022; Reyes-Harker et al., 2015; Wagner et al., 2017; Zapata et al., 2021).

deformational phases of this fault remain poorly constrained (Acosta et al., 2007; Deynoux et al., 2005; Velandia et al., 2005). However, the spatial relationship between the paleogeographic colonization patterns of high mountain palms and major strike-slip faults, such as the Algeciras Fault System, suggests that these faults were associated with structurally controlled valleys that prevented palm migration through the Central and Eastern Cordilleras before 5 Ma (Sanín, Cardona, et al., 2022; Sanín, Mejía-Franco, et al., 2022). The Chusma and Algeciras faults may have facilitated land connections between the Cauca and the Upper Magdalena Basin.

Despite the need for more temporal and structural constraints on the strike-slip deformational phases, available data suggest extensive strike-slip deformation in the Magdalena Basin and the Central Cordillera between the Oligocene and the Miocene. These findings support the hypothesis that strike-slip tectonics fragmented this mountain belt and thus modified the Middle Miocene sedimentary sources of the Magdalena Basin. Furthermore, these NE strike-slip faults may have been the structural paths that facilitated the land connections between the Cauca and the Magdalena basins. Early Miocene strike-slip deformation phases may have been related to the increase in the oblique convergence rates and the oblique collision of the Panamá-Chocó Block at ca. 16 Ma (Echeverri et al., 2015; León et al., 2018; Montes et al., 2012; Mora et al., 2013).

Thermal history models A1 and B1 suggest that there was accelerated cooling between 8 and 2 Ma (Figure 9), in model B1, this event implies ca. 1.5 km of differential exhumation (assuming a thermal gradient of 25°C/km) compare to block B2. This event is interpreted as the result of out-of-sequence deformation and exhumation in the core of the Southern Central Cordillera. During the same time interval (8 to 2 Ma), the Colombian, Quetame and Garzón massifs experienced major phases of uplift and exhumation (Figure 13) that led to the disconnection of the Upper Magdalena Basin and Western Amazonia (Figure 14) (Pérez-Consuegra, Hoke, et al., 2021; Saeid et al., 2017). This synchronous uplift of both flanks of the Upper Magdalena Basin caused the development of an endorheic basin and the deposition of the alluvial coarse-grained strata of the Gigante Formation (Figure 14).

Prolonged and accelerated Miocene to Pliocene exhumation and deformation in the AAP and the Southern Central and Eastern cordilleras (Montes et al., 2021; Pérez-Consuegra, Hoke, et al., 2021, Pérez-Consuegra et al., 2022; Ramon & Rosero, 2006) eventually led to the closure of the fluvial connections between the Cauca and Magdalena basins (Figure 14). Furthermore, volcanic arc magmatism along the Central Cordillera provided

abundant volcanoclastic materials (Anderson et al., 2016; Wagner et al., 2017), which contributed to the final closure of these passages (Sanín, Mejía-Franco, et al., 2022).

5.3 | Implications for the understanding of strike-slip deformation in Andean-type orogens

This contribution presents an example of how oblique convergence during compressive events can control orogen-scale deformation, drainage and sedimentation patterns in Andean-type orogens. Our results lead to a paleogeographic model that requires the development of fluvial connections and rock uplift and cooling along the same mountain belt (Central Cordillera) for a short time interval (ca. 6 Ma). Major changes in the sediment routing system, localized extension and compression in similar along-strike positions and mountain belt and basin fragmentation are diagnostic features of strike-slip tectonics (Cunningham & Mann, 2007; Fossen & Tikoff, 1998; Gibson et al., 2021; Liu et al., 2021).

We have documented at least two direct effects of strike-slip in the evolution of the deformation and sedimentation patterns in the Northern Andes. (1), Strike-slip deformation changed the drainage network and basin connectivity: after several compressive events, the Northern Andes hinterland (Cauca Basin) was completely separated from the foreland regions in the Magdalena, Llanos and Putumayo basins; however, Middle Miocene strike-slip deformation created at least two short-lived (ca. 6 Ma) passages between these regions. Sudden changes in the provenance signals and narrow and localized basin connections are the expressions of these events along the Central Cordillera of Colombia. These passages may have been critical for the evolution and connectivity of the highly diverse Amazonian and Pacific regions (Montes et al., 2021; Rodríguez-Muñoz et al., 2022; Sanín, Cardona, et al., 2022; Sanín, Mejía-Franco, et al., 2022). (2), Contrasting along-strike exhumation and deformation patterns: The Central and Eastern Cordilleras of Colombia are examples of mountain belts characterized by major along-strike variations in their deformation and exhumation histories, in the case of the Central Cordillera, the northern segment (AAP) was characterized by minor Miocene exhumation evidenced in old (>30 Ma) AHe ages (Zapata et al., 2021) while young ages (<15 Ma) suggest significant exhumation in the Southern Central Cordillera. In the presented paleogeographic and tectonic model, localized transpression in this segment of the mountain belt explains these along-strike differences in the amount of Miocene exhumation.

5.4 | Implications for the Pebas system

Available models of western Amazonia have proposed the existence of an immense wetland-like system characterized by extensive flood plains—the Pebas system. This system experienced two large-scale and short marine incursions during the Early and Middle Miocene, respectively. The system was terminated around 10Ma when the rise of the Andes increased the sediment flux, and subsidence in western Amazonia mostly ended (Hoorn et al., 2010; Hoorn, Boschman, et al., 2021). We have documented how strike-slip tectonics in the Northern Andes modified the drainage network, and sediment influx in the Upper Magdalena Basin resulted in the premature termination of lacustrine conditions and a transition to fluvial depositional systems. This finding implies that (1) the lacustrine deposits in the Upper Magdalena Basin were a byproduct of the Early Miocene marine incursion, and (2) the termination of the Pebas system was diachronous and controlled by local deformation patterns. Finally, the Middle Magdalena Basin presents an example of a lacustrine system that despite being disconnected from the Pebas system was affected by the Early Miocene marine incursions and the Miocene deformational phases in the Northern Andes.

6 | CONCLUSIONS

New U–Pb zircon detrital ages, sandstone petrography, stratigraphy from the Miocene strata in the Northern Andes hinterland basins and low-temperature thermochronology from the Central Cordillera are integrated with published data to present a new paleogeographic model of the Miocene evolution of this region. Our results suggest that the Lower Miocene lacustrine units preserved in the Upper and Middle Magdalena basins were disconnected from each other, while the Upper Magdalena Basin was connected to the Pebas System in Western Amazonia. Around 16Ma, the appearance of volcanic sources suggests the opening of at least two passages that connected the Cauca and Magdalena basins (western Colombian Andes). Simultaneously with the opening of these passages, the transition from lacustrine to fluvial depositional systems in the Magdalena Basin and the cooling events in the Central Cordillera are interpreted as the result of rock uplift, topographic growth and orogenic erosion. Coeval fragmentation and rock uplift along the Central Cordillera were likely the results of strike-slip tectonics promoted by oblique plate convergence and the oblique collision of the Panamá-Chocó Block. These results imply that despite regional subsidence and a marine incursion, deformation in the Andean margin did not allow lacustrine deposition in the Upper and Middle Magdalena basins during the

Middle Miocene. We present a model where strike-slip tectonic was responsible for the fragmentation and uplift of continuous orographic barriers that resulted in the development of trans-Andean passages and isolated topography.

ACKNOWLEDGEMENTS

We acknowledge the support for S. Zapata from the Missouri University of Science and Technology-STRI Bytnar Postdoctoral Fellowship. Colleagues from the EGEO research group at the National University of Colombia are acknowledged for their discussions, J. Gómez is acknowledged for his help with sample preparation. L. Calderon thanks the Asociación Colombiana de Geólogos y Geofísicos del Petróleo (ACGGP) and Ares Geological Corporation for the resources provided through Corrigan ACGGP—ARES found. J.S. Jaramillo received funding from the Universidad Nacional de Colombia (grant HERMES 47494). Finally, we thank B. Horton and an anonymous reviewer for their insightful comments.

CONFLICT OF INTEREST STATEMENT

Authors have no conflict of interest to declare.

PEER REVIEW

The peer review history for this article is available at <https://www.webofscience.com/api/gateway/wos/peer-review/10.1111/bre.12769>.

DATA AVAILABILITY STATEMENT

All the data used in this manuscript can be found in the supporting information and thermochronological and geochronological data are also stored in Geochron repository (https://www.geochron.org/dataset/html/geochron_dataset_2023_03_11_pOaYX).

ORCID

S. Zapata  <https://orcid.org/0000-0003-1213-544X>

L. Calderon-Diaz  <https://orcid.org/0000-0002-3523-9017>

C. Jaramillo  <https://orcid.org/0000-0002-2616-5079>

F. Oboh-Ikuenobe  <https://orcid.org/0000-0002-2223-9691>

M. Rodríguez-Cuevas  <https://orcid.org/0009-0008-5647-1035>

A. Cardona  <https://orcid.org/0000-0003-2813-4820>

E. R. Sobel  <https://orcid.org/0000-0001-5030-8773>

M. Parra  <https://orcid.org/0000-0002-5955-6105>

V. Valencia  <https://orcid.org/0000-0003-2508-651X>

A. Patiño  <https://orcid.org/0000-0001-5632-3376>

J. S. Jaramillo-Rios  <https://orcid.org/0000-0003-1067-9259>

M. Flores  <https://orcid.org/0000-0002-0246-7515>

J. Glodny  <https://orcid.org/0000-0002-7812-5933>

REFERENCES

- Abdul Aziz, H., Sanz-Rubio, E., Calvo, J. P., Hilgen, F. J., & Krijgsman, W. (2003). Palaeoenvironmental reconstruction of a middle Miocene alluvial fan to cyclic shallow lacustrine depositional system in the Calatayud Basin (NE Spain). *Sedimentology*, *50*, 211–236.
- Acosta, J., Lonergan, L., & Coward, M. P. (2004). Oblique transpression in the western thrust front of the Colombian Eastern Cordillera. *Journal of South American Earth Sciences*, *17*, 181–194. <https://doi.org/10.1016/j.jsames.2004.06.002>
- Acosta, J., Velandia, F., Osorio, J., Lonergan, L., & Mora, H. (2007). Strike-slip deformation within the Colombian Andes. *Geological Society, London, Special Publications*, *272*, 303–319.
- Amaya, S., Zuluaga, C. A., & Bernet, M. (2017). New fission-track age constraints on the exhumation of the central Santander Massif: Implications for the tectonic evolution of the Northern Andes, Colombia. *Lithos*, *282*, 388–402.
- Anderson, V. J., Horton, B. K., Saylor, J. E., Mora, A., Tesón, E., Breecker, D. O., & Ketcham, R. A. (2016). Andean topographic growth and basement uplift in southern Colombia: Implications for the evolution of the Magdalena, Orinoco, and Amazon river systems. *Geosphere*, *12*, 1235–1256. <https://doi.org/10.1130/GES01294.1>
- Antonelli, A., Kissling, W. D., Flantua, S. G. A., Bermúdez, M. A., Mulch, A., Muellner-Riehl, A. N., Kreft, H., Linder, H. P., Badgley, C., Fjeldsø, J., & Fritz, S. A. (2018). Geological and climatic influences on mountain biodiversity. *Nature Geoscience*, *11*, 718–725. <https://doi.org/10.1038/s41561-018-0236-z>
- Antonelli, A., Nylander, J. A. A., Persson, C., & Sanmartín, I. (2009). Tracing the impact of the Andean uplift on Neotropical plant evolution. *Proceedings of the National Academy of Sciences*, *106*, 9749–9754.
- Barbosa-Espitia, Á. A., Kamenov, G. D., Foster, D. A., Restrepo-Moreno, S. A., & Pardo-Trujillo, A. (2019). Contemporaneous Paleogene arc-magmatism within continental and accreted oceanic arc complexes in the northwestern Andes and Panama. *Lithos*, *348–349*, 105185. <https://doi.org/10.1016/j.lithos.2019.105185>
- Bayona, G., Baquero, M., Ramírez, C., Tabares, M., Salazar, A. M., Nova, G., Duarte, E., Pardo, A., Plata, A., Jaramillo, C., & Rodriguez, G. (2020). Unravelling the Widening of the Earliest Andean Northern Orogen: Maastrichtian to Early Eocene Intra-basinal Deformation in the Northern Eastern Cordillera of Colombia. *Basin Research*, *33*, 809–845. <https://doi.org/10.1111/bre.12496>
- Bayona, G., Bustamante, C., Nova, G., & Salazar-Franco, A. M. (2019). Jurassic evolution of the northwestern corner of Gondwana: Present knowledge and future challenges in studying Colombian Jurassic rocks. *The Geology of Colombia*, *2*, 161–202.
- Bayona, G., Cardona, A., Jaramillo, C., Mora, A., Montes, C., Valencia, V., Ayala, C., Montenegro, O., & Ibañez-Mejía, M. (2012). Early Paleogene magmatism in the northern Andes: Insights on the effects of Oceanic Plateau–continent convergence. *Earth and Planetary Science Letters*, *331*, 97–111.
- Bayona, G., Cortés, M., Jaramillo, C., Ojeda, G., Aristizabal, J. J., & Reyes-Harker, A. (2008). An integrated analysis of an orogen-sedimentary basin pair: Latest Cretaceous–Cenozoic evolution of the linked Eastern Cordillera orogen and the Llanos foreland basin of Colombia. *Bulletin of the Geological Society of America*, *120*, 1171–1197. <https://doi.org/10.1130/B26187.1>
- Bicudo, T. C., Sacek, V., & de Almeida, R. P. (2020). Reappraisal of the relative importance of dynamic topography and Andean orogeny on Amazon landscape evolution. *Earth and Planetary Science Letters*, *546*, 116423.
- Blair, T. C. (2003). Features and origin of the giant Cucomungo Canyon alluvial fan, Eureka Valley, California. *Geological Society of America Special Papers*, *370*, 105–126.
- Blanco-Quintero, I. F., García-Casco, A., Toro, L. M., Moreno, M., Ruiz, E. C., Vinasco, C. J., Cardona, A., Lázaro, C., & Morata, D. (2014). Late Jurassic terrane collision in the northwestern margin of Gondwana (Cajamarca Complex, eastern flank of the Central Cordillera, Colombia). *International Geology Review*, *56*, 1852–1872.
- Bookhagen, B., & Strecker, M. R. (2012). Spatiotemporal trends in erosion rates across a pronounced rainfall gradient: Examples from the southern Central Andes. *Earth and Planetary Science Letters*, *327*, 97–110. <https://doi.org/10.1016/j.epsl.2012.02.005>
- Briere, P. R. (2000). Playa, playa lake, sabkha: Proposed definitions for old terms. *Journal of Arid Environments*, *45*, 1–7.
- Brown, R. W., Beucher, R., Roper, S., Persano, C., Stuart, F., & Fitzgerald, P. (2013). Natural age dispersion arising from the analysis of broken crystals. Part I: Theoretical basis and implications for the apatite (U-Th)/He thermochronometer. *Geochimica et Cosmochimica Acta*, *122*, 478–497. <https://doi.org/10.1016/j.gca.2013.05.041>
- Bustamante, C., Archanjo, C. J., Cardona, A., & Vervoort, J. D. (2016). Late Jurassic to Early Cretaceous plutonism in the Colombian Andes: A record of long-term arc maturity. *Geological Society of America Bulletin*, *128*, 1762–1779.
- Bustamante, C., Cardona, A., Archanjo, C. J., Bayona, G., Lara, M., & Valencia, V. (2017). Geochemistry and isotopic signatures of Paleogene plutonic and detrital rocks of the Northern Andes of Colombia: A record of post-collisional arc magmatism. *Lithos*, *277*, 199–209.
- Bustamante, C., Cardona, A., Bayona, G., Mora, A., Valencia, V., Gehrels, G., & Vervoort, J. D. (2010). U–Pb LA-ICP-MS geochronology and regional correlation of middle Jurassic intrusive rocks from the Garzon massif, upper Magdalena Valley and Central Cordillera, Southern Colombia. *Boletín De Geología*, *32*, 93–105.
- Caballero, V., Parra, M., Mora, A., López, C., Rojas, L. E., & Quintero, I. (2013). Factors controlling selective abandonment and reactivation in thick-skin orogens: A case study in the Magdalena Valley, Colombia. *Geological Society, London, Special Publications*, *377*, 343–367. <https://doi.org/10.1144/sp377.4>
- Cardona, A., León, S., Jaramillo, J. S., Montes, C., Valencia, V., Vanegas, J., Bustamante, C., & Echeverri, S. (2018). The Paleogene arcs of the northern Andes of Colombia and Panama: Insights on plate kinematic implications from new and existing geochemical, geochronological and isotopic data. *Tectonophysics*, *749*, 88–109. [S0040195118303743](https://doi.org/10.1016/j.tecto.2018.04.011).
- Cardona, A., León, S., Jaramillo, J. S., Valencia, V., Zapata, S., Pardo-Trujillo, A., Schmitt, A. K., Mejía, D., & Arenas, J. C. (2020). Cretaceous record from a Mariana to an Andean-type margin

- in the central cordillera of the Colombian Andes. In J. Gómez & A. O. Pinilla-Pachón (Eds.), *The geology of Colombia* (Vol. 36, pp. 353–395). Servicio Geológico Colombiano.
- Carmona, O. O., & Pimentel, M. M. (2002). Rb–Sr and Sm–Nd isotopic study of the Puquí complex, Colombian Andes. *Journal of South American Earth Sciences*, *15*, 173–182.
- Carrillo, J. D., Forasiepi, A., Jaramillo, C., & Sánchez-Villagra, M. R. (2015). Neotropical mammal diversity and the Great American Biotic Interchange: spatial and temporal variation in South America's fossil record. *Frontiers in Genetics*, *5*, 451.
- Carroll, A. R., & Bohacs, K. M. (1999). Stratigraphic classification of ancient lakes: Balancing tectonic and climatic controls. *Geology*, *27*, 99–102.
- Carvalho, M. R., Jaramillo, C., de la Parra, F., Caballero-Rodríguez, D., Herrera, F., Wing, S., Turner, B. L., D'Apolito, C., Romero-Báez, M., & Narváez, P. (2021). Extinction at the end-Cretaceous and the origin of modern Neotropical rainforests. *Science*, *1979*(372), 63–68.
- Chang, Z., Vervoort, J. D., McClelland, W. C., & Knaack, C. (2006). U–Pb dating of zircon by LA-ICP-MS. *Geochemistry, Geophysics, Geosystems*, *7*, 1–14.
- Cochrane, R., Spikings, R., Gerdes, A., Ulianov, A., Mora, A., Villagómez, D., Putlitz, B., & Chiaradia, M. (2014). Permo-Triassic anatexis, continental rifting and the disassembly of western Pangaea. *Lithos*, *190–191*, 383–402. <https://doi.org/10.1016/j.lithos.2013.12.020>
- Correa-Martínez, A. M., Martens, U., & Rodríguez, G. (2020). Collage of tectonic slivers abutting the eastern Romeral Fault System in central Colombia. *Journal of South American Earth Sciences*, *104*, 102794.
- Costantino, D., Paton, D., & Mora, A. (2021). Structural style and kinematic history of the Colombian Eastern Cordillera. *Frontiers in Earth Science (Lausanne)*, *9*, 1–25. <https://doi.org/10.3389/feart.2021.636458>
- Coutts, D. S., Matthews, W. A., & Hubbard, S. M. (2019). Assessment of widely used methods to derive depositional ages from detrital zircon populations. *Geoscience Frontiers*, *10*, 1421–1435. <https://doi.org/10.1016/j.gsf.2018.11.002>
- Cunningham, W. D., & Mann, P. (2007). Tectonics of strike-slip restraining and releasing bends. *Geological Society, London, Special Publications*, *290*, 1–12.
- de La Parra, F., Pinzon, D., Rodriguez, G., Bedoya, O., & Benson, R. (2019). Lacustrine systems in the early Miocene of Northern South America—Evidence from the upper Magdalena Valley, Colombia. *Palaios*, *34*, 490–505. <https://doi.org/10.2110/palo.2019.025>
- De Porta, J. (1966). Geología del extremo S del valle Medio del Magdalena entre Honda y Guataquí (Colombia). *Boletín de Geología*, *22–23*, 5–341.
- Deynoux, M., Çiner, A., Monod, O., Karabiyikoglu, M., Manatschal, G., & Tuzcu, S. (2005). Facies architecture and depositional evolution of alluvial fan to fan-delta complexes in the tectonically active Miocene Köprüçay Basin, Isparta Angle, Turkey. *Sedimentary Geology*, *173*, 315–343.
- Dickinson, W. R. (1985). Interpreting provenance relations from detrital modes of sandstones. In G. G. Zuffa (Ed.), *Provenance of arenites* (pp. 333–361). Springer Dordrecht.
- Dumont, J. F. (1993). Lake patterns as related to neotectonics in subsiding basins: the example of the Ucamara depression, Peru. *Tectonophysics*, *222*, 69–78.
- Dunkl, I. (2002). Trackkey: A windows program for calculation and graphical presentation of fission track data. *Computational Geosciences*, *28*, 3–12. [https://doi.org/10.1016/S0098-3004\(01\)00024-3](https://doi.org/10.1016/S0098-3004(01)00024-3)
- Duque-Trujillo, J., Bustamante, C., Solari, L., Gómez-Mafla, Á., Toro-Villegas, G., & Hoyos, S. (2019). Reviewing the Antioquia batholith and satellite bodies: A record of Late Cretaceous to Eocene syn- to post-collisional arc magmatism in the Central Cordillera of Colombia. *Andean Geology*, *46*, 82–101.
- Eakin, C. M., Lithgow-Bertelloni, C., & Dávila, F. M. (2014). Influence of Peruvian flat-subduction dynamics on the evolution of western Amazonia. *Earth and Planetary Science Letters*, *404*, 250–260.
- Echeverri, S., Cardona, A., Pardo, A., Monsalve, G., Valencia, V. A., Borrero, C., Rosero, S., & López, S. (2015). Regional provenance from southwestern Colombia fore-arc and intra-arc basins: Implications for Middle to Late Miocene orogeny in the Northern Andes. *Terra Nova*, *27*, 356–363. <https://doi.org/10.1111/ter.12167>
- Escalona, A., & Mann, P. (2011). Tectonics, basin subsidence mechanism and paleogeography of the Caribbean-South American plate boundary zone. *Marine and Petroleum Geology*, *28*, 8–39.
- Espitia, W., Cortés, M., Beltran, W., Díaz, I. C. H., & Arias, J. (2022). Structural styles of the Upper Magdalena valley, Northern Andes, Colombia: Case studies. In G. Zamora & A. Mora (Eds.), *Andean structural styles* (pp. 139–148). Elsevier.
- Farley, K. A. (2002). (U–Th)/He dating: techniques, calibrations, and applications. *Reviews in Mineralogy and Geochemistry*, *47*, 819–844. <https://doi.org/10.2138/rmg.2002.47.18>
- Flowers, R. M. (2009). Exploiting radiation damage control on apatite (U–Th)/He dates in cratonic regions. *Earth and Planetary Science Letters*, *277*, 148–155. <https://doi.org/10.1016/j.epsl.2008.10.005>
- Flowers, R. M., & Kelley, S. A. (2011). Interpreting data dispersion and “inverted” dates in apatite (U–Th)/He and fission-track datasets: An example from the US midcontinent. *Geochimica et Cosmochimica Acta*, *75*, 5169–5186. <https://doi.org/10.1016/j.gca.2011.06.016>
- Flowers, R. M., Ketcham, R. A., Shuster, D. L., & Farley, K. A. (2009). Apatite (U–Th)/He thermochronometry using a radiation damage accumulation and annealing model. *Geochimica et Cosmochimica Acta*, *73*(8), 2347–2365. <https://doi.org/10.1016/j.gca.2009.01.015>
- Folk, R. L. (1980). *Petrology of sedimentary rocks*. Hemphill.
- Forero-Ortega, A. J., Campanha, G. A. D. C., Faleiros, F. M., & Yogi, M. (2020). Pure shear-dominated transpression and vertical extrusion in a strike-slip fault splay from the Itapirapuã Shear Zone, Ribeira Belt, Brazil. *Tectonophysics*, *786*, 228455.
- Fossen, H., & Tikoff, B. (1998). Extended models of transpression and transtension, and application to tectonic settings. *Geological Society, London, Special Publications*, *135*, 15–33.
- Galbraith, R. F., & Laslett, G. M. (1993). Statistical models for mixed fission track ages. *Nuclear Tracks and Radiation Measurements*, *21*, 459–470.
- Galindo, P. A., & Lonergan, L. (2020). Basin evolution and shale tectonics on an obliquely convergent margin: The Bahia Basin, offshore Colombian Caribbean. *Tectonics*, *39*, e2019TC005787.
- Gallagher, K. (2012). Transdimensional inverse thermal history modeling for quantitative thermochronology. *Journal of Geophysical*

- Research: *Solid Earth*, 117, 1–16. <https://doi.org/10.1029/2011JB008825>
- Gallagher, K., Charvin, K., Nielsen, S., Sambridge, M., & Stephenson, J. (2009). Markov chain Monte Carlo (MCMC) sampling methods to determine optimal models, model resolution and model choice for Earth Science problems. *Marine and Petroleum Geology*, 26, 525–535. <https://doi.org/10.1016/j.marpetgeo.2009.01.003>
- García-Castellanos, D. (2006). Long-term evolution of tectonic lakes: Climatic controls on the development of internally drained basins. *Special Papers-Geological Society of America*, 398, 283.
- Garzanti, E., & Vezzoli, G. (2003). A classification of metamorphic grains in sands based on their composition and grade. *Journal of Sedimentary Research*, 73, 830–837. <https://doi.org/10.1306/012203730830>
- Gaupp, R., Gast, R., & Forster, C. (2000). AAPG Studies in Geology# 46, Chapter 5: Late Permian Playa Lake Deposits of the Southern Permian Basin (Central Europe).
- Gehrels, G. (2012). Detrital zircon U-Pb geochronology: Current methods and new opportunities. In C. Busby & A. Azor (Eds.), *Tectonics of sedimentary basins: Recent advances* (1st ed., pp. 45–62). <https://doi.org/10.1002/9781444347166.ch2>
- George, S. W., Horton, B. K., Vallejo, C., Jackson, L. J., & Gutierrez, E. G. (2021). Did accretion of the Caribbean oceanic plateau drive rapid crustal thickening in the northern Andes? *Geology*, 49(8), 936–940.
- Gibson, T. M., Faehnrich, K., Busch, J. F., McClelland, W. C., Schmitz, M. D., & Strauss, J. V. (2021). A detrital zircon test of large-scale terrane displacement along the Arctic margin of North America. *Geology*, 49, 545–550.
- Gómez, E., Jordan, T. E., Allmendinger, R. W., Hegarty, K., Kelley, S., & Heizler, M. (2003). Controls on architecture of the Late Cretaceous to Cenozoic southern Middle Magdalena Valley Basin, Colombia. *GSA Bulletin*, 115, 131–147. [https://doi.org/10.1130/0016-7606\(2003\)115<0131](https://doi.org/10.1130/0016-7606(2003)115<0131)
- Gómez, E., Jordan, T. E., Allmendinger, R. W., Hegarty, K., & Kelley, S. (2005). Syntectonic Cenozoic sedimentation in the northern Middle Magdalena Valley Basin of Colombia and implications for exhumation of the Northern Andes. *Bulletin of the Geological Society of America*, 117, 547–569. <https://doi.org/10.1130/B25454.1>
- Gómez, J., & Montes, N. E. (2020). *Mapa Geológico de Colombia en Relieve 2020. Escala 1:1.000.000*. Servicio Geológico Colombiano.
- Green, P. F. (1981). A new look at statistics in fission-track dating. *Nuclear Tracks*, 5, 77–86. [https://doi.org/10.1016/0191-278X\(81\)90029-9](https://doi.org/10.1016/0191-278X(81)90029-9)
- Guenther, W. R., Reiners, P. W., Ketcham, R. A., Nasdala, L., & Gierster, G. (2013). Helium diffusion in natural zircon: Radiation damage, anisotropy, and the interpretation of zircon (U-Th)/He thermochronology. *American Journal of Science*, 313(3), 145–198.
- Guerrero, J. (1993). *Geology-paleomagnetism: Magnetostratigraphy of the upper part of the Honda Group and Neiva Formation. Miocene uplift of the Colombian Andes*. Duke University.
- Guzmán-Speziale, M., Valdés-González, C., Molina, E., Gómez, J. M., Guzmán, M., Valde, C., Molina, E., & Martí, J. (2005). Seismic activity along the Central America volcanic arc: Is it related to subduction of the Cocos plate? *Tectonophysics*, 400, 241–254. <https://doi.org/10.1016/j.tecto.2005.03.006>
- Hatano, N., & Yoshida, K. (2017). Sedimentary environment and paleosols of middle Miocene fluvial and lacustrine sediments in central Japan: Implications for paleoclimate interpretations. *Sedimentary Geology*, 347, 117–129.
- Hazzi, N. A., Moreno, J. S., Ortiz-Movliav, C., & Palacio, R. D. (2018). Biogeographic regions and events of isolation and diversification of the endemic biota of the tropical Andes. *Proceedings of the National Academy of Sciences of the United States of America*, 115, 7985–7990. <https://doi.org/10.1073/pnas.1803908115>
- Herrera C. (2008). *Estratigrafía de la Formación Urumaco y geología estructural entre el Domo de Agua Blanca y Hato Viejo (Edo. Falcón)* (Ms thesis). Universidad Simón Bolívar.
- Hoorn, C., Bogotá-A, G. R., Romero-Baez, M., Lammertsma, E. I., Flantua, S. G. A., Dantas, E. L., Dino, R., do Carmo, D. A., & Chemale, F., Jr. (2017). The Amazon at sea: Onset and stages of the Amazon River from a marine record, with special reference to Neogene plant turnover in the drainage basin. *Global and Planetary Change*, 153, 51–65.
- Hoorn, C., Boschman, L. M., Kukla, T., Sciumbata, M., & Val, P. (2022). The Miocene wetland of western Amazonia and its role in Neotropical biogeography. *Botanical Journal of the Linnean Society*, 199(1), 25–35.
- Hoorn, C., Guerrero, J., Sarmiento, G. A., & Lorente, M. A. (1995). Andean tectonics as a cause for changing drainage patterns in Miocene northern South America. *Geology*, 23, 237–240.
- Hoorn, C., Kukla, T., Bogotá-Angel, G., van Soelen, E., González-Arango, C., Wesselingh, F. P., Vonhof, H., Val, P., Morcote-Rios, G., & Roddaz, M. (2021). Cyclic sediment deposition by orbital forcing in the Miocene wetland of western Amazonia? New insights from a multidisciplinary approach. *Global and Planetary Change*, 210, 103717.
- Hoorn, C., Perrigo, A., & Antonelli, A. (Eds.) (2018). *Mountains, climate and biodiversity: An introduction*. John Wiley & Sons.
- Hoorn, C., Wesselingh, F. P. P., ter Steege, H., Bermudez, M. A. A., Mora, A., Sevink, J., Sanmartín, I., Sanchez-Meseguer, A., Anderson, C. L. L., Figueiredo, J. P. P., Jaramillo, C., Riff, D., Negri, F. R. R., Hooghiemstra, H., Lundberg, J., Stadler, T., Särkinen, T., Antonelli, A., ter Steege, H., ... Antonelli, A. (2010). Amazonia through time: Andean. *Science*, 330, 927–931. <https://doi.org/10.1126/science.1194585>
- Horton, B. K. (2018a). Sedimentary record of Andean mountain building. *Earth-Science Reviews*, 178, 279–309. <https://doi.org/10.1016/j.earscirev.2017.11.025>
- Horton, B. K. (2018b). Tectonic regimes of the Central and Southern Andes: Responses to variations in plate coupling during subduction. *Tectonics*, 37, 402–429. <https://doi.org/10.1002/2017TC004624>
- Horton, B. K., Anderson, V. J., Caballero, V., Saylor, J. E., Nie, J., Parra, M., & Mora, A. (2015). Application of detrital zircon U-Pb geochronology to surface and subsurface correlations of provenance, paleodrainage, and tectonics of the Middle Magdalena Valley Basin of Colombia. *Geosphere*, 11, 1790–1811. <https://doi.org/10.1130/GES01251.1>
- Horton, B. K., Parra, M., & Mora, A., Sr. (2020). Construction of the Eastern Cordillera of Colombia: Insights from the sedimentary record. In *The geology of Colombia. Servicio Geológico Colombiano* (Vol. 37, p. 22). Publicaciones Geológicas Especiales.
- Horton, B. K., Saylor, J. E., Nie, J., Mora, A., Parra, M., Reyes-Harker, A., & Stockli, D. F. E. (2010). Linking sedimentation in the northern Andes to basement configuration, Mesozoic extension and Cenozoic shortening: Evidence from detrital zircon U-Pb

- ages, Eastern Cordillera, Colombia. *Bulletin of the Geological Society of America*, 122, 1423–1442. <https://doi.org/10.1130/B30118.1>
- Howard, J. L. (1993). The statistics of counting clasts in rudites: a review, with examples from the upper Palaeogene of southern California, USA. *Sedimentology*, 40, 157–174. <https://doi.org/10.1111/j.1365-3091.1993.tb01759.x>
- Ibanez-Mejia, M., Pullen, A., Arenstein, J., Gehrels, G. E., Valley, J., Ducea, M. N., Mora, A. R., Pecha, M., & Ruiz, J. (2015). Unraveling crustal growth and reworking processes in complex zircons from orogenic lower-crust: The Proterozoic Putumayo Orogen of Amazonia. *Precambrian Research*, 267, 285–310.
- Jaramillo, C., Romero, I., D'Apolito, C., Bayona, G., Duarte, E., Louwye, S., Escobar, J., Luque, J., Carrillo-Briceño, J. D., Zapata, V., Mora, A., Schouten, S., Zavada, M., Harrington, G., Ortiz, J., & Wesselingh, F. P. (2017). Miocene flooding events of western Amazonia. *Science Advances*, 3, 1–11. <https://doi.org/10.1126/sciadv.1601693>
- Jaramillo, C., Rueda, M. J., & Mora, G. (2006). Cenozoic plant diversity in the Neotropics. *Science*, 1979(311), 1893–1896.
- Jaramillo, C., Torres, V., Parra, M., & Strecker, M. R. (2010). Tectonic controls on Cenozoic foreland basin development in the north-eastern Andes Colombia. *Basin Research*, 22(6), 874–903. <https://doi.org/10.1111/j.1365-2117.2009.00459.x>
- Jaramillo, C. A., Rueda, M., & Torres, V. (2011). A palynological zonation for the Cenozoic of the Llanos and Llanos Foothills of Colombia. *Palynology*, 35, 46–84.
- Jaramillo, C., Ochoa, D., Contreras, L., Pagani, M., Carvajal-Ortiz, H., Pratt, L. M., Krishnan, S., Cardona, A., Romero, M., & Quiroz, L. (2010). Effects of rapid global warming at the Paleocene-Eocene boundary on neotropical vegetation. *Science*, 1979(330), 957–961.
- Jaramillo, J. S., Cardona, A., León, S., Valencia, V., & Vinasco, C. (2017). Geochemistry and geochronology from Cretaceous magmatic and sedimentary rocks at 6°35' N, western flank of the Central cordillera (Colombian Andes): Magmatic record of arc growth and collision. *Journal of South American Earth Sciences*, 76, 460–481.
- Jaramillo, J. S., Cardona, A., Monsalve, G., Valencia, V., & León, S. (2019). Petrogenesis of the late Miocene Combia volcanic complex, northwestern Colombian Andes: Tectonic implication of short term and compositionally heterogeneous arc magmatism. *Lithos*, 330, 194–210.
- Jaramillo, J. S., Cardona, A., Zapata, S., & Valencia, V. (2014). Late Cretaceous ARC to MORB compositional switch in the Quebradagrande Complex, Colombian Andes: understanding the long term tectonic evolution of a magmatic arc. In *AGUFM* (Vol. 2014, pp. V33B–V4863B). American Geophysical Union.
- Jaramillo, J. S., Zapata, S., Carvalho, M., Cardona, A., Jaramillo, C., Crowley, J. L., Bayona, G., & Caballero-Rodríguez, D. (2022). Diverse magmatic evolutionary trends of the Northern Andes unraveled by Paleocene to early Eocene detrital zircon geochemistry. *Geochemistry, Geophysics, Geosystems*, 23(9), e2021GC010113.
- Jiménez, G., Rico, J., Bayona, G., Montes, C., Rosero, A., & Sierra, D. (2012). Analysis of curved folds and fault/fold terminations in the southern Upper Magdalena Valley of Colombia. *Journal of South American Earth Sciences*, 39, 184–201.
- Kennan, L., & Pindell, J. L. (2009). Dextral shear, terrane accretion and basin formation in the Northern Andes: Best explained by interaction with a Pacific-derived Caribbean Plate? *Geological Society, London, Special Publications*, 328, 487–531. <https://doi.org/10.1144/SP328.20>
- Ketchum, R. A., Carter, A., Donelick, R. A., Barbarand, J., & Hurford, A. J. (2007). Improved modeling of fission-track annealing in apatite. *American Mineralogist*, 92, 799–810.
- Krstekanić, N., Willingshofer, E., Broerse, T., Matenco, L., Toljić, M., & Stojadinovic, U. (2021). Analogue modelling of strain partitioning along a curved strike-slip fault system during backarc-convex orocline formation: Implications for the Cerna-Timok fault system of the Carpatho-Balkanides. *Journal of Structural Geology*, 149, 104386.
- Lara, M., Salazar-Franco, A. M., & Silva-Tamayo, J. C. (2018). Provenance of the Cenozoic siliciclastic intramontane Amagá Formation: Implications for the early Miocene collision between Central and South America. *Sedimentary Geology*, 373, 147–162. <https://doi.org/10.1016/j.sedgeo.2018.06.003>
- Leal-Mejia, H. (2011). *Phanerozoic gold metallogeny in the Colombian Andes: A tectono-magmatic approach* (Doctoral Thesis). Universitat de Barcelona.
- Leal-Mejía, H., Shaw, R. P., & Melgarejo i Draper, J. C. (2019). Spatial-temporal migration of granitoid magmatism and the Phanerozoic tectono-magmatic evolution of the Colombian Andes. In: F. Cedié & R. P. Shaw (Eds.), *Geology and Tectonics of Northwestern South America* (pp. 253–410). Springer.
- León, S., Cardona, A., Parra, M., Sobel, E. R., Jaramillo, J. S., Glodny, J., Valencia, V. A., Chew, D., Montes, C., Posada, G., Monsalve, G., & Pardo-Trujillo, A. (2018). Transition from collisional to subduction-related regimes: An example from Neogene Panama–Nazca–South America interactions. *Tectonics*, 37, 119–139. <https://doi.org/10.1002/2017TC004785>
- Lin, A., & Yamashita, K. (2013). Spatial variations in damage zone width along strike-slip faults: An example from active faults in southwest Japan. *Journal of Structural Geology*, 57, 1–15.
- Linares, O. J. (2004). Bioestratigrafía de la fauna de mamíferos de las Formaciones Socorro, Urumaco y Codore (Mioceno medio-Plioceno temprano) de la región de Urumaco, Falcón, Venezuela. *Paleobiología Neotropical*, 1, 1–26.
- Liu, K., Xiao, W., Wilde, S. A., Zhang, J., Alexandrov, I., Kasatkin, S. A., & Ge, M. (2021). Syn-subduction strike-slip faults shape an accretionary orogen and its provenance signatures: Insights from Sikhote-Alin in NE Asia during the late Jurassic to early Cretaceous. *Tectonics*, 40, e2020TC006541.
- Lundberg, J. G., & Chernoff, B. (1992). A Miocene fossil of the Amazonian fish Arapaima (Teleostei, Arapaimidae) from the Magdalena River region of Colombia—Biogeographic and evolutionary implications. *Biotropica*, 24, 2–14.
- Martens, U. C., Restrepo, J. J., & Solari, L. A. (2012). Sinifaná metasedimentites and relations with Cajamarca parañaises of the central cordillera of Colombia. *Boletín de Ciencias de la Tierra*, 32, 99–110.
- Miall, A. (1977). A review of the braided-river depositional environment. *Earth Science Reviews*, 13, 1–62. [https://doi.org/10.1016/0012-8252\(77\)90055-1](https://doi.org/10.1016/0012-8252(77)90055-1)
- Miall, A. (1985a). Architectural-element analysis: A new method of facies analysis applied to fluvial deposits. *Earth Science Reviews*, 22, 261–308. [https://doi.org/10.1016/0012-8252\(85\)90001-7](https://doi.org/10.1016/0012-8252(85)90001-7)
- Miall, A. D. (2014). *Fluvial depositional systems*. Springer International Publishing. <https://doi.org/10.1007/978-3-319-00666-6>
- Miller, K. G., Browning, J. V., Schmelz, W. J., Kopp, R. E., Mountain, G. S., & Wright, J. D. (2020). Cenozoic sea-level and cryospheric

- evolution from deep-sea geochemical and continental margin records. *Science Advances*, 6, eaaz1346.
- Montes, C., Cardona, A., Jaramillo, C., Pardo, A., Silva, J. C. C. C., Valencia, V., Ayala, C., Pérez-Angel, L. C., Rodríguez-Parra, L. A., Ramirez, V., & Niño, H. (2015). Middle Miocene closure of the Central American seaway. *Science*, 1979(348), 226–229. <https://doi.org/10.1126/science.aaa2815>
- Montes, C., Cardona, A., McFadden, R., Morón, S. E., Silva, C. A., Restrepo-Moreno, S., Ramírez, D. A., Hoyos, N., Wilson, J., Farris, D., Moron, S. E., Silva, C. A., Restrepo-Moreno, S., Ramirez, D., Hoyos, N., Wilson, J., Farris, D., Bayona, G., Jaramillo, C., ... Flores, J. A. (2012). Evidence for Middle Eocene and younger emergence in Central Panama: implications for Isthmus closure. *Geological Society of America Bulletin*, 124, 780–799.
- Montes, C., Guzman, G., Bayona, G., Cardona, A., & Valencia, V. (2010). Clockwise rotation of the Santa Marta Massif and simultaneous Paleogene to Neogene deformation of the Plato-San Jorge and Cesar-Ranchería basins. *Journal of South American Earth Sciences*, 29, 832–848.
- Montes, C., Hatcher, R. D., & Restrepo-Pace, P. (2005). Tectonic reconstruction of the northern Andean blocks: Oblique convergence and rotations derived from the kinematics of the Piedras-Girardot area, Colombia. *Tectonophysics*, 399, 250.
- Montes, C., Rodríguez-Corcho, A. F., Bayona, G., Hoyos, N., Zapata, S., & Cardona, A. (2019). Continental margin response to multiple arc-continent collisions: The northern Andes-Caribbean margin. *Earth-Science Reviews*, 198, 102903. <https://doi.org/10.1016/j.earscirev.2019.102903>
- Montes, C., Silva, C. A., Bayona, G. A., Villamil, R., & Stiles, E. (2021). A middle to late Miocene trans-Andean Portal: Geologic record in the Tatacoa Desert. *Frontiers in Earth Science*, 8, 1–19. <https://doi.org/10.3389/feart.2020.587022>
- Mora, A., Baby, P., Roddaz, M., Parra, M., Brusset, S., Hermoza, W., & Espurt, N. (2010). Tectonic history of the Andes and Sub-Andean Zones: Implications for the development of the Amazon drainage basin. In C. Hoorn & F. P. Wesselingh (Eds.), *Amazonia: Landscape and Species Evolution: A look into the past* (Vol. 388, pp. 115–127). Blackwell.
- Mora, A., Casallas, W., Ketcham, R. A., Gomez, D., Parra, M., Namson, J., Stockli, D., Almendral, A., & Robles, W. (2015). Kinematic restoration of contractional basement structures using thermokinematic models: A key tool for petroleum system modeling. *AAPG Bulletin*, 99, 1575–1598. <https://doi.org/10.1306/04281411108>
- Mora, A., Parra, M., Strecker, M. R., Sobel, E. R., Hooghiemstra, H., Torres, V., & Jaramillo, J. V. (2008). Climatic forcing of asymmetric orogenic evolution in the Eastern Cordillera of Colombia. *Geological Society of America Bulletin*, 120, 930–949.
- Mora, A., Reyes-Harker, A., Rodríguez, G., Tesón, E., Ramírez-Arias, J. C., Parra, M., Caballero, V., Mora, J. P., Quintero, I., & Valencia, V. (2013). Inversion tectonics under increasing rates of shortening and sedimentation: Cenozoic example from the Eastern Cordillera of Colombia. *Geological Society, London, Special Publications*, 377, 411–442.
- Mora, A., Tesón, E., Martínez, J., Parra, M., Lasso, A., Horton, B. K., Ketcham, R. A., Velásquez, A., Arias-Martínez, J. P., & Gómez, J. (2020). The eastern foothills of Colombia. *The Geology of Colombia*, 3, 123–142.
- Mora, A., Villagómez, D., Parra, M., Caballero, V. M., Spikings, R., Horton, B. K., Mora-Bohórquez, J. A., Ketcham, R. A., Arias-Martínez, J. P., & Gómez, J. (2020). Late Cretaceous to Cenozoic uplift of the northern Andes: Paleogeographic implications. *The Geology of Colombia*, 3, 89–121.
- Moreno, F., Hendsy, A. J. W., Quiroz, L., Hoyos, N., Jones, D. S., Zapata, V., Zapata, S., Ballen, G. A., Cadena, E., Cárdenas, A. L., Carrillo-Briceño, J. D., Carrillo, J. D., Delgado-Sierra, D., Escobar, J., Martínez, J. I., Martínez, C., Montes, C., Moreno, J., Pérez, N., ... Jaramillo, C. (2015). Revised stratigraphy of Neogene strata in the Cocinetas Basin, La Guajira, Colombia. *Swiss Journal of Palaeontology*, 134, 5–43. <https://doi.org/10.1007/s13358-015-0071-4>
- Muñoz Granados, M.D. (2019). *U-Th-Pb Detrital zircon geochronology of the Gualanday Group and its tectonic implications*. (undergraduated thesis, Universidad de los Andes). <http://hdl.handle.net/1992/45331>
- Naranjo, A., Horner, J., Jahoda, R., Diamond, L. W., Castro, A., Uribe, A., Perez, C., Paz, H., Mejia, C., & Weil, J. (2018). La Colosa Au porphyry deposit, Colombia: Mineralization styles, structural controls, and age constraints. *Economic Geology*, 113, 553–578.
- Nichols, G. (2009). *Sedimentology and stratigraphy* (2nd ed.). Wiley-Blackwell.
- Nie, J., Horton, B. K., Saylor, J. E., Mora, A., Mange, M., Garziona, C. N., Basu, A., Moreno, C. J., Caballero, V., & Parra, M. (2012). Integrated provenance analysis of a convergent retroarc foreland system: U–Pb ages, heavy minerals, Nd isotopes, and sandstone compositions of the Middle Magdalena Valley basin, northern Andes, Colombia. *Earth-Science Reviews*, 110, 111–126.
- Nuttall, C. P. (1990). A review of the Tertiary non-marine molluscan faunas of the Pebasian and other inland basins of northwestern South America. *Bulletin of the British Museum, Natural History. Geology*, 45(2), 165–371.
- Ordóñez-Carmona, O., Álvarez, J. J. R., & Pimentel, M. M. (2006). Geochronological and isotopic review of pre-Devonian crustal basement of the Colombian Andes. *Journal of South American Earth Sciences*, 21(4), 372–382.
- Ortiz, J. R., & Jaramillo, C. A. (2018). *[Dataset] SDAR: A Toolkit for Stratigraphic Data Analysis in R*. [MS Excel] Distributed by Smithsonian Research Online. <https://doi.org/10.25570/stri/10088/35917>
- Pardo-Trujillo, A., Cardona, A., Giraldo, A. S., León, S., Vallejo, D. F., Trejos-Tamayo, R., Plata, A., Ceballos, J., Echeverri, S., Barbosa-Espitia, A., Slattery, J., Salazar, A., Botello, G. E., Celis, S. A., & Osorio-Granad, C. A. (2020). Sedimentary record of the Cretaceous–Paleocene arc–continent collision in the northwestern Colombian Andes: Insights from stratigraphic and provenance constraints. *Sedimentary Geology*, 401, 105627.
- Parra, M., Mora, A., Jaramillo, C., Strecker, M. R., Sobel, E. R., Quiroz, L., Rueda, M., Torres, V., Parra, M., Mora, A., Strecker, M. R., Sobel, E. R., & Torres, V. (2009). Orogenic wedge advance in the northern Andes: Evidence from the Oligocene-Miocene sedimentary record of the Medina Basin, Eastern Cordillera, Colombia. *Bulletin of the Geological Society of America*, 121, 780–800. <https://doi.org/10.1130/B26257.1>
- Parra, M., Mora, A., Sobel, E. R., Strecker, M. R., & González, R. (2009). Episodic orogenic front migration in the northern Andes: Constraints from low-temperature thermochronology in the Eastern Cordillera, Colombia. *Tectonics*, 28(4), 1–27.
- Pérez-Consuegra, N., Cuervo-Gómez, A., Martínez, C., Montes, C., Herrera, F., Madriñán, S., & Jaramillo, C. (2017). Paleogene Salvinia (Salviniaceae) from Colombia and their

- paleobiogeographic implications. *Review of Palaeobotany and Palynology*, 246, 85–108.
- Pérez-Consuegra, N., Hoke, G. D., Fitzgerald, P., Mora, A., Sobel, E. R., & Glodny, J. (2022). Late Miocene–Pliocene onset of fluvial incision of the Cauca River Canyon in the Northern Andes. *Bulletin*, 134(9–10), 2453–2468.
- Pérez-Consuegra, N., Hoke, G. D., Mora, A., Fitzgerald, P., Sobel, E. R., Sandoval, J. R., Glodny, J., Valencia, V., Parra, M., & Zapata, S. (2021a). The case for tectonic control on erosional exhumation on the tropical Northern Andes based on thermochronology data. *Tectonics*, 40(4), 1–24 e2020TC006652.
- Pérez-Consuegra, N., Ott, R. F., Hoke, G. D., Galve, J. P., Pérez-Peña, V., & Mora, A. (2021). Neogene variations in slab geometry drive topographic change and drainage reorganization in the Northern Andes of Colombia. *Global and Planetary Change*, 206, 103641. <https://doi.org/10.1016/j.gloplacha.2021.103641>
- Pietras, J. T., Carroll, A. R., & Rhodes, M. K. (2003). Lake basin response to tectonic drainage diversion: Eocene Green River Formation, Wyoming. *Journal of Paleolimnology*, 30, 115–125.
- Pindell, J., Erikson, J. (1993). The Mesozoic margin of northern South America. In J. Salfity (Ed.), *Cretaceous tectonics of the Andes* (pp. 1–60). Springer.
- Pirie, M. D., Chatrou, L. W., Mols, J. B., Erkens, R. H. J., & Oosterhof, J. (2006). ‘Andean-centred’ genera in the short-branch clade of Annonaceae: testing biogeographical hypotheses using phylogeny reconstruction and molecular dating. *Journal of Biogeography*, 33, 31–46.
- Poulsen, C. J., Ehlers, T. A., & Insel, N. (2010). Onset of convective rainfall during gradual late Miocene rise of the central Andes. *Science*, 1979(328), 490–493.
- Rahbek, C., Borregaard, M. K., Antonelli, A., Colwell, R. K., Holt, B. G., Nogues-Bravo, D., Rasmussen, C. M. Ø., Richardson, K., Rosing, M. T., Whittaker, R. J., & Fjeldså, J. (2019). Building mountain biodiversity: Geological and evolutionary processes. *Science*, 365, 1114–1119. <https://doi.org/10.1126/science.aax0151>
- Ramon, J. C., & Rosero, A. (2006). Multiphase structural evolution of the western margin of the Girardot subbasin, Upper Magdalena Valley, Colombia. *Journal of South American Earth Sciences*, 21, 493–509. <https://doi.org/10.1016/j.jsames.2006.07.012>
- Réjaud, A., Rodrigues, M. T., Crawford, A. J., Castroviejo-Fisher, S., Jaramillo, A. F., Chaparro, J. C., Glaw, F., Gagliardi-Urrutia, G., Moravec, J., & Ignacio, J. (2020). Historical biogeography identifies a possible role of Miocene wetlands in the diversification of the Amazonian rocket frogs (Aromobatidae: Allobates). *Journal of Biogeography*, 47, 2472–2482.
- Renaut, R. W., Gierlowski-Kordesch, E. H., Dalrymple, R., & James, N. (2010). Lakes. In N. P. James & R. W. Dalrymple (Eds.), *Facies models* (Vol. 4, pp. 541–575). Geological Association of Canada.
- Restrepo, J. J., Ordóñez-Carmona, O., Armstrong, R., & Pimentel, M. M. (2011). Triassic metamorphism in the northern part of the Tahami Terrane of the central cordillera of Colombia. *Journal of South American Earth Sciences*, 32, 497–507.
- Restrepo-Moreno, S. A., Foster, D. A., Bernet, M., Min, K., & Noriega, S. (2019). Morphotectonic and orogenic development of the Northern Andes of Colombia: A low-temperature thermochronology perspective. In F. Cedie & R. P. Shaw (Eds.), *Geology and Tectonics of Northwestern South America: The Pacific-Caribbean-Andean Junction* (pp. 749–832). Frontiers.
- Reyes-Harker, A., Ruiz-Valdivieso, C. F., Mora, A., Ramírez-Arias, J. C., Rodríguez, G., De La Parra, F., Caballero, V., Parra, M., Moreno, N., Horton, B. K., Saylor, J. E., Silva, A., Valencia, V., Stockli, D., & Blanco, V. (2015). Cenozoic paleogeography of the Andean foreland and retroarc hinterland of Colombia. *AAPG Bulletin*, 99(8), 1407–1453. <https://doi.org/10.1306/061814111110>
- Rodríguez, G., Arango, M. I., Zapata, G., & Bermúdez, J. G. (2016). Catálogo de unidades litoestratigráficas de Colombia, Formación Saldaña. Cordilleras Central y Oriental Tolima, Huila, Cauca y Putumayo. In *Catálogos estratigráficos* (pp. 1–91). Servicio Geológico Colombiano.
- Rodríguez-Muñoz, E., Montes, C., Rojas-Runjaic, F. J. M., & Crawford, A. J. (2022). Synthesis of geological data and comparative phylogeography of lowland tetrapods suggests recent dispersal through lowland portals crossing the Eastern Andean Cordillera. *PeerJ*, 10, e13186.
- Saeid, E., Bakioglu, K. B., Kellogg, J., Leier, A., Martínez, J. A., & Guerrero, E. (2017). Garzón Massif basement tectonics: Structural control on evolution of petroleum systems in upper Magdalena and Putumayo basins, Colombia. *Marine and Petroleum Geology*, 88, 381–401.
- Sanín, M. J., Cardona, A., Valencia-Montoya, W. A., Jiménez, M. F. T., Carvalho-Madrigal, S., Gómez, A. C., Bacon, C. D., Tangarife, T. R., Jaramillo, J. S., & Zapata, S. (2022). Volcanic events coincide with plant dispersal across the Northern Andes. *Global and Planetary Change*, 103, 757.
- Sanín, M. J., Mejía-Franco, F. G., Paris, M., Valencia-Montoya, W. A., Salamin, N., Kessler, M., Olivares, I., Jaramillo, J. S., & Cardona, A. (2022). Geogenomics of montane palms points to Miocene–Pliocene Andean segmentation related to strike-slip tectonics. *Journal of Biogeography*, 49(9), 1711–1725.
- Sarmiento, L. F., & Rangel, A. (2004). Petroleum systems of the upper Magdalena Valley, Colombia. *Marine and Petroleum Geology*, 21, 373–391.
- Sarmiento-Rojas, L. F., van Wess, J. D., & Cloetingh, S. (2006). Mesozoic transtensional basin history of the Eastern Cordillera, Colombian Andes: Inferences from tectonic models. *Journal of South American Earth Sciences*, 21, 383–411. <https://doi.org/10.1016/j.jsames.2006.07.003>
- Shuster, D. L., Flowers, R. M., & Farley, K. A. (2006). The influence of natural radiation damage on helium diffusion kinetics in apatite. *Earth and Planetary Science Letters*, 249, 148–161. <https://doi.org/10.1016/j.epsl.2006.07.028>
- Siravo, G., Faccenna, C., Gérault, M., Becker, T. W., Fellin, G., Herman, F., & Molin, P. (2019). Slab flattening and the rise of the Eastern Cordillera, Colombia. *Earth and Planetary Science Letters*, 512, 100–110. <https://doi.org/10.1016/j.epsl.2019.02.002>
- Siravo, G., Speranza, F., Mulas, M., & Costanzo-Alvarez, V. (2021). Significance of Northern Andes terrane extrusion and genesis of the interandean valley: Paleomagnetic evidence from the “Ecuadorian orocline”. *Tectonics*, 40, e2020TC006684.
- Spencer, C. J., Kirkland, C. L., & Taylor, R. J. M. (2016). Strategies towards statistically robust interpretations of in situ U–Pb zircon geochronology. *Geoscience Frontiers*, 7, 581–589. <https://doi.org/10.1016/j.gsf.2015.11.006>
- Spikings, R., Cochrane, R., Villagomez, D., Van Lelij, R., Der Vallejo, C., Winkler, W., & Beate, B. (2014). The geological history of northwestern South America: From Pangaea to the early collision of the Caribbean Large Igneous Province (290–75 Ma). *Gondwana Research*, 27(1), 95–139. <https://doi.org/10.1016/j.gr.2014.06.004>
- Spikings, R., & Paul, A. (2019). The Permian–Triassic history of magmatic rocks of the northern Andes (Colombia and Ecuador):

- Supercontinent assembly and disassembly. *The Geology of Colombia*, 2(36), 1–43.
- Valencia-Gómez, J. C., Cardona, A., Bayona, G., Valencia, V., & Zapata, S. (2020). Análisis de procedencia del registro sin-orogénico Maastrichtiano de la Formación Cimarrona, flanco occidental de la Cordillera Oriental colombiana. *Boletín de Geología*, 42, 171–204.
- van der Lelij, R., Spikings, R., & Mora, A. (2016). Thermochronology and tectonics of the Mérida Andes and the Santander massif, NW South America. *Lithos*, 248, 220–239.
- van der Wiel, A. M. M., van den Bergh, G. R. D., & Hebeda, E. H. (1992). Uplift, subsidence, and volcanism in the southern Neiva Basin, Colombia, Part 2: Influence on fluvial deposition in the Miocene Gigante Formation. *Journal of South American Earth Sciences*, 5, 175–196. [https://doi.org/10.1016/0895-9811\(92\)90037-Y](https://doi.org/10.1016/0895-9811(92)90037-Y)
- Velandia, F., Acosta, J., Terraza, R., & Villegas, H. (2005). The current tectonic motion of the Northern Andes along the Algeciras Fault System in SW Colombia. *Tectonophysics*, 399, 313–329.
- Vermeesch, P. (2012). On the visualisation of detrital age distributions. *Chemical Geology*, 312–313, 190–194. <https://doi.org/10.1016/j.chemgeo.2012.04.021>
- Vermeesch, P. (2013). Multi-sample comparison of detrital age distributions. *Chemical Geology*, 341, 140–146.
- Vermeesch, P. (2018a). IsoplotR: A free and open toolbox for geochronology. *Geoscience Frontiers*, 9, 1479–1493.
- Vermeesch, P. (2018b). Dissimilarity measures in detrital geochronology. *Earth-Science Reviews*, 178, 310–321.
- Villagómez, D., & Spikings, R. (2013). Thermochronology and tectonics of the Central and Western Cordilleras of Colombia: Early Cretaceous–Tertiary evolution of the Northern Andes. *Lithos*, 160–161, 228–249. <https://doi.org/10.1016/j.lithos.2012.12.008>
- Villagómez, D., Spikings, R., Magna, T., Kammer, A., Winkler, W., & Beltrán, A. (2011). Geochronology, geochemistry and tectonic evolution of the Western and Central cordilleras of Colombia. *Lithos*, 125, 875–896. <https://doi.org/10.1016/j.lithos.2011.05.003>
- Villamizar-Escalante, N., Bernet, M., Urueña-Suárez, C., Hernández-González, J. S., Terraza-Melo, R., Roncancio, J., Muñoz-Rocha, J. A., Peña-Urueña, M. L., Amaya, S., & Piraquive, A. (2021). Thermal history of the southern Central Cordillera and its exhumation record in the Cenozoic deposits of the Upper Magdalena Valley, Colombia. *Journal of South American Earth Sciences*, 107, 103105. <https://doi.org/10.1016/j.jsames.2020.103105>
- Vinasco, C., Cordani, U. G., González, H., Weber, M., & Pelaez, C. (2006). Geochronological, isotopic, and geochemical data from Permo-Triassic granitic gneisses and granitoids of the Colombian Central Andes. *Journal of South American Earth Sciences*, 21, 355–371.
- Wagner, G. A., Gleadow, A. J. W. W., & Fitzgerald, P. G. (1989). The significance of the partial annealing zone in apatite fission-track analysis: Projected track length measurements and uplift chronology of the transantarctic mountains. *Chemical Geology: Isotope Geoscience Section*, 79, 295–305. [https://doi.org/10.1016/0168-9622\(89\)90035-3](https://doi.org/10.1016/0168-9622(89)90035-3)
- Wagner, L. S., Jaramillo, J. S., Ramírez-Hoyos, L. F., Monsalve, G., Cardona, A., & Becker, T. W. (2017). Transient slab flattening beneath Colombia. *Geophysical Research Letters*, 44, 6616–6623. <https://doi.org/10.1002/2017GL073981>
- Wellman, S. S. (1970). Stratigraphy and petrology of the nonmarine Honda Group (Miocene), Upper Magdalena Valley, Colombia. *Geological Society of America Bulletin*, 81, 2353–2374.
- Wesselingh, F., & Salo, J. A. (2006). A Miocene perspective on the evolution of the Amazonian biota. *Scripta Geologica*, 133, 439–458.
- Wozniak, J., & Wozniak, M. H. (1987). Biostratigrafía de la región nor-central de la Serranía de Falcón, Venezuela nor-occidental. *Boletín de Geología*, 16, 101–139.
- Zapata, S., Cardona, A., Jaramillo, J. S., Patiño, A., Valencia, V., León, S., Mejía, D., Pardo-Trujillo, A., & Castañeda, J. (2019). Cretaceous extensional and compressional tectonics in the Northwestern Andes, prior to the collision with the Caribbean oceanic plateau. *Gondwana Research*, 66, 207–226. <https://doi.org/10.1016/j.gr.2018.10.008>
- Zapata, S., Sobel, E. R., del Papa, C., Muruaga, C., & Zhou, R. (2019). Miocene fragmentation of the Central Andean foreland basins between 26 and 28°S. *Journal of South American Earth Sciences*, 94, 102238. <https://doi.org/10.1016/j.jsames.2019.102238>
- Zapata, S., Zapata-henao, M., Cardona, A., Jaramillo, C., & Silvestro, D. (2021). Long-term topographic growth and decay constrained by 3D thermo-kinematic modeling: Tectonic evolution of the Antioquia Altiplano, Northern Andes. *Global and Planetary Change*, 203, 103553. <https://doi.org/10.1016/j.gloplacha.2021.103553>
- Zapata-Villada, J. P., Cardona, A., Serna, S., & Rodríguez, G. (2021). Late Cretaceous to Paleocene magmatic record of the transition between collision and subduction in the Western and Central Cordillera of northern Colombia. *Journal of South American Earth Sciences*, 112, 103557.
- Zavala, C., Arcuri, M., Di Meglio, M., Diaz, H. G., & Contreras, C. (2011). A genetic facies tract for the analysis of sustained hyperpycnal flow deposits. *AAPG Studies in Geology*, 61, 31–52. <https://doi.org/10.1306/13271349St613438>
- Zhou, R., Schoenbohm, L. M., Sobel, E. R., Davis, D. W., & Glodny, J. (2017). New constraints on orogenic models of the southern Central Andean Plateau: Cenozoic basin evolution and bedrock exhumation. *Bulletin of the Geological Society of America*, 129, 152–170. <https://doi.org/10.1130/B31384.1>
- Zhou, Y., Cheng, R., Shen, Y., Xu, Z., & Liu, G. (2022). Early Cretaceous provenance-depositional systems and volcano-sedimentary responses to strike-slip faulting in southern Jilin and eastern Liaoning provinces, NE China: A case study of the Tonghua Basin. *International Geology Review*, 1–20. <https://doi.org/10.1080/00206814.2022.2111725>

SUPPORTING INFORMATION

Additional supporting information can be found online in the Supporting Information section at the end of this article.

How to cite this article: Zapata, S., Calderon-Diaz, L., Jaramillo, C., Oboh-Ikuenobe, F., Piedrahita, J. C., Rodríguez-Cuevas, M., Cardona, A., Sobel, E. R., Parra, M., Valencia, V., Patiño, A., Jaramillo-Rios, J. S., Flores, M., & Glodny, J. (2023). Drainage and sedimentary response of the Northern Andes and the Pebas system to Miocene strike-slip tectonics: A source to sink study of the Magdalena Basin. *Basin Research*, 00, 1–44. <https://doi.org/10.1111/bre.12769>